69-18,281

CHURCH, David Arthur, 1939-

STORAGE AND RADIATIVE COOLING OF LIGHT ION GASES IN RADIO-FREQUENCY QUADRUPOLE TRAPS.

University of Washington, Ph.D., 1969
Physics, spectroscopy

University Microfilms, Inc., Ann Arbor, Michigan

STORAGE AND RADIATIVE COOLING OF LIGHT ION GASES IN RADIO-FREQUENCY QUADRUPOLE TRAPS

by

DAVID ARTHUR CHURCH

A dissertation submitted in partial fulfillment of the requirements for the degree of

DOCTOR OF PHILOSOPHY

UNIVERSITY OF WASHINGTON

1969

Approved by Hans S. Dehmelt
(Chairman of Supervisory Committee)

Department Physics Dept
(Departmental Faculty sponsoring candidate)

Date February 6, 1969

UNIVERSITY OF WASHINGTON

Date: January 16, 1969

We have carefully read the dissertation entitled "Storage and Radiative Cooling of Light Ion Gases in Radio-Frequency Quadrupole Traps" submitted by David Arthur Church in partial fulfillment of the requirements of the degree of Doctor of Philosophy and recommend its acceptance. In support of this recommendation we present the following joint statement of evaluation to be filed with the dissertation.

The goal of Mr. Church's thesis was twofold, firstly to investigate experimentally new types of radio-frequency traps which might be useful in the rf spectroscopy of stored ions and secondly to attempt to cool the ions through radiation damping by coupling to a resonant circuit tuned to one of their oscillatory frequencies in the trap. Cooling of the ion gas is important to prevent quick evaporation from the trap and to reduce the second order Doppler shift of the rf spectrum. The first trap structure studied was race-track shaped, the $\sim$ 5" long straight sections providing ideal regions for interaction of the stored ions with a beam of particles or photons. The short storage times for $_3He^+$ attainable with this first apparatus (a few seconds) independent of the background pressure below 10^{-8} torr were tentatively analyzed as caused by ion heating by the rf fields due to constructional imperfections. The relative complex structure made it difficult to keep tolerances below a critical margin. As the next structure to be studied a circular quadrupole trap was chosen. In this design much closer tolerances were achieved and it was possible to obtain storage times up to 200 sec for $_3He^+$ and H^+. By radiation damping the lifetime for protons could be increased to 490 sec at a background pressure of 2×10^{-10} torr, but no worthwhile cooling was observable. For the purpose of demonstrating the radiative colling a small axially symmetric trap apparatus was now constructed in which the trap capacity limiting the damping resistance and the background - pressure could be appreciably reduced. With this trap reduction of the ion temperature by a factor three to as low as 1000°K

DISSERTATION READING COMMITTEE: Hans J. Dehmelt

Edwin A. Uehling

Mark A. Heald

UNIVERSITY OF WASHINGTON

Date: January 16, 1969

We have carefully read the dissertation entitled "Storage and Radiative Cooling of Light Ion Gases in Radio-Frequency Quadrupole Traps" submitted by David Arthur Church in partial fulfillment of the requirements of the degree of Doctor of Philosophy and recommend its acceptance. In support of this recommendation we present the following joint statement of evaluation to be filed with the dissertation.

and lifetimes of 56 min. were observed for protons at a background pressure of 5×10^{-11} torr. Randomization times for the axial motion in the proton gas, presumably due to ion-ion collisions, as short as 0.3 sec were measured. In conclusion then, Mr. Church's work has demonstrated the potential usefulness of race-track and circular traps for future spectroscopy work on stored ions and proven the feasibility of radiative cooling of the ions.

DISSERTATION READING COMMITTEE: Hans J. Dehmelt

Edwin G. Wilson

Mark A. Heald

In presenting this thesis in partial fulfillment of the requirements for an advanced degree at the University of Washington I agree that the Library shall make it freely available for inspection. I further agree that permission for extensive copying of this thesis for scholarly purposes may be granted by my major professor, or, in his absence, by the Director of Libraries. It is understood that any copying or publication of this thesis for financial gain shall not be allowed without my written permission.

Signature 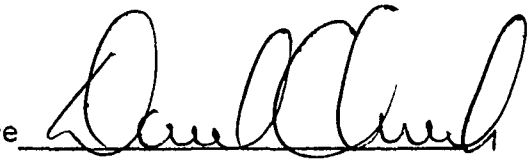

Date 7 February, 1969

ACKNOWLEDGMENTS

I am indebted to many people who contributed in their own way to the success attained in this research. In particular, Professor H. G. Dehmelt suggested the work, and his support, advice, and interest led to the final outcome. During the course of the work I had many valuable discussions with Dr. E. N. Fortson, Dr. C. B. Richardson, Dr. H. A. Schuessler, Mr. F. L. Walls, and Mr. S. C. Menasian concerning their work and my own. Mr. S. J. Hoverson carefully assembled the final ion trap and performed much of the experimental vacuum work. The dominant contributions to the construction of the vacuum systems and ion traps were made by Messrs. W. Pursel, H. Guldenmann, T. Hellesto, and R. Jochim of the machine shop and J. Jonson of the glass shop.

I also wish to express my appreciation to Dr. F. G. Major, who guided my early research experience, and to my wife Diane, who faced the difficulties attendant with graduate school in a creative and constructive manner.

TABLE OF CONTENTS

LIST OF FIGURES

List of Figures (continued) Page

LIST OF TABLES

I INTRODUCTION

1. The Ion-Storage Collision technique has recently been applied to ground state measurements in two important ionic systems: the $_3$He ion[1,2] and the H_2 molecular ion.[3,4] Both fine and hyperfine[5] splittings have been observed in the H_2 molecular ion, and the hyperfine structure of the $_3$He ion has been measured[6] with a fractional linewidth of 10^{-9}. Both of these systems are simple enough to allow precise theoretical calculations to be made. In the past, narrow linewidths have made precise tests of physical theories possible. The ISC technique offers the possibility of linewidths smaller than previously reported in a frequency range convenient for precision frequency standards.

In order to illumine the direction taken by the research reported here, the basic experimental method used in the measurements cited above will be briefly outlined. The ionic systems of interest are localized in space and stored by means of an inhomogeneous rf electric field, and are polarized by interaction with a suitable polarized beam of neutral systems. The ionic polarization is monitored by a polarization dependent neutralization interaction with the same neutral beam, which destroys the ions. As a result, the ion number observed after a fixed time interval is related to the ion polarization. The ion number measured after resonant depolarization is compared to the number when no

depolarizing mechanism is applied, resulting in a resonance signal.

The basic feature of this method that makes the narrow linewidths possible is the long available ion storage time, during which the energy states of interest in the ion are essentially isolated. The perturbation of the states produced by the rf electric field used to generate the effective harmonic well in which the ions move has been shown to be quite weak.[7] The other essential element of this technique is the neutral beam, by which the polarization is generated. The isolation time of the ions is limited by these interactions, but weaker beams and longer storage times can reduce this limitation. The primary virtue of the rf trapping technique is the possibility of ion confinement without the use of large magnetic fields required by other storage devices, such as the Penning trap.[8]

A fundamental limitation on the measured linewidth is produced by the motion of the trapped ions. The relativistic Doppler shift given by $\Delta\nu/\nu_o = -3kT/2W$, where T is the temperature and W is the rest energy of the ion, can be relatively large for light ions. The ions may have an energy spread of several electron volts in their effective harmonic well. A substantial fraction of the measured $_3He$ ion hfs linewidth[6] was attributed to this resultant broadening.

2. At the time this work was begun, a method of reducing the temperature of electrons in a Penning gauge trap had just been devised and demonstrated.[8] The aim of the following work has been the generalization of this cooling technique to ions in a radio-frequency quadrupole trap with the goal of making higher precision ion linewidths attainable. A further aim was the construction of modified rf quadrupole traps which would be suitable for future ISC experiments in which ion cooling and weak polarized beams could be effectively used. These aims divided the research effort into three separate, but dependent, areas: attainment of low pressures; ion trapping technique to achieve long term ion storage; and, once adequate traps were constructed, the study of the properties and results of ion cooling.

3. Ion storage times long compared to the time constant for ion cooling, expected to be many seconds, were required. Preliminary experimental tests on existing apparatus indicated that long term ion storage times were limited by collisions with the background gas in the vacuum system, as at higher pressures,[9,10] so the initial work centered on the construction and operation of a room temperature ultrahigh vacuum system and the testing of techniques to reach low pressures. Attempts to lower the attainable base pressures continued throughout the course of the work.

The second objective was the construction and operation of a "storage ring" ion trap in which to cool the ions.

A trap of this type would allow the physical separation of the functions of ion creation, polarization, and detection; and when built in a racetrack shape, would have a long beam interaction region. A "racetrack" trap was constructed which trapped $_3$He and H ions with modest success. The experience gained from this preliminary attempt was then used to build a circular storage ring trap. Despite ion lifetimes of minutes, it was not possible to cool ions in this trap although some effects of the cooling process were observed.

Rather than modify the storage ring trap once more, a small three-dimensional axially symmetric quadrupole ion trap was used to demonstrate the ion cooling technique with protons. Cooling the ions made information about ion-ion interactions accessible.

II CONCEPT OF THE RESEARCH

1. The development of getter-ion pumps has made the use of room temperature vacuum systems with base pressures in the 10^{-11} Torr range quite feasible. Vacuum bakeout procedures are necessary to reach these pressures, putting stringent requirements on materials and assembly techniques. However, no expensive cryopumping techniques are required, and the system is immune to power failures. Extrapolation of previously measured ion storage times to this pressure region indicated that storage times of minutes could be expected if no pressure independent lifetime limiting effects became dominant.

The design of the storage ring ion trap was based on a modification of the linear quadrupole rf mass filter structure. The potential between the electrodes of a linear mass filter ideally has the form[11]

$$\phi(x,y,z,t) = r_o^{-2} \, (U_o + V_o \mathrm{Cos}\Omega t)(x^2-y^2) \qquad \text{II-1}$$

where $r_o = x_o = y_o$ is the radius of the inter-electrode region, and U_o and V_o are respectively the applied dc and peak rf voltages. This potential clearly satisfies LaPlace's equation and leads to separable equations of motion for an ion with charge e, mass m, of the type

$$d^2\lambda/d\xi^2 + (a_\lambda - 2q_\lambda \mathrm{Cos}2\xi)\,\lambda = 0 \qquad \lambda = x,y \qquad \text{II-2}$$

where

$$\xi = \Omega t/2,\ a_x = 8eU_o/m\Omega^2 r_o^2 = -a_y \quad \text{and} \quad q_x = 4eV_o/m\Omega^2 r_o^2 = -q_y$$

Equation II-2 is the normalized form of the Mathieu equation.[12] The solutions are either bounded or unbounded, depending upon the choice of the parameters a and q. In a particular region of the composite (a,q) plane, defined as the stability region, both the x and y motions are bounded while the ions move freely in the z direction.[11]

The length of a physical structure constructed to the above specifications must be finite, and ions will be lost from the ends. Moreover, constructional misalignments will distort the potential from the ideal value, making application of the Mathieu theory to describe the ion motion no longer strictly appropriate.

We instead rely on an approximate theory[13,14] which indicates that, when given a general field $\vec{E}(x,y,z)\mathrm{Cos}\Omega t$ derivable from a potential that satisfies LaPlace's equation, the one dimensional equation of motion can be written in the form

$$d^2\lambda/dt^2 + (e/m)\frac{\partial \psi}{\partial \lambda} = 0 \qquad \lambda = x,y,z \qquad \text{II-3}$$

where the time average in the pseudopotential $\psi = e\overline{E^2}/4m\Omega^2$ is taken over the period $2\pi/\Omega$. When the electric field is linear in space, the resultant motion is harmonic.

We now imagine a slightly distorted structure in which, instead of lying parallel to the z axis, the electrodes are

bent into an arc of radius R, with $R>>r_o$. Since the change is small, the new potential inside the electrodes should differ only slightly from the original. Taking r_o/R as a measure of the perturbation, we assume that the new electric field can be written as a sum of terms composed of the original field plus new components weighted, to first order, by r_o/R. The approximate theory now indicates that the ions will still be bound in directions perpendicular to the arc, with the motion remaining basically harmonic. The equations of motion will not now in general be linear. Small typical nonlinear effects such as a shift in the center of oscillation and higher order harmonics of the fundamental motion can be expected. If the arc is now completed to form a circle, the ions should be stably bound in this "storage ring" structure. Placing straight sections between sections of arc should only reduce the nonlinearities in these regions. The practicality of a round structure of this type for the trapping of an electron-ion plasma for short times had been demonstrated,[15] indicating that the long term storage of ions might be feasible.

The standard method of creating ions in the trap is to ionize the background gas with a pulse of electrons. Particular ions could be produced by leaking the appropriate gas into the vacuum system. The storage efficiency of the trap was determined by measuring the number of ions remaining in the trap as a function of the elapsed time after ion creation. The storage time for ions is assumed to be limited

by ionic energy gain at a rate which may depend on background gas pressure, ion number and temperature, or other parameters. Large energy ions have orbits that intersect the trap electrodes, resulting in ion loss. An ion storage time limited only by the lowest base pressure attainable was considered to be the merit criterion of a successful trap design.

2. The harmonic motion of the ions in the radio-frequency trap is used as the basis of a technique to "radiatively" cool the ions.[8,16] Before continuing with the approximate theory of ion motion, we return to the exact theory to note that if $\lambda(\xi)$ is the exact solution to the Mathieu equation (II-2) then the solution to the modified equation[12]

$$d^2y/d\xi^2 + 2Kdy/d\xi + (\bar{a} - 2qCos2\xi)y = 0 \qquad \bar{a} = a + K^2$$

is $y(\xi) = e^{-K\xi}\,\lambda(\xi)$, indicating that when the motion is bounded, the addition of a damping mechanism decreases the amplitude of motion exponentially.

To illustrate the radiative cooling concept,[17] we consider an idealized model consisting of a single ion with charge Ze, mass Am, bound harmonically in one dimension to a plane midway between two infinite parallel plates separated by a distance $2x_o$. The plates, shown in Figure I-(a), are assumed to have negligible capacitance and are connected externally with a resistance R taken to be noiseless. The equation of motion of the ion is

Figure I-(a) Model for the ion cooling theory.

Figure I-(b) Experimental realization of the model. The capacitance of the trap electrodes which replace the parallel plates is tuned out by an inductance to produce a resistance effective at the ion oscillation frequency.

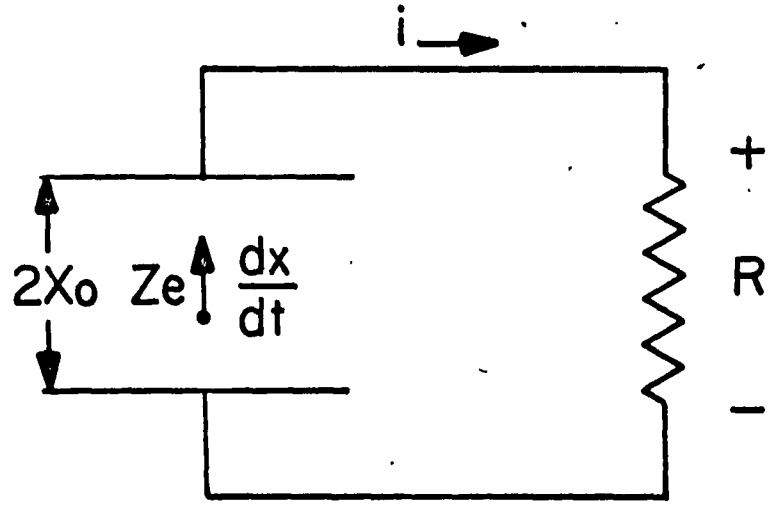

(a)

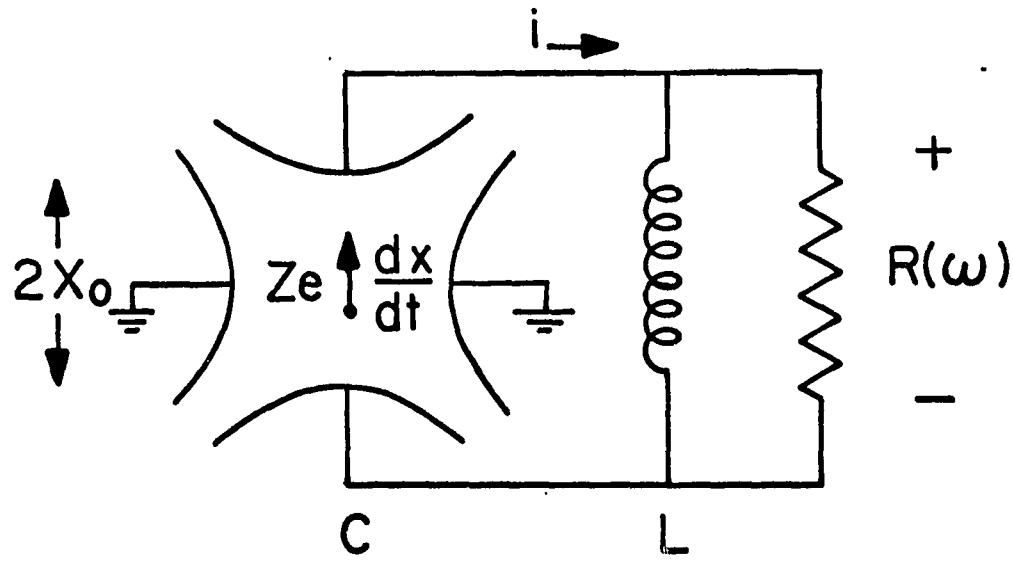

(b)

$$d^2x/dt^2 + \omega_o^2 x = -ZeV(t)/2Amx_o$$

where $-V(t)/2x_o$ is any electric field appearing across the plates. Charge is induced on the plates by the ion, and the motion of the ion between the plates causes charge to flow from one plate to the other through the resistance R. The current induced at a particular plate is[18,19] $i(t) = (Ze/2x_o)dx/dt$ which, flowing through the resistor, produces a voltage between the plates. This reaction of the circuit on the charge may be incorporated into the equation of motion of the ion, giving

$$d^2x/dt^2 + \tau_{xo}^{-1}\, dx/dt + \omega_o^2 x = 0$$

where $\tau_{xo} = 4Amx_o^2/Z^2e^2R$. The solution of this equation is a damped oscillation with time constant $2\tau_{xo}$ or alternatively, the ion energy averaged over a period of the motion, $\bar{W}_x = Am\omega_o^2\overline{x^2}$, decreases exponentially at the rate

$$d\bar{W}/dt = -\overline{i^2}R = -\bar{W}/\tau_{xo}$$

To maximize the damping rate, clearly A and $2x_o$ should be small, while R and Z should be large. In an experimental situation, the parallel plates will have a capacitance C which can be tuned out by an inductance L at the ion oscillation frequency ω_o , as in Figure I-(b). This produces a resistance effective at ω_o given by $R = Q/\omega_o C$ where Q is the quality factor of the tuned circuit. This makes $R(\omega)$ dependent upon frequency. If the well depth of the harmonic

motion, defined as $D = Am\omega_o^2 x_o^2/2Ze$ is held constant while the mass and charge of the ion are varied, the frequency can be eliminated from the time constant for a given ion type. The resultant expression is

$$\tau_{xo} = \frac{4x_o C}{QZe}\left(\frac{2AmD}{Ze}\right)^{1/2} \qquad \text{II-4}$$

The magnitude of the time constant depends strongly on the capacitance of the trapping structure, as well as the electrode separation. $A = Z = 1$ for a proton, and using the physical parameters given in Tables II and III a time constant of a few seconds is obtained.

Using linear superposition, the cooling of N ions can be dealt with in a manner similar to the single ion case. The superposition assumption should be valid as long as all motional relaxation times are long compared to coherence times set by the ion oscillation bandwidth. For coherent ion motion, such as that produced by external excitation, the currents due to each ion add. The ion equation of motion incorporating the voltage induced by this current has a damping time constant N/τ_{xo} indicating that the coherent motion of N ions is rapidly damped with a rate dependent on ion number. When the phases of the individual ion currents are randomly distributed, however, the time averaged total ion current vanishes. The averaged mean square current is

$$\overline{i^2(t)} = \sum_{j=1}^{n} \overline{i_j^2(t)} + \sum_{\substack{j=1 \\ j\neq k}}^{n}\sum_{k=1}^{n} \overline{i_j(t)i_k(t)} = \frac{NZ^2e^2}{4x_o^2}\left(\overline{\frac{dx}{dt}}\right)^2$$

so power is dissipated in the resistor at N times the single ion rate. Since the average total energy of the ion cloud is a factor of N larger, the time constant for cooling N ions is unchanged from the single ion rate.

Ions at temperature T harmonically bound in all three dimensions have a total energy 3NkT. Assuming a relaxation time between the degrees of freedom of the motion short compared to the radiation time constant, the time constant for ion cooling becomes $\tau_o = 3\tau_{xo}$, if the energy loss still occurs only in one dimension as previously discussed.

A cooling resistor at an absolute temperature T_o will cause a fluctuating Johnson noise voltage to appear across the capacitor plates which is independent of the voltage fluctuation produced by the ion motion at temperature T. As a result of the lack of phase correlation between the ion motion and the thermal voltage fluctuation, the ions will come into temperature equilibrium with the resistor. The thermal energy input to the ions is at the constant rate $3NkT_o/\tau_o$, with the time required to establish this equilibrium characterized by the damping time constant τ_o. The time averaged rate of ion energy loss can now be written

$$3Nkd(T-T_o)/dt = -3Nk(T-T_o)/\tau_o \qquad \text{II-5}$$

The "bolometric" technique[8] of detecting the presence of the hot ions consists of observing the added fluctuating noise voltage across the tank circuit generated by the random

ion motion. The tank circuit is heated by the ions at the rate given by equation (II-5), which can be generalized by adding an appropriate heating rate to describe any ionic energy gain. The tank circuit dissipates its energy as heat with a time constant $\tau_{to} = Q/\omega_o$ dependent on the tank circuit Q. The rate of exchange of energy in the tank circuit is described by the equation

$$kd(T_t-T_o)/dt = 3Nk(T-T_t)/\tau_o - k(T_t-T_o)/\tau_{to} \qquad \text{II-6}$$

The tank circuit reaches a quasi-equilibrium with the ions in a time comparable to τ_{to}. The signal is the difference between the quasi-equilibrium temperature of the tank circuit and room temperature, assuming that the tank circuit temperature differs only slightly from T_o. With this assumption the sensitivity[8] for ion detection is

$$(T_t-T_o)/(T-T_o) = 3N\tau_{to}/\tau_o \equiv \eta \qquad \text{II-7}$$

In the ideal situation so far assumed we have a harmonically bound, undisturbed ion gas at temperature T with relaxation rates between motional coordinates fast compared to the expected ion cooling rate. The ions should cool exponentially to the tuned circuit equilibrium temperature T_o with time constant $3\tau_{xo}$ when tuned to resonance with the tuned circuit. The tuned circuit temperature should abruptly increase when the ions are brought into resonance, and then should follow the ion temperature back to equilibrium, as long as the sensitivity η is small and constant.

Several experimental factors produce changes in the magnitude of the cooling time constant. Figure I-(b) shows how two trap electrodes take the place of the parallel plates used in the simplified theory. The general expression for the current to an electrode is given by[18,19]

$$i(t) = ZeE_v(x)dx/dt$$

where $E_v(x)$, the electric field measured at the instantaneous position of the ion, is determined by setting the electrode of interest at unit potential and grounding all other electrodes. This electric field is clearly not uniform due to the distortion of the field lines produced by the other electrodes of the ion trap. Charge flows to and from the added electrodes without passing through the resistance $R(\omega)$ at the frequency ω_o . Moreover, the potential difference produced in reaction to the ion motion is distorted by the added electrodes, resulting in nonlinear damping. The smallness of the damping rate should make nonlinear effects negligible, however.

The amount the induced ion current is changed by the use of a trap structure instead of parallel plates can be calculated in the limit of small ion temperature using an approximate geometry consisting of a hollow cylinder with two flat end plates. This approximate geometry is most appropriate for the axially symmetric trap which will be discussed later. When the current to one end plate is

calculated, the electric field can be obtained in terms of standard functions.[20] Using ion trap parameters to fix the geometric dimensions, a thirty per cent increase in the cooling time constant is obtained. This gives a measure of the degree of accuracy of time constant calculations.

Due to structural misalignments or modifications of the harmonic potential well by space charge effects, the trapped ions do not all oscillate at the same frequency, but occupy a band of frequencies centered on ω_o . The width of this band can be characterized by a quality factor $Q_I = \omega_o/\Delta\omega_I$. Likewise, the tuned circuit which acts as the resistance R has a bandwidth defined by $Q_t = \omega_o/\Delta\omega_t$. As the resistance is increased by increasing Q_t, the bandwidth decreases. The cooling rate increases with increased resistance until the bandwidth of the resistance becomes less than the ion frequency spread. In this situation, only those ions with frequencies in the bandwidth of $\Delta\omega_t$ will dissipate energy directly. For the case where the ion linewidth is much greater than the tank circuit bandwidth, the number of ions dissipating energy varies inversely with the resistance bandwidth, so the cooling time constant should be independent of tank circuit Q. A resistance effective over the whole ion bandwidth can be defined as $R_I = Q_I/\omega_o C$ for use in cooling rate calculations.

To summarize the preceding paragraph, the cooling rate for the ions is maximized when the Q of the tank circuitis made at least as large as the Q of the ion line. Higher tank

circuit Q's do not increase the cooling rate. The mean squared voltage fluctuation generated by the ions per unit bandwidth is proportional to the square of both the ion current and the resistance in that bandwidth, however. Since the thermal noise voltage fluctuation varies directly with the resistance, a large tank circuit Q is desirable to increase the signal to noise ratio.

When the corrections discussed above are applied to the cooling time constant, the magnitude does not change substantially. The small electrode separations necessary for efficient ion cooling are appropriate for the storage ring trap. The dimension $2r_o$ in the storage ring, which corresponds to the plate separation in the cooling theory, must of necessity be small if R/r_o is to be reasonably large in a conventional vacuum system. On the other hand, the long electrode length and close spacing produces a fairly large capacitance to be tuned out at the ion oscillation frequency. For the cylindrical electrode case this capacitance varies only as the logarithm of the electrode diameter to spacing ratio,[21] so for shorter time constants close spacing is desirable.

III DESIGN OF THE EXPERIMENT

1. The motion of a charged particle in a sinusoidally time varying inhomogeneous electric field has been treated approximately by a number of workers, and detailed accounts are available.[13,14,22] A few aspects of this theory which pertain to the work to be described are reviewed here for convenience.

The instantaneous effect on an ion of a uniform rf electric field with frequency Ω is to produce a rapid driven oscillatory motion at the same frequency, with a small amplitude proportional to the field. When the field is made non-uniform, the motion becomes more complex. The "micro-motion", as the small amplitude oscillation is called, becomes a small perturbation on the large amplitude "secular" motion which is obtained by an averaging procedure. The secular acceleration can be described by the gradient of the pseudopotential ψ used in equation (II-3). If a dc potential exists in the same region, a gradient of a constant potential must be added to equation (II-3). Unlike the pseudopotential, the dc potential does not bind the ions in all dimensions. Any defocusing effect produced by the dc must be overcome by the rf for the ions to remain bound. Taking for illustration the individual components of the potential defined in equation (II-1), the equations of motion for the mass filter structure are

$$d^2\bar{x}/dt^2 + \omega_{xo}^2\bar{x} = 0 \qquad \omega_{xo} = \left(\frac{2e^2V_o^2}{m^2\Omega^2r_o^4} + \frac{2eU_o}{mr_o^2}\right)^{1/2}$$

$$d^2\bar{y}/dt^2 + \omega_{yo}^2\bar{y} = 0 \qquad \omega_{yo} = \left(\frac{2e^2V_o^2}{m^2\Omega^2r_o^4} - \frac{2eU_o}{mr_o^2}\right)^{1/2} \qquad \text{III-1}$$

The oscillation frequencies are degenerate when no dc voltage is applied.

When the micromotion is added to the secular motion, the expression for the ion coordinate can be written

$$\bar{x} = \bar{x}_m \text{Cos}(\omega_o t + \phi_x)[1 - (\sqrt{2}\omega_o/\Omega)\text{Cos}(\Omega t + \phi_{rf})] \qquad \text{III-2}$$

Expanding the trigonometric functions we find sidebands at the frequencies $\Omega + \omega_o$ and $\Omega - \omega_o$ with amplitudes proportional to the amplitude of the secular motion but reduced by the factor ω_o/Ω . Successive approximations give the higher frequency terms $s\Omega \pm \omega_o$, $s = 2,3,---$ found in the exact theory.

The region of the potential just illustrated is defined by the position of the electrodes which establish the fields. The maximum coordinate reached by the ions without striking the electrodes is r_o, so well depths in each dimension can be defined by the equation $D_x = m\omega_{xo}^2x_o^2/2e$ and $D_y = m\omega_{yo}^2y_o^2/2e$. When the dc voltage is zero, insertion of the frequencies given by equation (III-1) into these expressions yields $D_x = D_y = V_o\omega/\sqrt{2}\Omega$.

The effectiveness of the rf voltage in producing a potential well, when compared to the dc voltage, is reduced by roughly the frequency ratio ω/Ω . For a given well depth, a large frequency ratio requires a correspondingly large rf voltage. The validity of the approximate theory is not uniform over the whole range of stable solutions allowed by the exact theory. The use of this theory is most appropriate when the parameter ω/Ω is small.[22] In the experimental work to be discussed here, this was the case.

The approximate theory outlined here indicates that an ion should be bound to the region of minimum electric field irrespective of the exact shape of the field. The one-dimensional treatment presented here is inadequate for the general case, which would include field components depending on more than one coordinate. However, the approximate magnitude of effects can be determined. For the special case of the storage ring trap configuration with a linear perturbation of the electric field proportional to r_o/R , the oscillation frequency is shifted by $(\omega-\omega_o)/\omega_o \approx \pm r_o/R$ indicating the amount of expected deviation from the mass filter situation.

2. Since the approximate theory indicated that an experimental or mathematical analysis of the electric field was unnecessary, a racetrack storage ring trap shown in Figure II was built to test the prediction. Four 0.1 inch diameter molybdenum rods were used as electrodes. The bent rods were

Figure II "Racetrack" storage ring trap

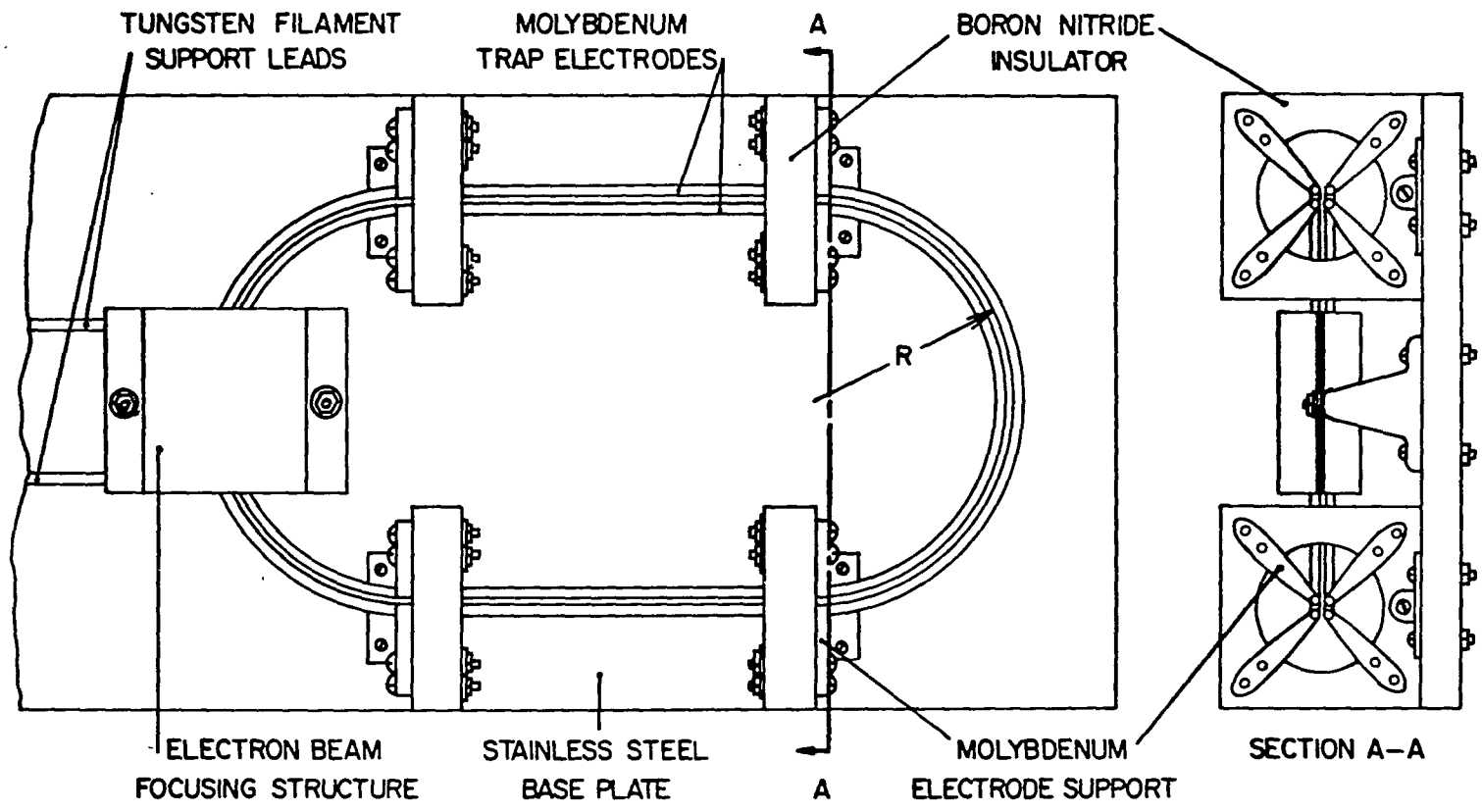
TUNGSTEN FILAMENT
SUPPORT LEADS
MOLYBDENUM
TRAP ELECTRODES
A
BORON NITRIDE
INSULATOR
R
ELECTRON BEAM
FOCUSING STRUCTURE
STAINLESS STEEL
BASE PLATE
A
MOLYBDENUM
ELECTRODE SUPPORT
SECTION A–A
INTERELECTRODE RADIUS
r_o =0.043 INCH
STRUCTURE RADIUS
R=2 INCH
ONE INCH

supported by Boron Nitride ceramic insulators on a stainless steel table. The rigidity of the molybdenum eliminated the problem of sagging during vacuum bakeout, observed by others who used OFHC copper,[23] but bending the rods to an exact curvature was impossible using available techniques. As a result, the radius of the trapping field region varied along the arc of the trap and the ion oscillation frequency became a function of position. The ends of the bent rods were connected by inserting one end of each rod into a stainless steel foil sleeve resistance welded to the other end. This allowed some thermal expansion without distortion. The field radius r_o was 0.043 inches and the ratio of structure radius to field radius R/r_o was 46 to one. The trap electrode rods were resistance welded to molybdenum supports using stainless steel foil strips wrapped around the rods. The supports were bolted to the ceramic insulators with stainless steel screws using lock washers to hold the nuts tight during vacuum bake-out. The table supporting the trap was bolted to the front flange of the vacuum system described in section IV-2. The rf and dc connections to the rods were made at a single point close to the feedthroughs bringing the voltages through the vacuum flange. A spring loaded tungsten filament heated by 60 Hz current produced the electrons that created the ions from the gas in the vacuum system. A negatively biased shield around the rods and filament focused the electrons on the trap rods.

The detection of the ions in a similar structure will be described in a later section. The trapping rf voltage was applied at frequencies $\Omega/2\pi$ of 14, 21, and 28 MHz at various times. The longest storage time for $_3$He ions was found to be independent of background gas pressure below 10^{-8} Torr, and was limited to at most a few seconds. The storage times seemed to improve slightly when the ratio Ω/ω was made large while the well depth was held constant. The Ω/ω ratio could be varied from about 7/1 to 14/1. The ions seemed to be gaining energy from the trapping fields, resulting in premature loss at the electrodes. The lack of sensitivity to frequency change exhibited by the energy input process was probably due to the large range of ion oscillation frequencies over the arc of the structure.

3. Experimentally observed frequency dependent instabilities in a linear mass filter were investigated by v. Busch[24] in terms of subharmonic excitation of a nonlinear oscillator by a driving force, produced in this case by the trapping rf field with frequency Ω . In the mass filter such instabilities reduced the transmitted ion current, while in an ion trap they would lead to shortened storage times. Some basic characteristics of this excitation can be obtained with a simple one-dimensional approximation by calculating the time averaged rate of change of energy of a system acted upon by a force: $\overline{dW_x/dt} = \overline{F_x dx/dt}$. This of course neglects nonlinear coupling between coordinates which exists in general. We

assume that both rf and dc fields in each dimension can be expanded in a power series in the coordinate, with appropriate coefficients to describe the strength of each nonlinear term. The dominant terms in each expansion will be the linear ones, which generate the basic harmonic motion of the ions. To calculate the rate of energy gain, it is assumed that only the field component of a particular order nonlinearity produces the excitation, and that the excitation is weak enough to keep the basic motion essentially unchanged for short times. The expression for the rate of energy gain is then linearized by using the harmonic oscillator expressions at frequency ω for position and velocity. The time averaged rate vanishes except at resonance, and for a nonlinearity of order K-1 in the field, $\Omega/\omega = K$ is the highest integer frequency ratio for which there is a non-vanishing time average. The resonant rate of energy gain by the ions is proportional to the rf voltage and the strength of the nonlinear term, and is most rapid for large amplitude motion. The effect of such excitation is to segment the stability region for the parameters of the ion equation of motion into smaller stable regions bounded by regions of instability. Stable motion should result for the correct choice of operating parameters.

The effect of the dc field on nonlinear excitation is small compared to that of the rf field, due to the much smaller voltages involved. The coefficients of a given order nonlinear term will in general be different, since the rf and

dc bias arrangements are independent. Nevertheless, the effect of the dc voltage on the excitation should be observable only insofar as it changes the frequency of the ion motion. The coefficients of the lower order nonlinear terms are in general expected to be the largest, so it appears favorable to keep the ratio Ω/ω as large as possible. This can be accomplished by using small well depths or by utilizing high Ω - rf frequencies. On the other hand, for large Ω/ω the frequency separation between neighboring instabilities is small. For a finite ion oscillation linewidth, the ion line will overlap several orders of excitation simultaneously producing continuous, although weak, excitation if all field expansion coefficients are present. Experimentally, increasing the Ω/ω ratio by increasing the rf frequency produced longer ion storage times, so this solution to the problem was used. As an example of the overlap of the excitation orders, the unstable frequencies ω_1 and ω_2 are separated by

$$(\omega_1-\omega_2)/\omega \approx \omega/\Omega = 0.06 \text{ for } \Omega/\omega = 15/1.$$

The Q of the ion line must be much greater than twenty to avoid simultaneous excitation.

In summary, the short storage times exhibited by the racetrack trap were attributed to the following causes: unnecessary field nonlinearities were caused by uneven electrode spacing, contact potential differences between different materials on the electrodes, and the penetration of external fields into the trapping region. In addition, unwanted emissions from the trapping rf oscillator were produced by

frequency multiplication. These shortcomings were removed or reduced by using a trapping rf not generated by frequency multiplication which was a large non-integral multiple of the ion oscillation frequency, and by the design of the circular storage ring ion trap to be described.

IV CIRCULAR STORAGE RING TRAP APPARATUS

1. On the basis of the experience gained with the first attempt at storage ring ion trapping, a second structure was built with substantial success. The construction and operation of this trap will be described in detail to illustrate the factors involved in long term ion storage at low pressures.

A simplified block diagram of the apparatus, including the details of the ion detection circuit and the rf bias circuit, appears in Figure IV. Two of the trap electrodes were grounded directly; the rf voltage was capacitively coupled to the other two; and the ion motion was detected between these two "hot" electrodes. The dc bias on these electrodes was supplied through an rf choke from a low impedence source.

The trapping rf input lead is effectively grounded at the ion detection frequency ω through the large capacity C_Ω. As a result, the coupling capacitors C_c appear in parallel with the trap electrode capacitance. The trapping rf voltage is divided across these coupling capacitors and the trap electrode capacitance. To minimize the capacitance to be tuned out at ω, this division ratio should be large; but a large division ratio may lead to uncertainties in trap voltage due to asymmetric stray capacitance. The value one-to-one was chosen for this ratio, with C_c = 45 pF. Rf chokes

with an impedance of about 1000 ohms at the frequency Ω were put in the detection circuit leads inside the vacuum system to inhibit possible Ω rf current bypass to ground. The coil forming the resonant circuit at ω is at the high voltage V_o, and is coupled to the receiver through a shielded one-to-one transformer at low impedance.

2. The ultrahigh vacuum system was constructed from #304 austenitic stainless steel, using Varian Associates Conflat flanges and OFHC copper gaskets. The main chamber, eight inches inside diameter and sixteen inches long, was connected to an 80 liter/second Varian Vac-Ion pump through a four inch diameter, seven inch long pump lead. Two one and one half inch diameter arms projected at right angles to the pump lead. One arm held a General Electric Triggered Discharge Gauge (TDG) to monitor the system pressure, and the other arm held a pulsed helium leak, described in Appendix III. A two and one half inch diameter arm mounted near the front of the main chamber held a Varian nude ion gauge of the Bayard-Alpert type for pressure measurement. The ten inch outside diameter front flange on the main chamber contained all electrical feedthroughs to the ion trap, and acted as the trap support. The feedthrough for the Ω rf was specially constructed of copper, glass, and stainless steel. This nonmagnetic construction was found to be necessary to avoid excessive heat generation when carrying the high frequency at appreciable power levels. The feedthrough was essentially a cylinder of

Pyrex insulation, sealed at one end to a stainless steel cylinder welded to the flange, and at the other end to an OFHC copper cup. A one-half inch diameter OFHC copper rod, brazed to the copper cup, acted as the rf lead. All other electrical connections were made through commercial ceramic insulators welded to the flange. The input leads were 0.1 inch diameter tungsten rods brazed with electron beam heating in vacuum to the insulators. Leaks in several of these insulators apparently resulted from the welding. All unflanged joints in the vacuum shell were Tungsten-Inert Gas welded.

The procedures used in cleaning, assembling and evacuating the vacuum system are outlined in Appendix I. Measuring pressure in the ultrahigh vacuum region is difficult due to the limitations of the various types of gauges. The gas composition at base pressure was unknown, and the gauge sensitivity for each gas component tended to be pressure dependent in the low pressure region for the TDG. Pressure measurements will generally be given in TDG gauge current units (Amperes), which must be multiplied by the appropriate sensitivity to obtain the pressure. This calibration is discussed in Appendix II. When a pressure is given in Torr, the gas composition was relatively unambiguous and the appropriate calibration has already been made.

3. When a high frequency trapping rf is used, the requirements on physical and electrical symmetry become more stringent. Multiple feed connections to the trap electrodes

were used to make sure that the trapping rf voltage did not vary along the circumference of the trap, since at high frequencies the wavelength is not negligible compared to the trap circumference. The use of higher frequencies required higher voltages and currents, and made better shielding of the trapping volume necessary.

The materials used in construction were chosen to keep the structure as non-magnetic as feasible while at the same time providing enough rigidity to withstand the 400°C vacuum bake without loss of dimensional tolerance. Metals, chosen on the basis of their rigidity, conductivity, vapor pressure and non-magnetic properties were #304 and #316 austenitic stainless steel, molybdenum, tungsten, OFHC copper, and Advance metal. Ceramics were chosen on the basis of their machining and vacuum properties. Boron Nitride,[25] Alsimag,[26] and standard commercial glazed ceramic standoff insulators were used. Corning 7740 and 7052 glasses were used in parts of the vacuum envelope, as well as Vicor and sealing glasses.

The trap structure, shown in detail in Figure III-(a), (b), and (c), was constructed between two stainless steel plates which served as electrostatic shields. The 3/8 inch thick bottom plate was bolted to the front flange of the vacuum system, and acted as a supporting table. The upper plate was about 1/4 inch thick, as thinner plates tended to warp. The insulators holding the ion trap electrodes in place were clamped between these two plates, which were held

Figure III - (a) Circular storage ring trap, top view. The top plate of the structure and the rf choke attached to it have been removed to reveal the internal construction.

Figure III - (b) Circular storage ring trap, section view A-A. A cross section in one plane is shown to avoid additional confusing detail.

Figure III - (c) Circular storage ring trap, section view B-B. A cross section in one plane is again used.

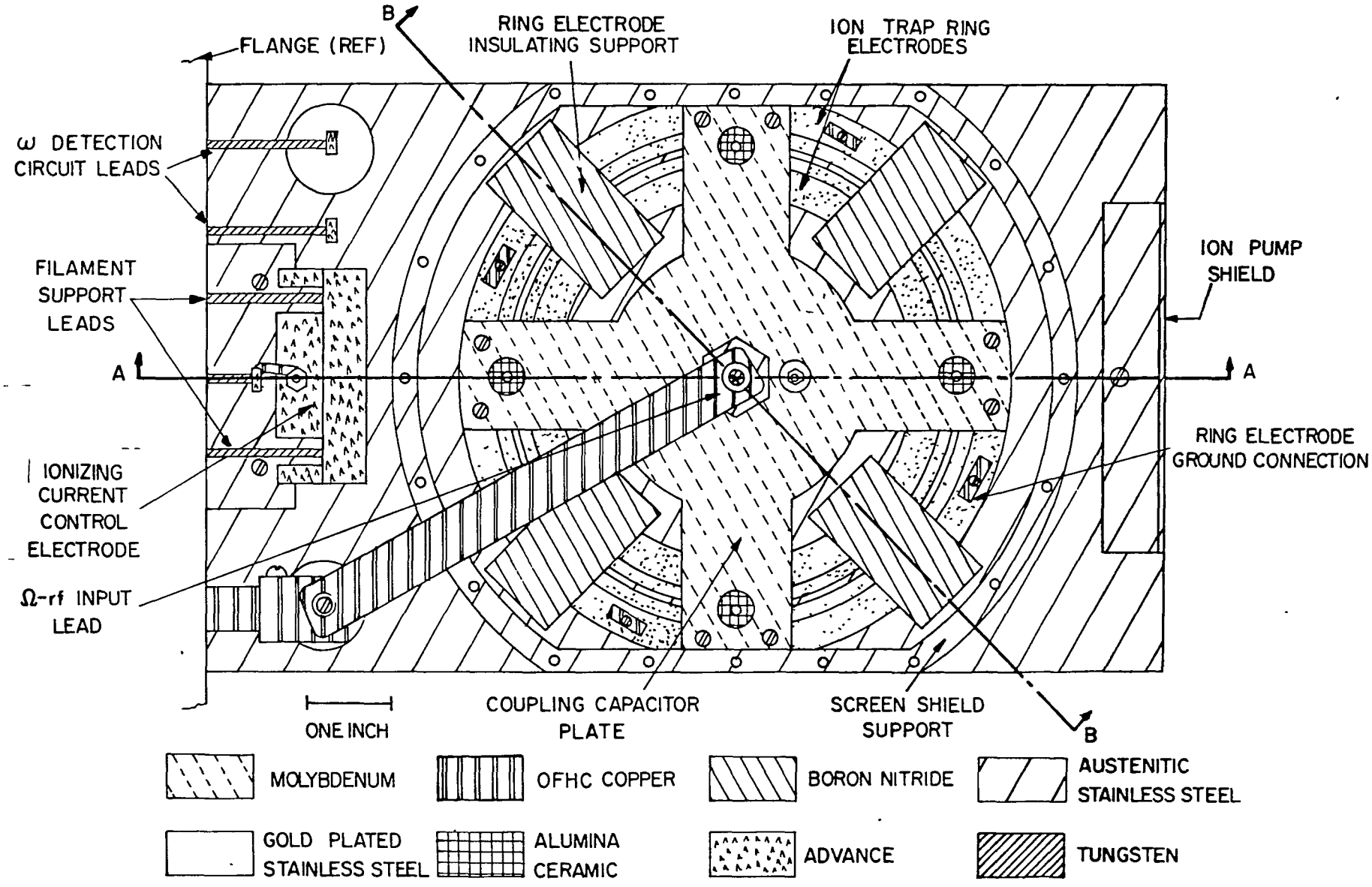
B
FLANGE (REF)
RING ELECTRODE INSULATING SUPPORT
ION TRAP RING ELECTRODES
ω DETECTION CIRCUIT LEADS
FILAMENT SUPPORT LEADS
ION PUMP SHIELD
A
A
RING ELECTRODE GROUND CONNECTION
IONIZING CURRENT CONTROL ELECTRODE
Ω-rf INPUT LEAD
ONE INCH
COUPLING CAPACITOR PLATE
SCREEN SHIELD SUPPORT
B
MOLYBDENUM
OFHC COPPER
BORON NITRIDE
AUSTENITIC STAINLESS STEEL
GOLD PLATED STAINLESS STEEL
ALUMINA CERAMIC
ADVANCE
TUNGSTEN

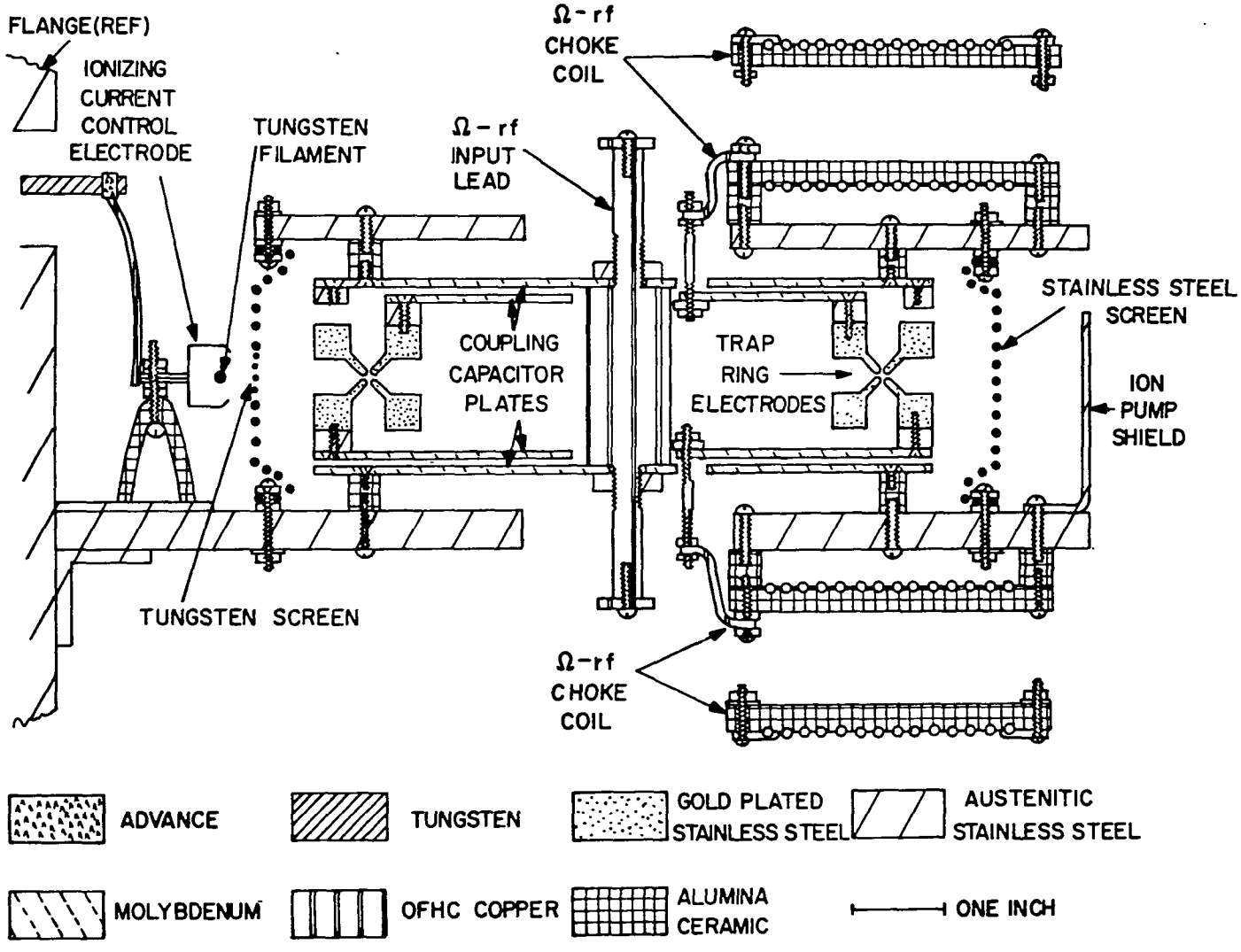
FLANGE(REF)
IONIZING CURRENT CONTROL ELECTRODE
TUNGSTEN FILAMENT
Ω - rf INPUT LEAD
Ω - rf CHOKE COIL
COUPLING CAPACITOR PLATES
TRAP RING ELECTRODES
STAINLESS STEEL SCREEN
ION PUMP SHIELD
TUNGSTEN SCREEN
Ω - rf CHOKE COIL
ADVANCE
TUNGSTEN
GOLD PLATED STAINLESS STEEL
AUSTENITIC STAINLESS STEEL
MOLYBDENUM
OFHC COPPER
ALUMINA CERAMIC
ONE INCH

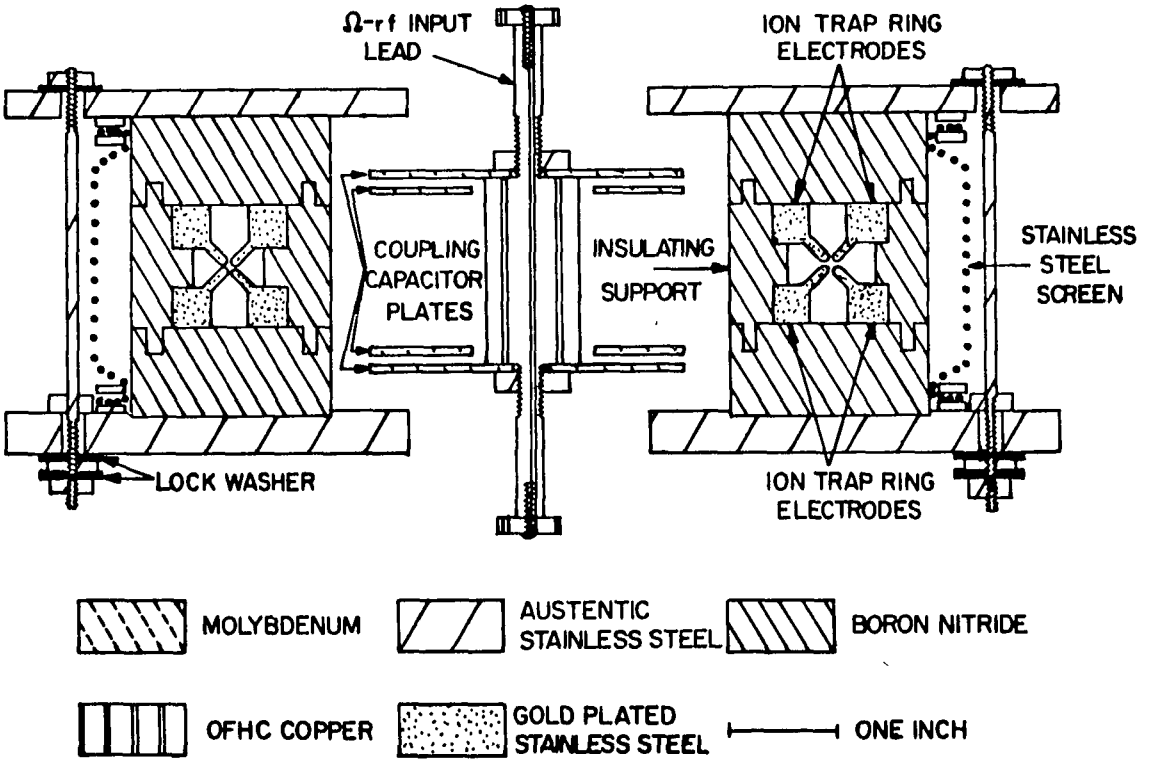
Ω-rf INPUT LEAD
ION TRAP RING ELECTRODES
COUPLING CAPACITOR PLATES
INSULATING SUPPORT
STAINLESS STEEL SCREEN
LOCK WASHER
ION TRAP RING ELECTRODES
MOLYBDENUM
AUSTENTIC STAINLESS STEEL
BORON NITRIDE
OFHC COPPER
GOLD PLATED STAINLESS STEEL
ONE INCH

together by nuts and lockwashers on threaded stainless steel rods. Stainless steel screen, held by clamping rings bolted to the plates, shielded the outside of the trap while not inhibiting the vacuum pumpdown. This screen also served as an rf ground return.

An OFHC copper cylinder formed the symmetry axis of the trapping structure, projecting through holes drilled in the top and bottom plates. Massive copper straps external to these plates connected this cylinder to the rf feedthrough in the front flange. These straps were bolted to the cylinder and to a vertical rod connected to the rf feedthrough, and could slide and rotate slightly to accommodate thermal expansion. The copper cylinder acted as the central rf feed point for the trap electrodes. Molybdenum plates, chosen for rigidity, capacitively coupled the high voltage rf to the appropriate trap electrodes. Small stainless steel tabs were bolted on to balance the capacitance where necessary. The other two trap electrodes were grounded directly at regular intervals with copper straps bolted to the nearest of the two supporting plates. Lockwashers were used on all bolted connections to maintain tension during the vacuum bakeout.

The shape of the trap electrodes was chosen to maintain symmetry and to make the trapping region accessible to the ionizing electrons and to any beam that might be directed across one section of the arc if desired. The massive square cross sections of the electrodes made positioning and support

relatively easy, and provided enough mass to prevent warping under thermal stress. The electrodes were machined from #316 stainless steel, and were stress relieved several times during the machining process to inhibit any subsequent warping under thermal stress. They were plated with 2×10^{-5} inches of rhodium, which acted as a diffusion barrier for a 10^{-4} inch plated layer of gold. The ratio of the diameter of the ring structure to the diameter of the trapping region was $R/r_o = 42/1$, with $r_o = 0.16$ cm. The end of the projection on each electrode, which defines the trapping region boundary, was machined round in cross section with a radius 1.16 times the radius of the ion storage region to provide a good approximation to a harmonic potential.[27]

The insulating supports for the trap electrodes are best shown in Figure III-(c). These supports were made from Boron Nitride, which can be machined to the same tolerance as stainless steel and requires no subsequent bake which might change the dimensions. These insulating supports were designed to interlock in a rigid manner when the trap electrodes were in place. The clamping action of the top and bottom plates held the supports as units. The insulators were positioned by shallow milled slots in the bottomplate.

The rf chokes were made from copper wire wound on a coil form machined from Alsimag ceramic, which tends to chip and crumble more than the Boron Nitride. The chokes were connected between the appropriate molybdenum coupling plate

Figure IV Block diagram of the electronic apparatus for the circular storage ring trap.

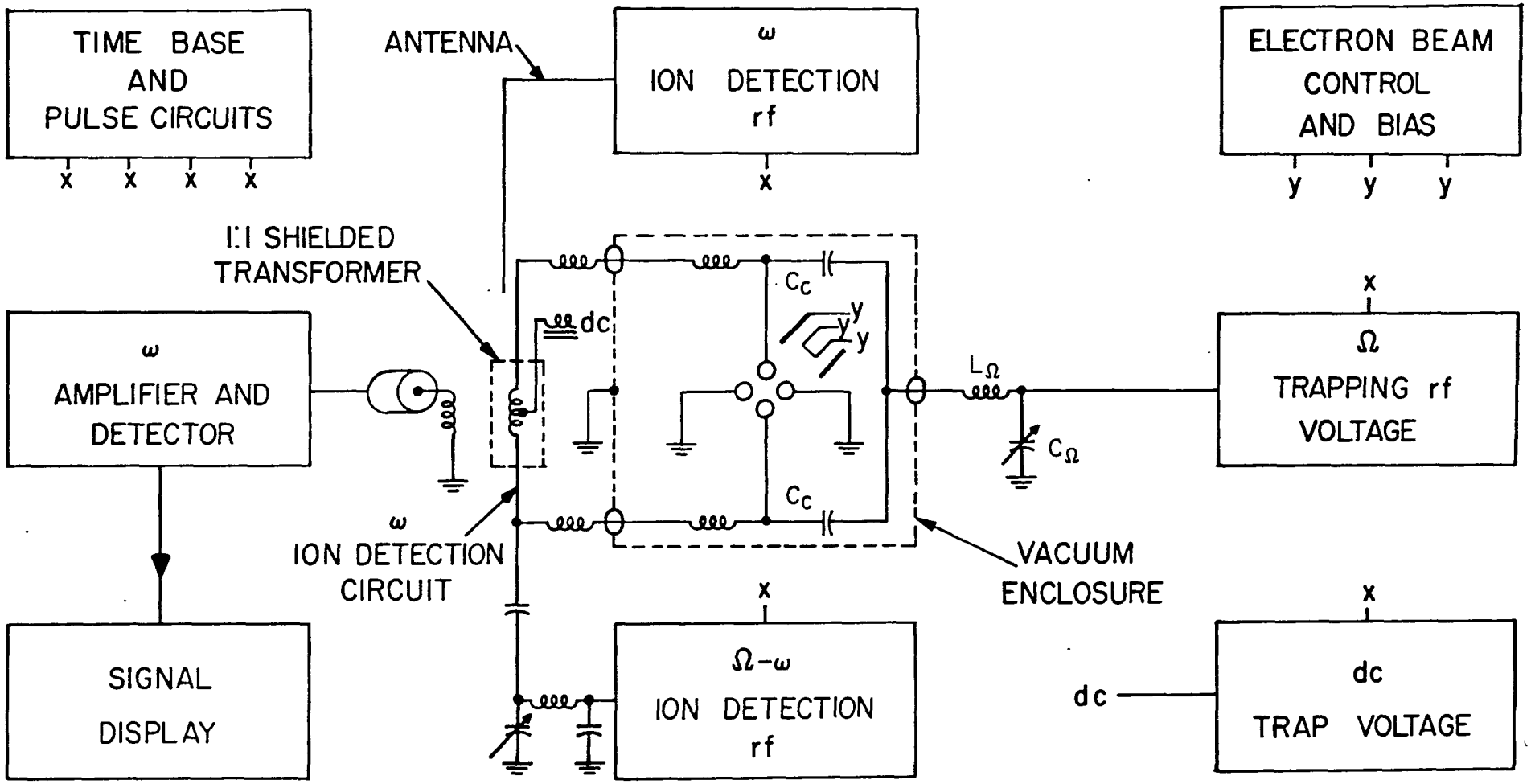
TIME BASE AND PULSE CIRCUITS
x x x x
ANTENNA
ω
ION DETECTION rf
x
ELECTRON BEAM CONTROL AND BIAS
y y y
1:1 SHIELDED TRANSFORMER
dc
C_c
y
y
y
x
Ω
TRAPPING rf VOLTAGE
L_Ω
C_Ω
ω
AMPLIFIER AND DETECTOR
ω
ION DETECTION CIRCUIT
C_c
VACUUM ENCLOSURE
SIGNAL DISPLAY
x
Ω−ω
ION DETECTION rf
x
dc
dc
TRAP VOLTAGE

and the ion detection feedthroughs in the vacuum flange. The coil forms were bolted to the top and bottom plates using ceramic standoff insulators for support.

The spring loaded 0.008 inches diameter tungsten filament was resistance welded to the tungsten feedthrough leads using Advance metal as filler. A focusing electrode made of Advance metal directed the emission current toward the trap. A tungsten wire section in the stainless steel screen served to accelerate the electrons when the filament was negatively biased. The electron pulse was modulated by a large negative bias on the focusing electrode.

A stainless steel plate external to the electrostatic shield protected the trapping volume from the ionic and molecular beam generated by the ion pump. A stainless steel screen in the pump throat further attenuated the ion beam.

4. A large six inch deep aluminum chassis attached to the front flange of the vacuum system acted as a shield for the circuit components shown in Figure IV. The front cover of the shield, attached with sheet metal screws, allowed easy access to the circuits inside.

The high frequency trapping rf circuit consisted of an International Crystal Co. 52 MHz crystal oscillator coupled through a matching network to a Boonton 230A linear amplifier. The rf power was further amplified by a Gonset 6 meter linear amplifier, filtered by a multistage high pass filter, and

coupled to the trap electrodes by the step-up pi network shown in Figure IV. The dc bias for the trap was provided by an emitter follower circuit with an output impedance of a few ohms. The dc bias was modulated by a ramp sweep when the ion signal was detected. Low pass filters were installed in all low frequency leads to block the rf.

The ion detection tank circuit consisted of two separate coils connected by a shielded one to one transformer. The transformer consisted of two concentric coils wound on bakelite forms with a slotted aluminum cylinder between them. The capacitance tuned out by the detection circuit coil was about 70 pF. Originally a Hammarlund HQ-180A radio receiver was used as an amplifier and detector. The one to one transformer coupled the tank circuit signal to the receiver at an impedance of about one hundred ohms. Later the receiver was replaced by two Tektronix 1121 low noise broad band amplifiers, and the impedance was transformed at one tenth of the tuned circuit maximum resistance. The bandwidth was narrowed with step-up pi networks between and after the amplifiers, and a conventional peak detecting diode circuit was used as detector. The detection frequencies used were in the two to five MHz range. The ion signal was observed on a Tektronix type 503 oscilloscope.

Two methods of ion number detection were used, both involving excitation of the ions at particular frequencies. The excitation at ω was provided by a General Radio 1213B

unit oscillator, which was keyed on by a gate actuated plate circuit relay for an appropriate interval during the detection process. The same oscillator retuned in frequency generated the excitation at $\Omega-\omega$ when this frequency was used to drive the ions. This frequency was pulsed with a gate operated diode switch, amplified by a Boonton 230A linear amplifier, stepped up to high impedance with a pi network and capacitively coupled at high impedance to one electrode of the ion trap.

Tektronix 160 series pulse and waveform generators were used to generate a repetitive ion detection time sequence consisting of an electron pulse followed, with variable delay, by a sawtooth sweep of the dc trap bias accompanied by a pulse of the appropriate detection rf. This sequence of events was controlled by a variable duration master time base. All gates, pulses, and sawtooth sweeps were produced by these generators. The events were initiated manually during long storage time interval measurements.

The tungsten filament was heated by an auto-transformer controlled 60 Hz filament transformer. The line current could be interrupted by a gate actuated relay to pulse the emission. The filament was biased 600 volts negative with respect to ground, with the emission control electrode at minus 750 volts. Emission currents in the range of five to ten mA with pulse durations of five to ten seconds were

used to create the ions. These large currents were necessary as only a small fraction of the total current penetrated the trapping volume. Using the experimental helium ionization cross section[28] at a pressure of 10^{-9} Torr, about 5×10^{7} ions were produced in the trapping volume per pulse. The pulsed helium leak was used to increase the helium gas pressure during the electron pulse when helium ions were being trapped.

V PROCEDURE AND RESULTS FOR STORAGE RING ION CONTAINMENT

1. Two different detection methods were used to determine the ion number, as indicated in Figure IV. The "absorption" method has been widely used,[9] and analyzed in detail.[2] Briefly, a weak voltage at the resonant frequency ω is coupled at high impedance to the detection tank circuit by an antenna. When the oscillation frequency of the ions is swept through this resonant frequency by varying the trap voltage, the ions absorb energy from the exciting dipole field. The current in the tank circuit induced by the driven ion motion produces a voltage across the tank circuit which modulates the carrier voltage. The ion signal is the modulation on the carrier, amplified and detected. The peak induced voltage has been shown to be [2] $e_{max} = NeQ_t/4C$, where N is the ion number and $R = Q_t/\omega_o C$ is the resonant tank circuit resistance.

The second method of detection, "sideband excitation" operates on the same principle, but the exciting frequency differs from the detection frequency.[7] This eliminates the carrier, and the voltage induced across the tank circuit by the ion motion is observed directly. The excitation principle can be understood with an argument of the following type.[17] When the ion motion is excited by a uniform electric field with a frequency corresponding to a sideband frequency such as $\Omega-\omega$, the total field seen by the ions is

the superposition of the harmonic field with frequency Ω and this linear field. Since the pseudopotential is proportional to $\overline{E^2}$, these field components are mixed. When a time average is taken over the short interval $2\pi/\Omega$, ψ has an added time averaged term varying at the frequency ω indicating that the ions see a force at this frequency which produces a resonance similar to the absorption case.

The peak signal to rms noise ratio in the bandwidth of the tank circuit can be written

$$S = e_{max}/\overline{(V_n^2)}^{1/2} \approx (NeQ_t/4C)(4RkT\Delta f)^{-1/2} . \qquad V\text{-}1$$

For typical storage ring trap values given in Table I, with an optimum signal to noise ratio of about 10^3 in a bandwidth of 40 KHz, the ion number observed was $N \approx 10^5$.

The sideband excitation detection method has the disadvantage of requiring the ion exciting voltage at $\Omega-\omega$ to be the order of Ω/ω larger than that required for absorption detection, due to the smaller sideband amplitude. This large voltage increases the chance of mixing with the large trapping voltage at Ω in any nonlinear element of the system. The frequency ω resulting from this mixing can be picked up by the sensitive receiver. This effect was useful for tuning $\Omega-\omega$ to resonance, but it necessitated careful filtering before all voltage monitoring diodes, and after the final stages of amplifiers, before measurements could be made. The small frequency difference ω between the two high frequencies added to the filtering problem.

Figure V A weak $_3$He ion signal observed with the absorption method in the circular storage ring trap. A tracing of the photographed signal is shown. The curvature of the baseline is produced by hum on the rf envelope.

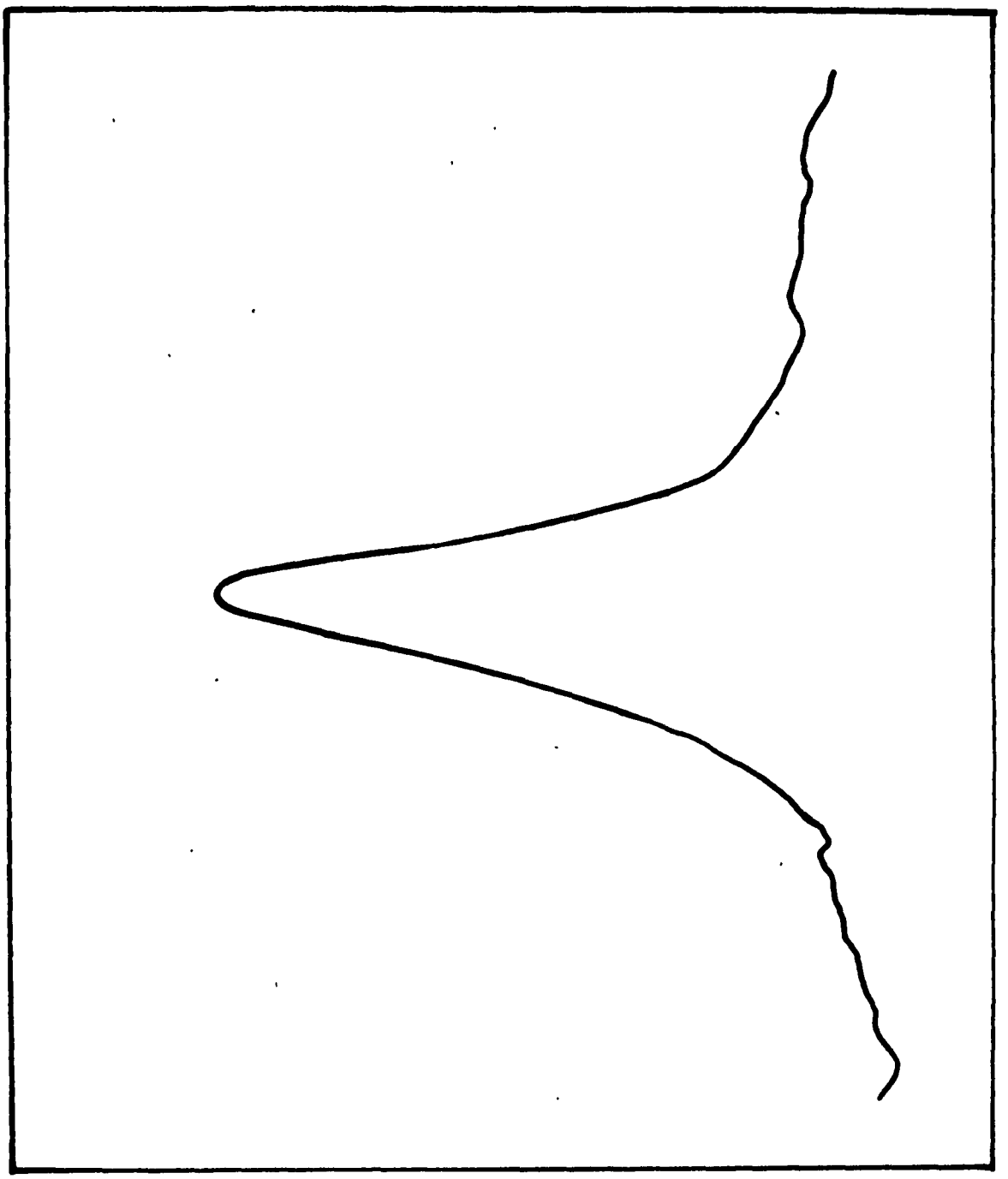

2. Using either of the detection methods, a signal proportional to the number of a single ion type could be measured as a function of storage time in the trap. The ions $_3He^+$, H_2^+, and H^+ were identified in the trap by taking the ratios of the rf voltages at which they were detected while holding the detection frequency constant. This method was used since the magnitude of the rf voltage could not be determined with great accuracy. The ion oscillation frequency is proportional to V_o/m so the rf voltage varies directly as the mass, for singly charged ions. $_3He^+$ was identified by increasing the background gas partial pressure of $_3He$ with a steady leak rate into the system. At constant storage time, with the electron pulse held constant in magnitude and duration below saturation, the $_3He^+$ signal increased relative to the other ion signals while the pressure increased, due to the increased creation rate.

Degeneracies in the charge to mass ratio occur for the ion pairs $_4He^{++}$ - H_2^+ and $_3He^+$ - H_3^+. Here the more abundant species will mask the presence of the other. Little $_4He^+$ was expected in the predominantly metal system, however, and no $_4He^+$ resonance was observed. The H_3^+ will only come from the reaction[29] $H_2^+ + H_2 \rightarrow H_3^+ + H$, so destroying the H_2^+ also eliminates the H_3^+.

3. The lifetime of the ions in the trap appeared to be unaffected by subharmonic excitation over broad detection frequency ranges in the band investigated, although the ion

lifetime did appear to be limited at the frequency ratios of $\Omega/\omega = 12$ and 21. The unstable frequency ranges were surprisingly narrow, since long term storage could be attained at only slightly different frequency ratios. This indicates that some other cause might have limited the observed lifetime. The existence and properties of instabilities in the operating range were not investigated in detail due to the interest in the long term storage properties of the trap.

Graphs of ion number versus storage time for $_3He^+$ and H^+ appear in Figures VI and VII. Other types of ions were removed from the trap during these measurements by varying the dc trap voltage to make certain charge to mass ratios unstable or by applying the appropriate resonant frequencies to throw out specific ion types. It was not convenient to operate the trap in a mode where only one ion type was stable due to the small ion number that could be trapped at low well depths. All such limited stability modes operate near the stability diagram border, where the well depth in one dimension is quite shallow.

The initial sharp drop in ion number for short times after ion creation shown for $_3He^+$ is typical for both ion species studied in detail. It is probably due in part to the increased pressure during this interval produced by outgassing of the trap electrodes by the electron pulse. The ion pump did not decrease the pressure to the base value as rapidly as might be desired.

Figure VI Decay of the $_3$He ion population for short times in the storage ring trap. The short term loss rate for protons is similar to the $_3$He ion results. The error bars indicate the standard deviation for an individual ion number determination made in similar circumstances.

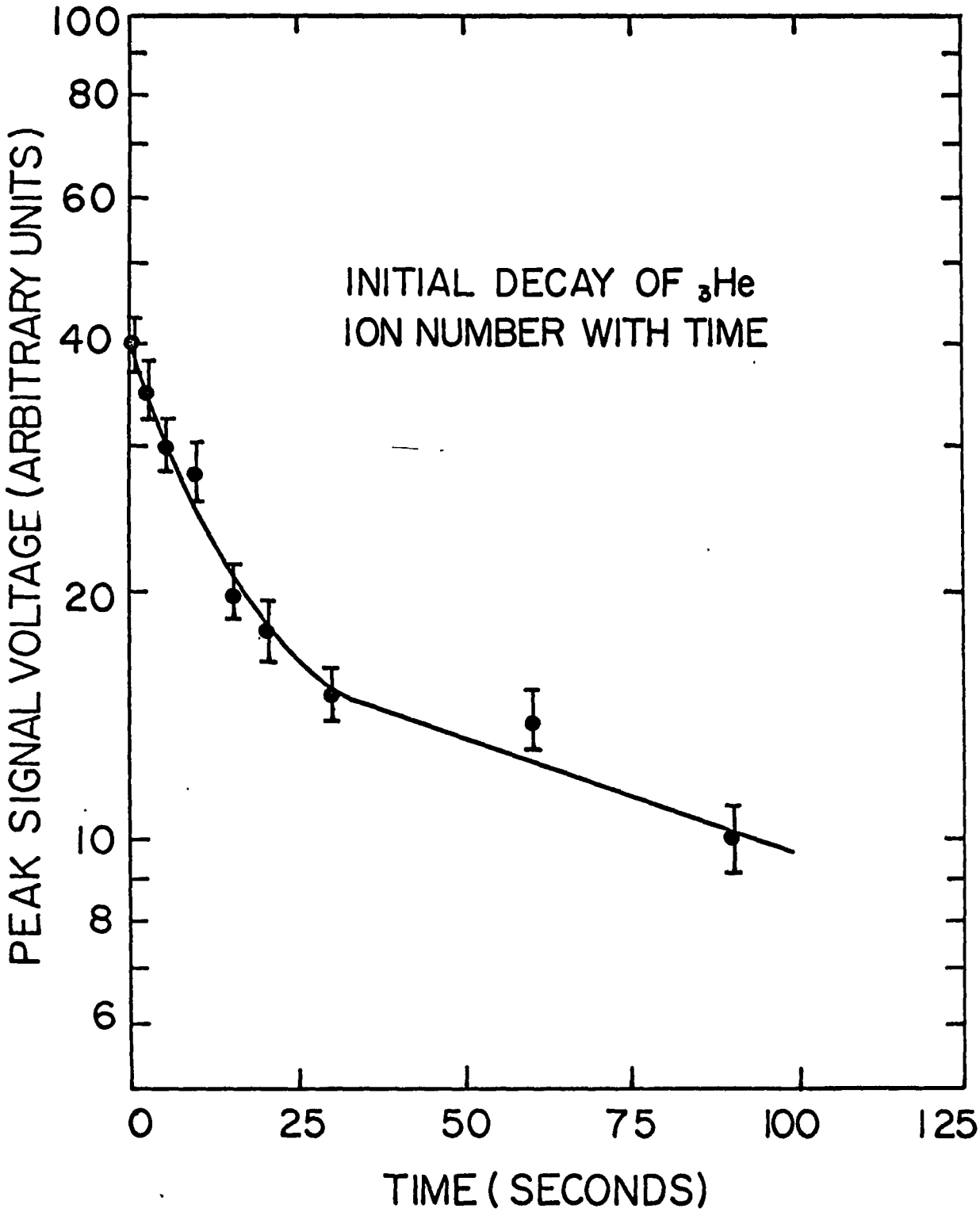
INITIAL DECAY OF ₃He
ION NUMBER WITH TIME
PEAK SIGNAL VOLTAGE (ARBITRARY UNITS)
100
80
60
40
20
10
8
6
0
25
50
75
100
125
TIME (SECONDS)

Figure VII Decay of the stored proton population in the circular storage ring trap for long time intervals at several pressures. The long term loss rate of $_3$He ions is similar to the proton results.

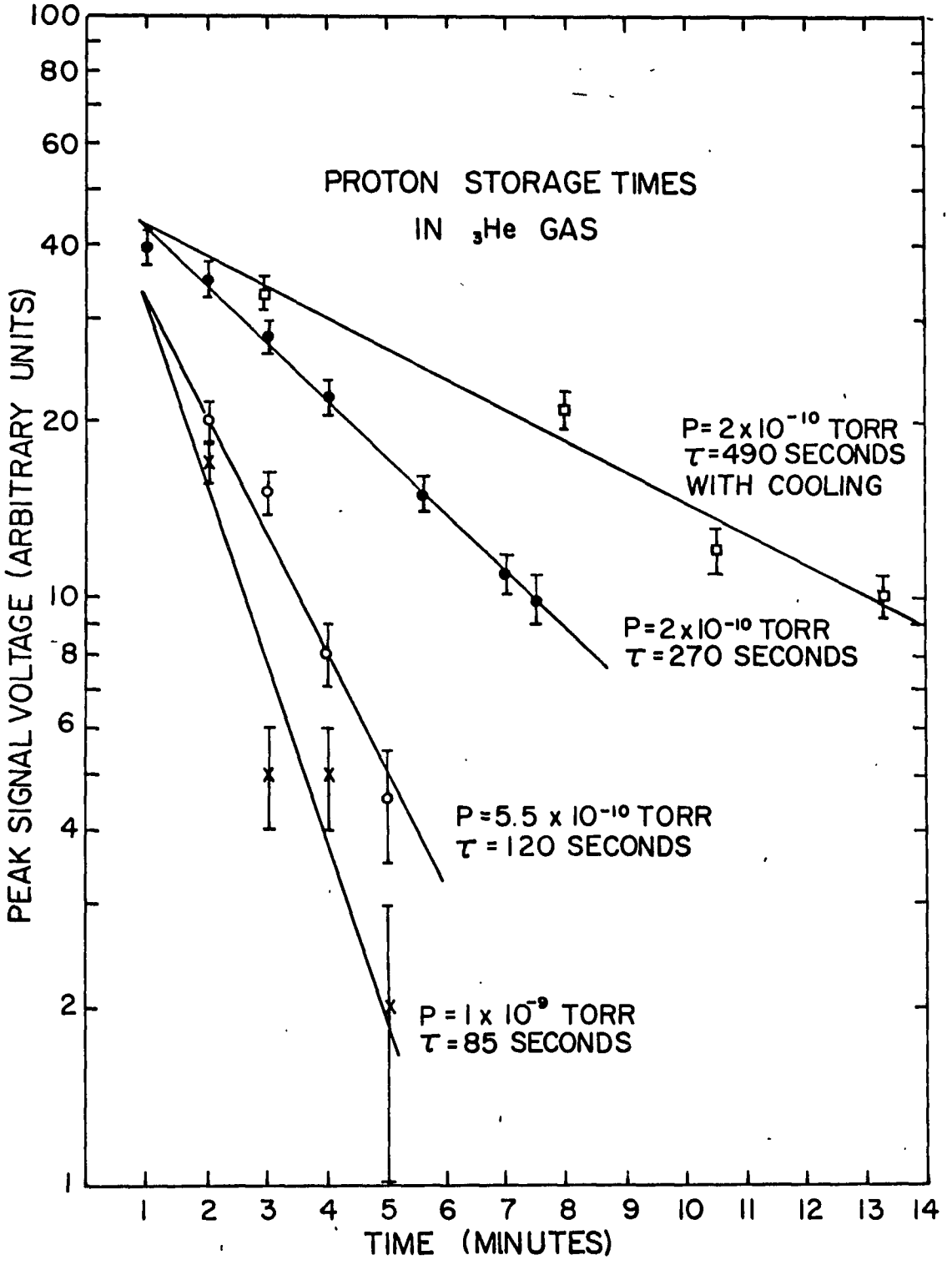
PROTON STORAGE TIMES
IN ₃He GAS
P= 2 x 10⁻¹⁰ TORR
τ=490 SECONDS
WITH COOLING
P=2 x 10⁻¹⁰ TORR
τ = 270 SECONDS
P=5.5 x 10⁻¹⁰ TORR
τ = 120 SECONDS
P = 1 x 10⁻⁹ TORR
τ = 85 SECONDS
PEAK SIGNAL VOLTAGE (ARBITRARY UNITS)
TIME (MINUTES)
100
80
60
40
20
10
8
6
4
2
1
1
2
3
4
5
6
7
8
9
10
11
12
13
14

This outgassing was reduced by about two orders of magnitude by electron bombardment heating, but could not be entirely eliminated. The pressure from outgassing rose to about 7×10^{-10} A during the pulse interval, and dropped to about 3×10^{-11} A in thirty seconds. The equilibrium pressure associated with each lifetime was measured at times long after this transient had vanished.

4. As indicated for protons in Figure VII, the ion number decay was exponential after the initial transient. The ion storage lifetime, defined as the time interval in which the stored ion number decreases by e^{-1}, is measured by the slope of this decay. The dependence of the proton lifetime on pressure was made by increasing the $_3$He background gas partial pressure with the leak. Figure VIII shows that the proton lifetime was inversely proportional to pressure in this situation. The high pressure point used is based on the adjusted measured lifetime of $_3He^+$ in $_3$He gas by Major.[10] The $_3He^+$ lifetime is about 2.5 times longer than the proton lifetime at the same pressure of $_3$He gas. This is in agreement with the predictions of Major and Dehmelt[2] for ion heating due to elastic collisions of ions with gas atoms in a radio-frequency electric field. Collisions with atoms heavier than the ion are expected to increase the ion energy on the average, producing a larger ion loss rate. Collisions with lighter atoms should have a cooling effect. Since equal mass collisions are not heating, the loss rate of $_3He^+$ is

Figure VIII Pressure dependence of the proton storage time constant T_B. The small departure from unity slope is within the limits set by the nonlinear sensitivity of the pressure gauge (reference 48).

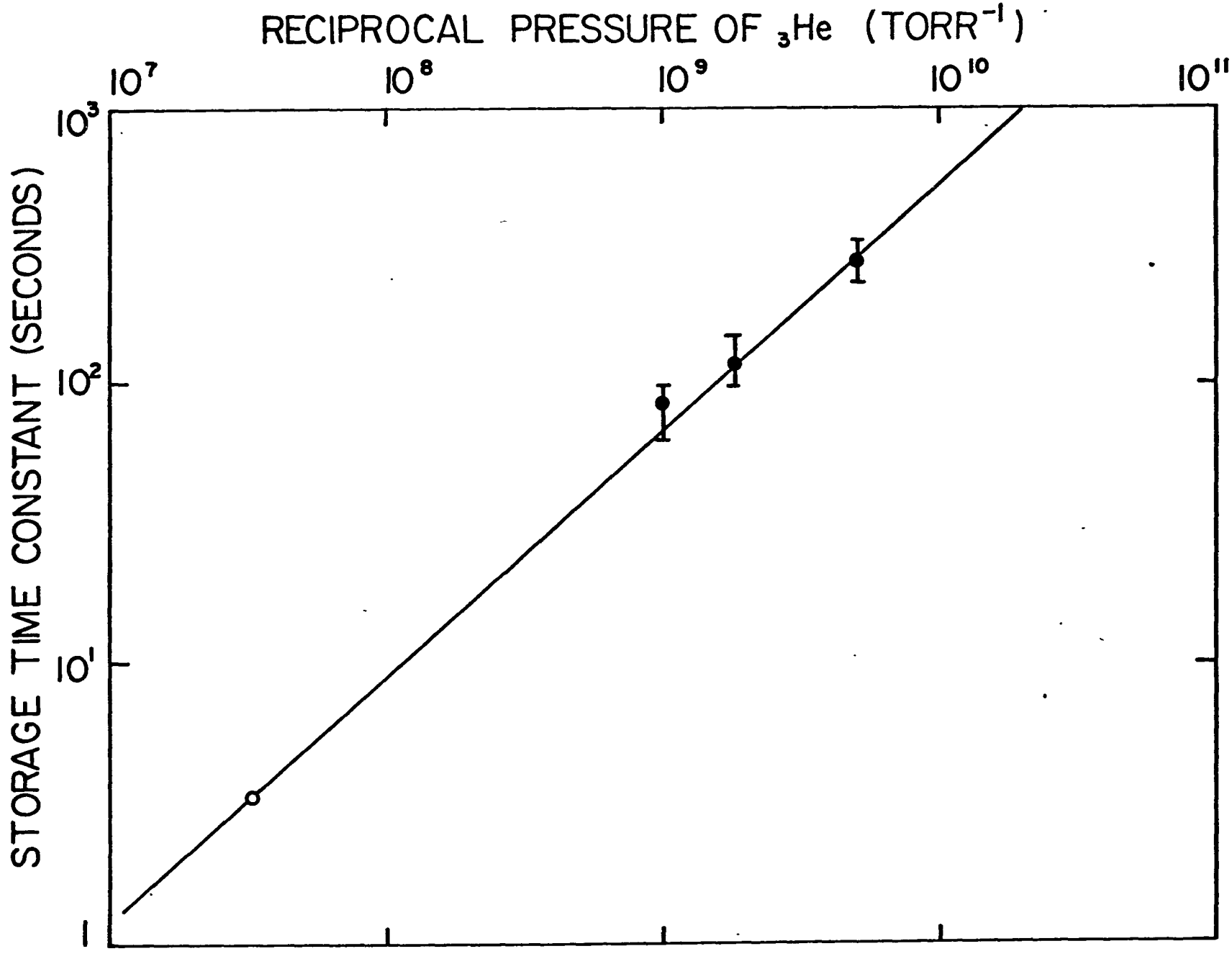
RECIPROCAL PRESSURE OF $_3$He (TORR^{-1})
10^7
10^8
10^9
10^{10}
10^{11}
STORAGE TIME CONSTANT (SECONDS)
10^3
10^2
10^1
1

presumably due to spin exchange heating or to collisions with other gas molecules.

5. The presence of the ions could also be detected by monitoring the detected noise signal from the tank circuit when no detection rf was applied. When the ions were tuned to resonance, the detected noise increased due to the voltage induced by the motion of the ions, as discussed in section II-2. The increase in tank circuit temperature is proportional to both ion number and temperature, equation II-7. If the heating rate of the ions is greater than the cooling rate, the measured tank circuit temperature above equilibrium will decrease as ions are lost. For the opposite case, the tank circuit temperature will decrease as the ion temperature decreases. A noise signal decrease proportional to the rate of ion loss was observed.

6. The effect of radiative cooling on the ion lifetime was determined by keying off the detection rf and storing the ions at the tank circuit resonance frequency. After a measured storage interval, the ions were detuned from resonance and the number detected in the normal manner with an rf pulse and dc ramp sweep. The effect of the radiative cooling on the proton lifetime at 2×10^{-10} Torr is shown in Figure VII. It is clear that the ions are gaining energy at too fast a rate to be cooled. To estimate the improvement in ion storage time or cooling time constant required,

we assume an exponential heating rate with time constant τ_h in equation II-5. When the ions are being cooled, the effective net heating time constant becomes $\tau_{he}^{-1} = \tau_h^{-1} - \tau_o^{-1}$. We now assume, and will justify later, that the ions distribute energy rapidly among their degrees of freedom, and can be assumed to be in thermal equilibrium. In this picture, the loss of ions due to energy input can be taken as the loss of the high energy tail from the distribution over the edge of the potential well. Each lost ion then carries the well depth energy eD. To maintain temperature equilibrium while a heating mechanism is operative, the rate of energy loss must equal the rate of energy input. When the ions are not cooled, the ions are lost with a time constant T_B, while with cooling this time constant becomes T_{BC}. Writing down the rate equilibrium conditions for the two cases of cooled and uncooled ions and taking the ratio, the heating time constant can be found in terms of the cooling time constant and the loss time constants, i.e. $\tau_h = \tau_o(1 - T_B/T_{BC})$. By calculation, $\tau_o = 190$ seconds, so $\tau_h = 90$ seconds, indicating a factor of three or four decrease in pressure was necessary. All attempts to reach these lower pressures failed.

7. The large magnitude of the cooling time constant is produced by two main causes: the large capacitance of the electrode structure and the linewidth of the ion oscillation frequency. The ion oscillation frequency depends on the electrode spacing along the arc of the trap, which is

determined by the machining and positioning accuracy. Assuming that the whole linewidth is due to errors of this type, an ion line Q of twenty gives a tolerance for each electrode of about 1.5×10^{-3} inches. This may be difficult to improve on, but the capacitance to be tuned out could be reduced by changing the rf voltage division ratio. Moreover, with a different biasing arrangement it might be possible to cool both oscillations of the ion motion simultaneously, reducing the time constant by a factor of two. Rather than pursue any such alternatives immediately, a small three-dimensional axially symmetric ion trap was constructed to demonstrate the cooling technique. This is discussed in the following sections.

It should be emphasized that the lack of success with ion cooling in no way detracts from the long term storage properties of the storage ring trap. These storage times demonstrate that moderate perturbations of the trap electrode structure do not produce fields that modify the ion motion substantially, or heat the ions in a manner that can not be overcome by the proper choice of operating parameters. The ion signal to noise ratios achieved compare quite well with those observed in the large axially symmetric traps used to date for spectroscopic purposes.

Some of the important properties of ion storage in the circular storage ring ion trap, both measured and derived, are summarized in Table I.

Table I Circular storage ring trap parameters

CIRCULAR STORAGE RING TRAP DATA

Field dimension $2x_o \approx 2y_o = 2r_o$	0.32 cm
Structure dimension 2R	14.3 cm
Ratio R/r_o	45/1
Storage volume $V = 2\pi^2 R r_o^2$	3.6 cm^3
Trapping rf frequency $\Omega/2\pi$	52 MHz
Trapping rf voltage for a 10 V well V_o	160 volts
Typical proton oscillation frequency $\omega/2\pi$	4.5 MHz
Proton well depth	10.6 volts
Typical $_3$He ion oscillation frequency $\omega/2\pi$	2.4 MHz
$_3$He ion well depth	9.0 volts
Calculated maximum ion number density n_{max}	6×10^8 cm^{-3}
Calculated maximum ion number N_{max}	2×10^9
Maximum measured ion density n	3×10^4 cm^{-3}
Maximum measured ion number N	10^5
Maximum proton storage time constant	490 seconds
Estimated proton cooling time constant $3\tau_{xo}$	190 seconds
Tank circuit capacitance	70 pF
Tank circuit Q_t	100
Ion resonance line Q_I	20
Estimated base pressure	2×10^{-10} Torr

VI CONCEPT AND DESIGN OF THE EXPERIMENT

1. The axially symmetric quadrupole ion trap,[9,10,22] shown schematically in Figure IX, was used to test the properties of very small trapping structures as well as demonstrate the ion cooling technique. The potential inside the electrodes ideally has the form

$$\phi(x,y,z,t) = z_o^{-2}(U_o + V_o \mathrm{Cos}\Omega t)(r^2/2 - z^2) \qquad \text{VI-1}$$

giving the equations of motion:

$$d^2z/dt^2 + \omega_z^2 z = 0 \qquad \omega_z = \left(\frac{2e^2V_o^2}{m^2\Omega^2 z_o^4} - \frac{2eU_o}{mz_o^2}\right)^{1/2} \qquad \text{VI-2}$$

$$d^2r/dt^2 + \omega_r^2 r = 0 \quad , \quad \omega_r = \left(\frac{e^2V_o^2}{2m^2\Omega^2 z_o^4} + \frac{eU_o}{mz_o^2}\right)^{1/2}$$

For $U_o = 0$, $\omega_r = \omega_z/2$ for this trap, and for equal well depths in the r and z dimensions, $\omega_r = \omega_z/2^{1/2}$.

2. To make the cooling time constant conveniently short, the dimensions of the trap were chosen to be the same as in the storage ring; $2z_o = 0.125$ inches. This makes the trap a factor of twenty smaller than the one used in the $_3He^+$ hfs measurement.[2] In principle, the small size should not severely limit the storage capacity of the trap.[14] The space charge repulsion of the ions produces a repulsive potential

which effectively decreases the depth of the well in which the ions move. For charges at rest, the well would be completely filled when the pseudopotential is exactly balanced by the repulsive potential generated by the space charge. Under these circumstances, $n_{max} = 3D_z\varepsilon_o/ez_o^2$ so the maximum ion number $N_{max} = 8\pi\varepsilon_o D_z z_o/e$ and decreases only linearly with z_o. Estimated values for maximum ion number and charge density are given in Table II.

The motion of the ions in the trap will cause the ion number N in the trap to be much less than N_{max}. However, as the ions are cooled off, the charge cloud will collapse until the maximum density situation discussed above is approached in a limited region of the trap volume. The energy depth D_q of this minimum volume situation for N ions at rest has been shown to be[14] $D_q/D = (N/N_{max})^{2/3}$. VI-3 Ions cooled to this limit will still possess a micromotion due to the electric field even if the temperature of the motion in the pseudowell is negligible. This will set a lower limit on the Doppler linewidth which can be attained for a given ion number and again emphasizes the value of a storage ring configuration in which a larger number of ions can be stored along the length of the arc.

3. The Coulomb ion-ion elastic scattering interaction results in the distribution of the ion energy among the different motional coordinates even when the ion-gas collision rate becomes negligible at low pressures. A characteristic

relaxation time to an equilibrium distribution for a uniform plasma is the Spitzer time[30,14]

$$t_{II} = 7.8 \times 10^{6} A^{1/2} (kT/e)^{3/2} n^{-1} Z^{-4} (\ln\Lambda)^{-1} \text{ seconds} \qquad \text{VI-4}$$

for n ions/cm^3 with mass number A, charge Ze, and temperature T. Λ is the ratio of the Coulomb interaction cutoff distance to the distance of closest approach in a collision. The Coulomb shielding distance in a plasma is produced by charge of the opposite sign from the ions of interest, and so does not exist for a single type of ion in the trap. The ions induce charge of the opposite sign on the trap electrodes, however, and since the trap structure acts as a shield from external charge, the trap radius is taken as analogous to the Coulomb cutoff distance in the following calculations. This assumption makes $\ln\Lambda \approx 20$.

4. An analysis of the establishment of equilibrium in an ion trap by Coulomb elastic scattering has been made by Dehmelt.[14] A time constant for ion loss from the trap was obtained, which can be written

$$T_B = \frac{25.76 \times 10^{5} (D)^{3/2} z_o^{3}}{N} (kT/eD)^{2} \exp(eD/kT) \qquad \text{VI-5}$$

for protons, where T is the ion temperature and D is the well depth. D is in volts, while z_o is in centimeters. The derivation is based on the exchange of energy among the ions via ion-ion collisions, which establish an equilibrium

distribution in the well. The high energy tail of this distribution "evaporates" from the well, and the rate at which hot ions in the tail are replenished gives the temperature and well depth dependence in the ion loss time constant T_B. It is clear that a small decrease in ion temperature produced by cooling should make a substantial change in the ion loss rate. Stored ion loss rates with a dependence on ion number similar to that derived have been observed.[31]

VII APPARATUS FOR ION COOLING

1. During the completion of the storage ring measurements an entirely different apparatus was constructed to demonstrate the ion cooling technique. The goal of the construction was to produce a small, clean surfaced, non-magnetic trap which would allow long term ion storage. A small vacuum system which could reach low pressures was also constructed.

The vacuum system had a volume of about one liter. The metal portion of the vacuum shell was constructed from one and one half inch outer diameter #304 stainless steel tubing while the glass portion, shown schematically in Figure IX, was constructed from Corning 7740 Pyrex glass, except for the region of the tungsten rod seals. The glass to metal joint was a stainless steel to Pyrex Housekeeper seal. All flanged joints were made with Varian Conflat flanges and OFHC copper gaskets except the joint between the General Electric TDG and the system, where one Varian and one General Electric flange were used. The mismatch produced no sealing problems.

A 15 liter/second Varian Vac-Ion pump evacuated the system and the pressure was monitored with a TDG as before. The pump and glass section were mounted on the parallel arms of a metal "T" while the discharge gauge was mounted on the perpendicular arm. Three 0.060 inch diameter tungsten rods sealed in each of two stems provided the support

Figure IX Axially symmetric quadrupole ion trap and glass portion of the vacuum system.

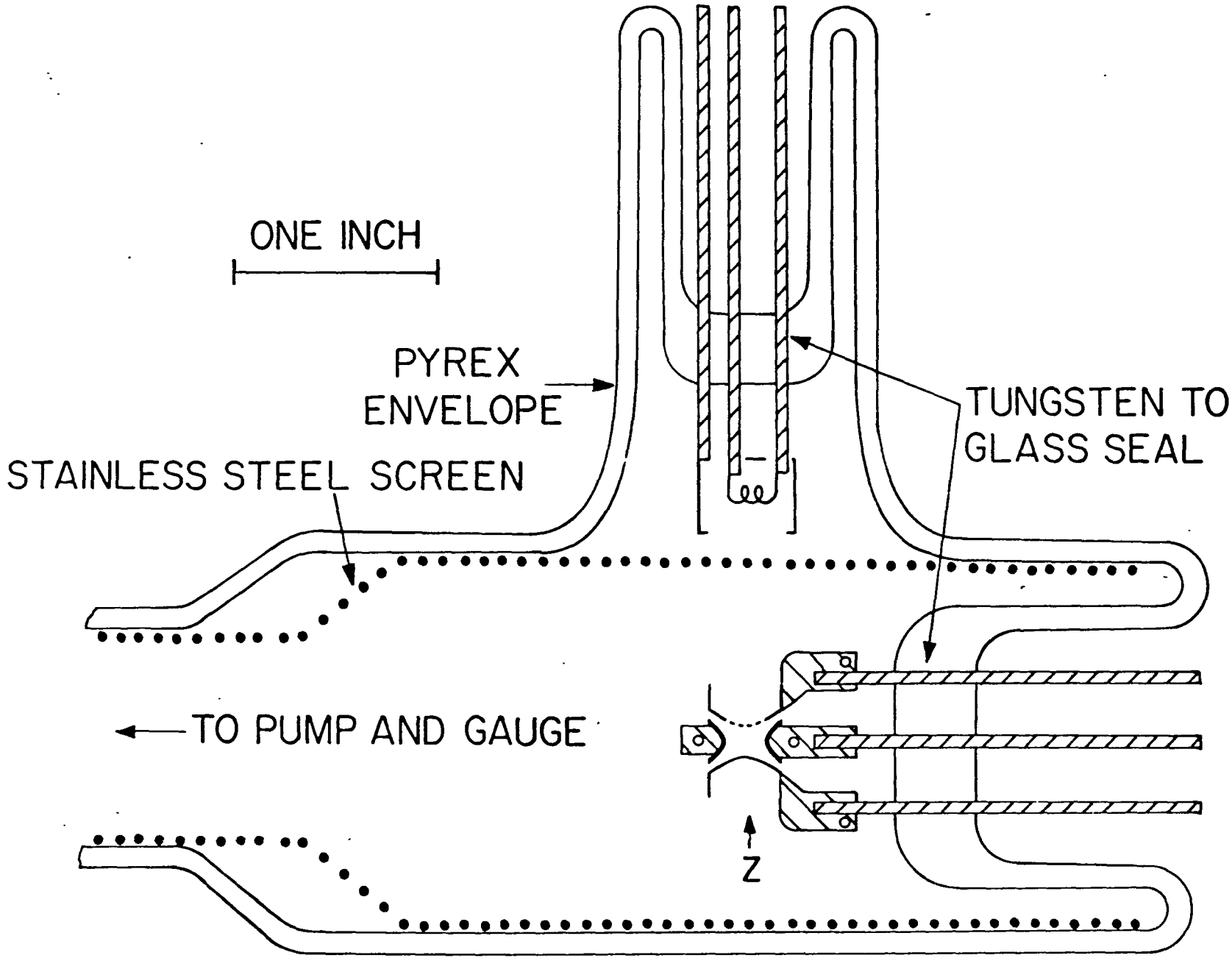
ONE INCH
PYREX
ENVELOPE
STAINLESS STEEL SCREEN
TUNGSTEN TO
GLASS SEAL
TO PUMP AND GAUGE
Z

and electrical connections for the ion trap and electron gun. A cylinder of stainless steel screen inside the glass tube acted as an electrostatic shield and provided a conduction path for surface charges that might form on the glass walls. The screen acted also as an accelerating grid for the ionizing electrons. The screen was resistance welded to the metal portion of the system.

To facilitate replacement in case of failure, the electron gun was installed as a unit on a stem perpendicular to the symmetry axis of the tube. The filament was five centimeters of 0.008 inch diameter tungsten wire closely wound in a helix of about one centimeter length. The ends of the filament were resistance welded to strips of Advance metal, which in turn were resistance welded to the tungsten electrodes in the seal. The third electrode supported a molybdenum Wehnelt cylinder used to control the electron beam. By choosing the correct voltages for the filament and Wehnelt cylinder with respect to the grounded screen, a slight focusing action could be obtained. Prior to installation the filament was heated to 2600 degrees C for thirty minutes in a vacuum bell jar to stabilize the tungsten crystal structure and outgas the tungsten.[32]

2. The method of mounting the ion trap electrode system is shown schematically in Figure IX. The electodes are equipotentials of $(r^2/2 - z^2) =$ constant out to a radius $2z_o$ from the symmetry axis. Specially ground tools were used

to form the ring electrode from 0.030 inch thick gold sheet, while the end caps were formed from 0.020 inch thick gold sheet. It was necessary to anneal the gold frequently with a hydrogen flame to prevent tearing due to work hardening. In one end cap approximately one hundred 0.006 inch diameter holes were drilled to serve as ducts for the electron beam. It was necessary to use paraffin as a support for the end cap during the drilling procedure to prevent the pivot drills from tearing the gold. As a final step the gold electrodes were polished with Jewelers Rouge which was then dissolved with HCL. The electrodes were then carefully cleaned and examined under a one hundred power microscope. No trace of the polishing agent could be observed embedded in the gold.

The ring electrode was tightly clamped to the tungsten rod by an OFHC copper clamp machined to a close fit with the outside surface of the electrode. The clamp was bolted together with #316 stainless steel screws with lock washers to maintain tension. As usual, all screw threads were slotted to prevent virtual leaks due to trapped gas. Each end cap electrode of the trap was clamped by a molybdenum ring, which was also held together by a stainless steel screw assembly. An extension on this ring was resistance welded to the appropriate tungsten rod using Advance metal for filler. The molybdenum ring was also resistance welded directly to the gold end cap in several spots. The electrodes were held in position by a jig to about 0.001 inch while being mounted.

The two stems holding the trap and electron gun were sealed to the glass cylinder on the glass to metal seal while a non-explosive mixture of 15-per cent H_2 and 85 per cent argon was passed through the tube to inhibit oxidation. The flange on the glass section was then bolted to the previously assembled metal portion of the system, which was evacuated and baked with the technique discussed in Appendix I. After the system had cooled, each trap electrode was heated by electron bombardment to a dull red color, and the stainless steel screen was outgassed at the same temperature with a Lepel induction heater. Some distortion of the end caps due to the relaxation of residual stresses in the molybdenum clamps was observed after this outgassing procedure. The system was then rebaked to bring the pressure down again, and the electrodes were outgassed again by the same method. Despite these precautions the TDG still indicated a current of 5×10^{-10} A when the trap was bombarded by 5 mA of 450 volt electrons. The pressure dropped rapidly into the 10^{-11} range when this bombardment ceased, however.

After the completion of most of the measurements to be described, the system was disassembled and the ring electrode was found to have rotated about its support by an angle of about five and one half degrees, apparently during the second outgassing procedure. This perturbation would appear to lift the degeneracy of the x and y dimensions in the trap as well as generate additional field nonlinearities. To determine the effect of this perturbation, the electrode was ro-

tated back into place and many of the measurements were repeated, as discussed in section VIII-8. The distortions in the end electrodes could not be corrected.

3. The use of a sensitive detection circuit and large voltages at high frequencies made good shielding essential. The goal of the system layout was physical and electrical symmetry and the avoidance of ground loops. Two large aluminum chassis, each four inches deep, were clamped together back to back. A section of the back of each was sawed out to enclose the glass portion of the vacuum system with the ground plane along the symmetry axis of the tube. The rf circuits at Ω were installed with their own ground plate on one side of this ground plane, while the ion detection circuits at ω were placed on the other side. The axes of the coils of these circuits were orthogonal to reduce inductive coupling. The glass portion of the vacuum system was wrapped in brass shim stock which was grounded at the symmetry point taken as the basic ground point of the system. The layout of the circuit components inside the shield is shown in Figures XI-(a) and (b). Whenever possible, filters in external shields were installed on the electrical inputs to the shielded box.

A simplified block diagram of the electronics, including bias and detection circuits, is shown in Figure X. The ion trap bias electronics are similar to those used for the storage ring, but the frequency $\Omega/2\pi$ = 146 MHz was used.

Figure X Block diagram of the electronic apparatus used in the ion cooling measurements.

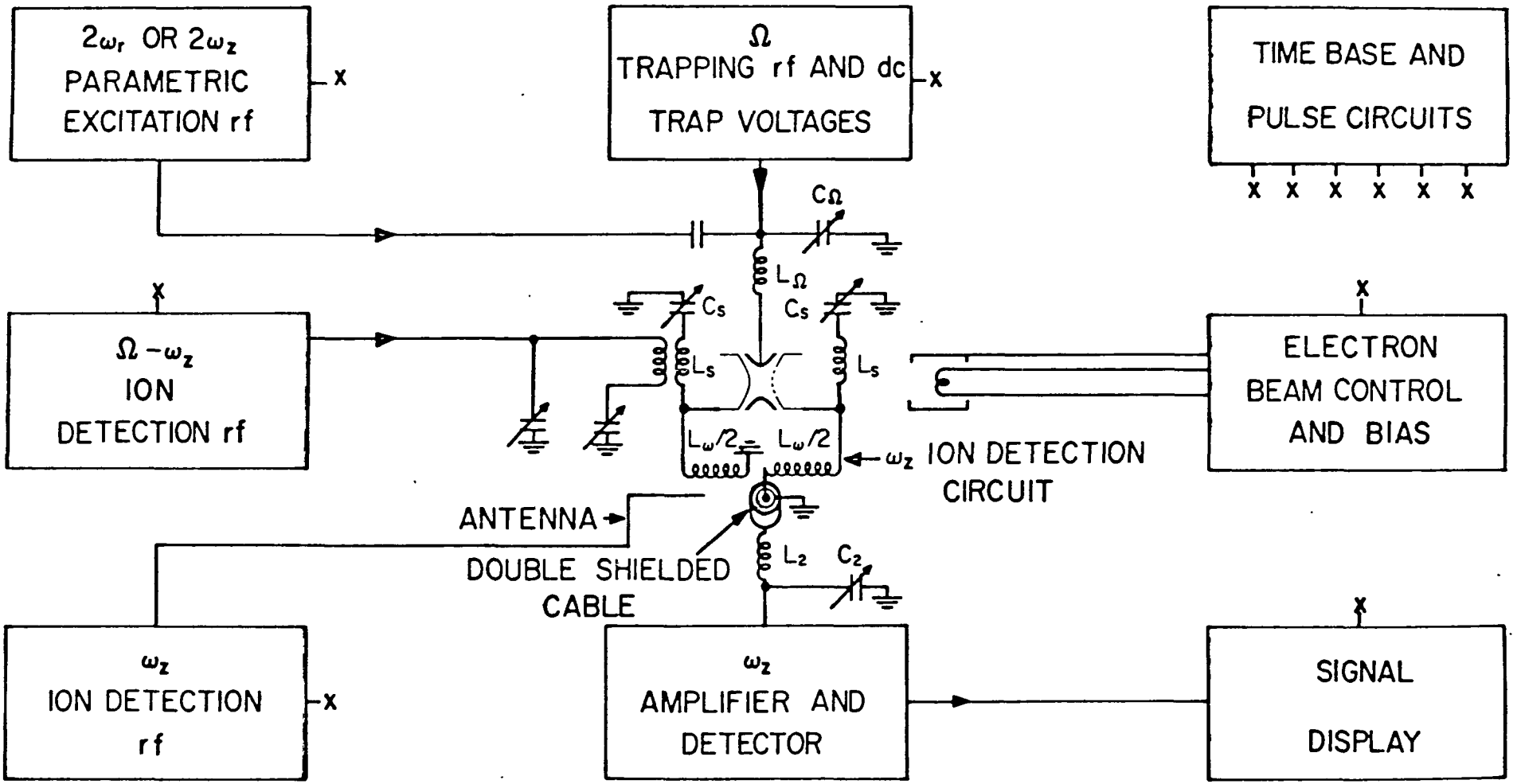
$2\omega_r$ OR $2\omega_z$
PARAMETRIC
EXCITATION rf
x
Ω
TRAPPING rf AND dc
TRAP VOLTAGES
x
TIME BASE AND
PULSE CIRCUITS
x x x x x x
C_Ω
L_Ω
C_s
C_s
L_s
L_s
$L_\omega/2$
$L_\omega/2$
ω_z ION DETECTION
CIRCUIT
x
$\Omega - \omega_z$
ION
DETECTION rf
x
ELECTRON
BEAM CONTROL
AND BIAS
ANTENNA
DOUBLE SHIELDED
CABLE
L_2
C_2
ω_z
ION DETECTION
rf
x
ω_z
AMPLIFIER AND
DETECTOR
x
SIGNAL
DISPLAY

Figure XI-(a) Block diagram layout of Ω - rf trapping circuits. The shunts L_s, C_s ground the end caps at Ω , while the voltage on the ring electrode is stepped up by the pi network C_Ω , L_Ω .

Figure XI-(b) Block diagram of trapping rf and ω_z detection circuit layout seen looking from the ion trap. Access to the circuits was from either the top or bottom as shown in the diagram.

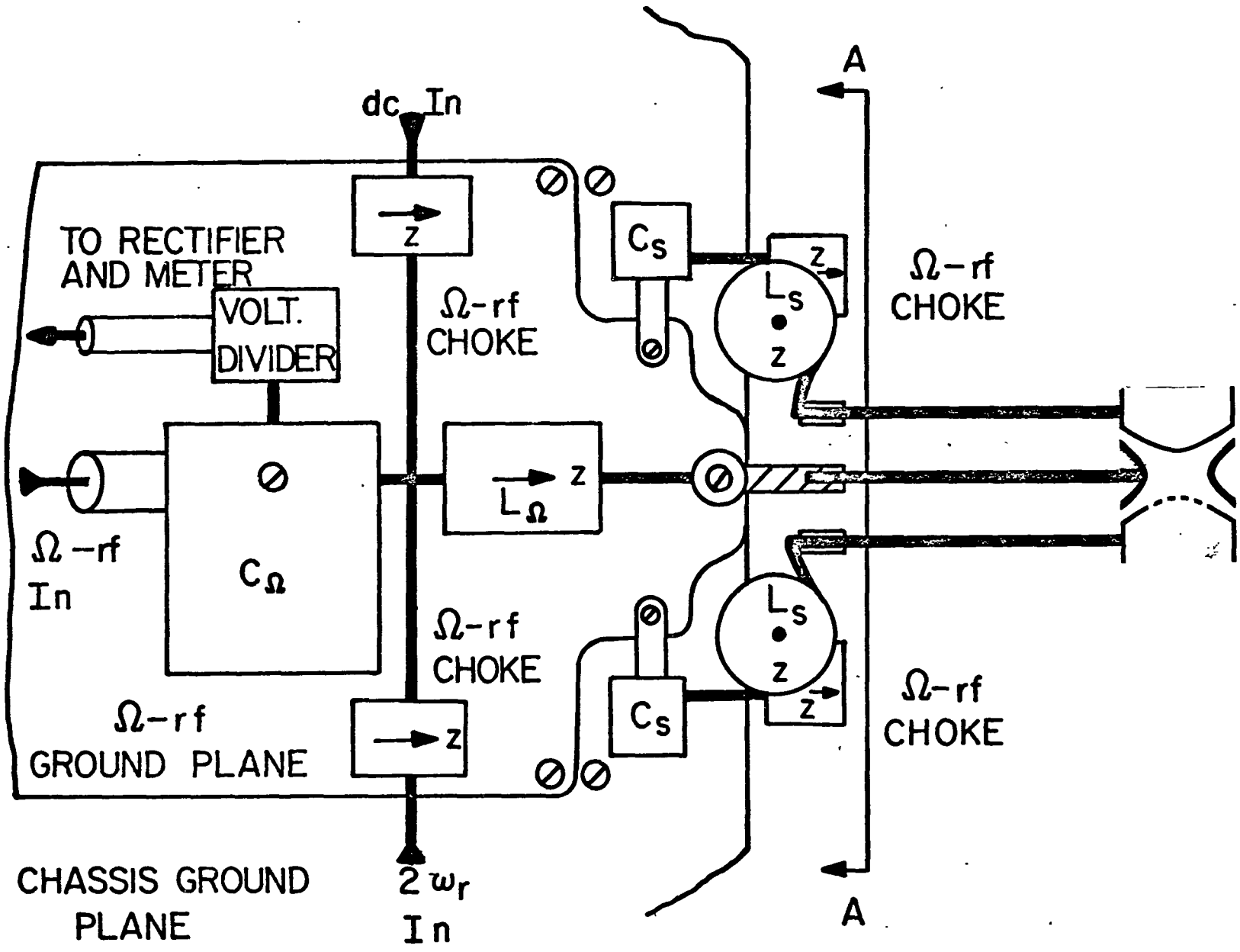
dc In
A
TO RECTIFIER
AND METER
VOLT.
DIVIDER
z
Ω-rf
CHOKE
Cs
Ls
z
z
Ω-rf
CHOKE
z
LΩ
Ω-rf
In
CΩ
Ls
z
z
Cs
Ω-rf
CHOKE
Ω-rf
GROUND PLANE
z
CHASSIS GROUND
PLANE
2 ωr
In
A

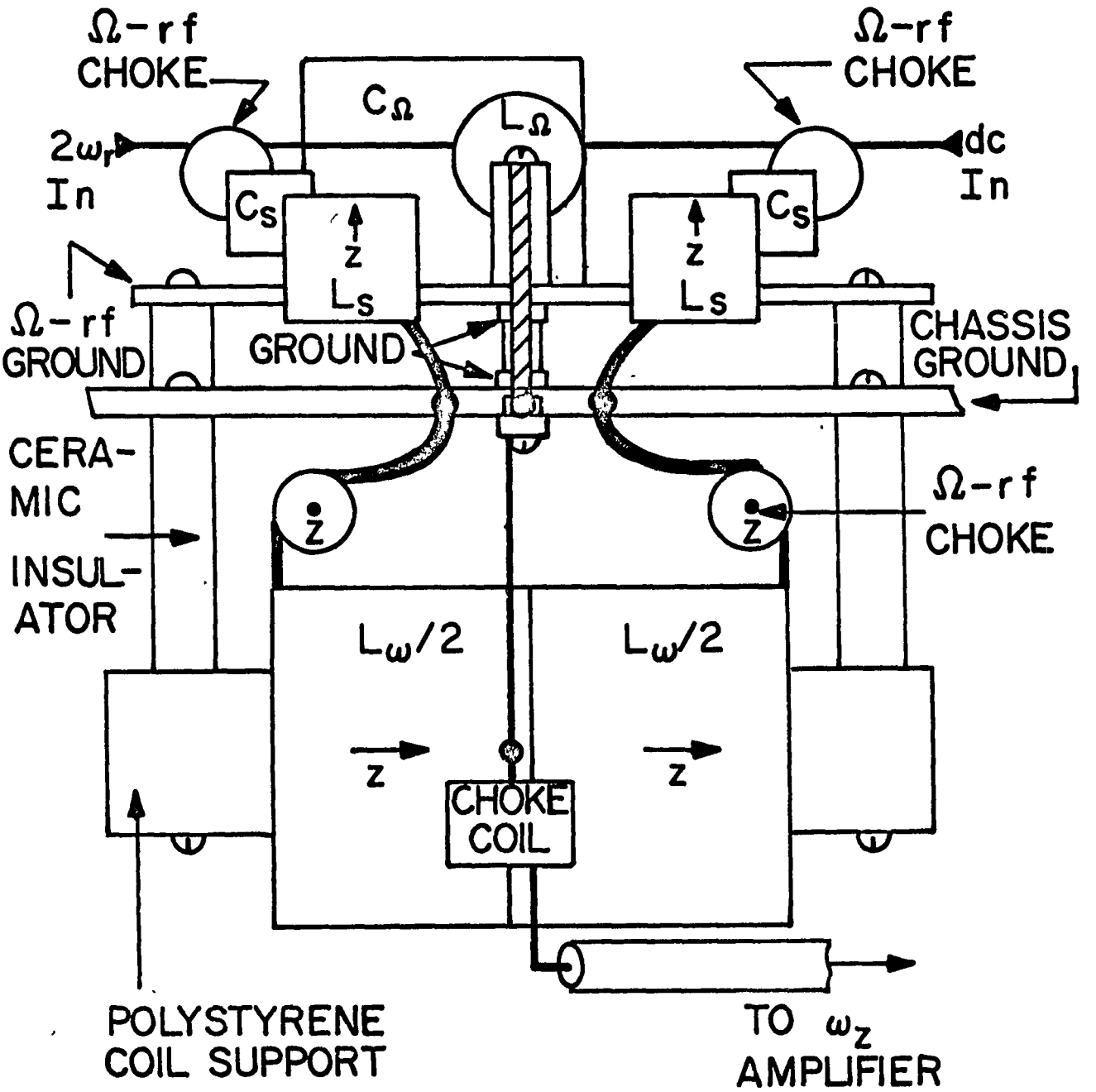
Ω-rf CHOKE
Ω-rf CHOKE
C_Ω
L_Ω
$2\omega_r$ In
dc In
C_s
C_s
z
L_s
z
L_s
Ω-rf GROUND
GROUND
CHASSIS GROUND
CERA-MIC INSUL-ATOR
Ω-rf CHOKE
z
z
$L_\omega/2$
$L_\omega/2$
z
z
CHOKE COIL
POLYSTYRENE COIL SUPPORT
TO ω_z AMPLIFIER

Ω was generated by a General Radio 1215-B unit oscillator, amplified by a Boonton 230A linear amplifier to a few watts, and then re-amplified by a Gonset 2 meter linear amplifier. The output of the Gonset was passed through a λ/2 filter with a loaded Q of 200 and was then stepped up by a pi network. The ring electrode of the trap acted as the final capacitor for the pi. The Q of the pi was spoiled by constructing the coil from Nichrome wire, to dissipate the amplifier power and keep the rf voltage from changing substantially when the ionizing electron current reached the ring electrode. Forced air blown on the coil kept it below red heat. The input voltage to the pi was sampled by a capacitive divider and converted to dc by a peak reading diode. The dc voltage was filtered and then bucked out with a mercury reference cell. The difference voltage was amplified by a Nexus SQ-10a operational amplifier and was then applied to the cathode modulation input of the General Radio oscillator with a high current emitter follower. The loop gain of the feedback circuit was set at ten, which reduced the hum on the rf voltage to 0.1 per cent. The narrow locking range of this circuit was its major disadvantage.

The dc bias on the ring electrode of the trap was produced by the circuit discussed in section IV-4.

Several ion detection circuits were used in the course of this work. One of the two ultimately employed appears in Figure X. The values of the circuit components are given

in the text.

Taking the capacitance from the ring electrode of the trap to one end cap as C_1, the pi network comprised of C_Ω, L_Ω, and $2C_1$, tuned to the frequency Ω, is the rf biasing circuit just described. Both end caps of the trap are at virtual ground at the frequency Ω as C_s is tuned to resonate L_s at this frequency. This had the advantage of reducing the high frequency rf voltage across the coil L_ω as well as diminishing the load on the rf pi network produced by the ionizing electrons striking the end caps. At the ion oscillation frequency ω the reactances of L_Ω and C_Ω are small, so the ring electrode of the trap is a virtual ground at this frequency.

The remainder of the circuit is the high impedance ion detection circuit tuned to the ion oscillation frequency ω. Neglecting L_s, the two coil halves $L_\omega/2$ in series resonate the effective capacitance $C_t = (C_1 + C_s)/2$. The input to the double shielded cable is a low impedance point, since L_2 resonates C_2 at ω. C_2 is in part made up of the amplifier input capacitance. Finally, to prevent each half of the circuit from resonating separately, they were coupled by the mutual inductance of each $L_\omega/2$ and by the small direct capacitance from one end cap of the trap to the other. This ion detection circuit acts as a step-down pi network which couples the voltage across the trap end caps to the high impedance input of a low noise amplifier.

It is desirable to make C_t small, since the capacitance limits the impedance used to damp the ion motion. This is done by reducing C_s which in practice was made comparable to C_1 . Stray capacity and the self-capacity of the coil L_ω raised the total capacitance of the circuit resonant at ω to about seven pF. The capacitance C_2 was chosen to make the Johnson noise of the tank circuit much greater than the noise generated by the amplifier in a comparable bandwidth, while keeping the amplifier input impedance from loading the tank circuit. The amplifier can be physically separated from the trap as long as the double shielded cable is short compared to a quarter wavelength at the frequency ω . A further advantage is the reduction of the rf voltage at Ω by the divider composed of $L_\omega/2$ and the cable capacitance. Despite these precautions, it was necessary to insert a voltage divider circuit with a high impedance at Ω in series with the double shielded cable to further decrease the high frequency voltage at the amplifier input. Rectification of this voltage, which generated noise at ω and interfered with ion detection, made this precaution necessary. The approximate experimental values for the circuit components used at 4.4 MHz were $C_1 \approx C_s \approx 3$ pF, $L_\Omega \approx L_s \approx 0.2\mu$H, $C_\Omega = 100$ pF, $C_2 \approx 45$ pF and $L_2 \approx 30\mu$H . The dc connection to ground for the floating end cap was provided by a choke to ground across the cable input, not shown in Figure X.

The circuit just described does suffer from the disadvantage that the tuning of the Ω shunt circuits L_s , C_s may be fairly critical, and non-uniform coupling between the several coils due to small asymmetries in circuit layout may occur. The second circuit used after trap resymmetrization was identical with the first, except that the Ω shunts were replaced by gang tuned butterfly capacitors C_s , C_s^1 so arranged that a positive increment of capacitance on one was matched by an equal negative increment on the other, preserving circuit symmetry and tuning while the rf voltage appearing on the end caps could be varied to measure the sensitivity of the trap to this type of well distortion.

The ion detection amplifier circuit was the same as that discussed in section IV-4. The detection diode was operated in the linear region for all types of measurements as the diode response to low level inputs was not strictly square law. The coherent ion number signal was displayed on an oscilloscope as before but to measure the tank circuit noise temperature the detected voltage was passed through an FET source follower to provide a low impedance for a variable time constant circuit and the Varian G-10 strip-chart recorder. Alternatively the difference between the detected voltage and a mercury reference cell was amplified by a Nexus SQ-10a operational amplifier for an analog input to the multi-channel analyzer system, which consisted of a Vidar 241 voltage to frequency convertor, a Dymec 222A pulse shaper, and the RIDL 24-2 memory.

The voltage to detect the ions by the sideband excitation method was generated by a General Radio 1215-B unit oscillator at $\Omega-\omega$. The voltage was passed through a single stage grounded grid rf amplifier which could be keyed on and off by a plate circuit relay driven by a voltage gate. This allowed the rf voltage to be pulsed on only during the detection sweep of the dc voltage. The voltage was then amplified by a Boonton 230A linear amplifier and coupled through a four stage high pass filter to a pi network matched to the transmission line. The coil of this pi was coupled inductively to one of the coils L_s , causing a voltage to appear across the trap end caps. Most of the ion number measurements were made by the absorption method.

The parametric heating circuit was used to excite the ions at twice the oscillation frequency in either coordinate direction. The voltage produced by another GR unit oscillator was coupled to the ring electrode of the trap through a gate controlled diode switch. Both pulsed and continuous excitation were used.

The timing circuits have already been discussed in section IV-4. The filament circuit is also the same used in the storage ring measurements, except for the bias voltages. A negative bias of 370 volts on the filament allowed temperature limited electron flow while minus 1100 volts on the control electrode cut it off.

VIII EXPERIMENTAL PROCEDURE AND RESULTS

1. After the vacuum processing was completed, the temperature limited emission from the filament was measured as a function of the current heating the filament by collecting the electrons with the focusing electrode. Following this, the fraction of the emission current reaching the far trap electrode was determined to estimate the number of electrons passing through the trap. About two per cent of the total current reached the far end cap. The bias on the focusing electrode necessary to cut off electron flow was also found.

For sufficiently long ion lifetimes, both a large electron current and a long pulse length appeared to be desirable for producing large ion signals. For a given pulse length of five seconds, the ion number increased linearly with emission current up to about eight mA. The number continued to increase with further current increases, but at a slower rate. This may be due to ion lifetime limitations produced by gas generated from the electrodes during the electron pulse. Assuming the evolved gas to be hydrogen, the pressure during the pulse approached 10^{-8} Torr. About 10^{7} ions should have been produced in the trap by such an electron pulse.

The detection of ion number by absorption and sideband excitation was performed in the manner discussed in section V-1. In a trap with a short ion cooling time constant

the number dependent damping time τ_{zt}/N that appears in the ion detection theory of Major and Dehmelt[2] when the ions are excited coherently can no longer be neglected. This time can easily become comparable to the detection sweep time for large N. Signal instabilities observed with long sweep intervals were removed by decreasing the detection sweep time. A symmetric signal could be obtained, as Figure XII-(a) shows for about 3×10^3 ions observed with a sweep duration of five msec. The ion signal was quite broad, having a Q close to twenty. The Q was measured by sweeping the dc voltage linearly and measuring the voltages at which the signal dropped to $2^{-1/2}$ of the maximum amplitude. Using the expression for ω_z given in equation VI-2, $Q_i = \omega/\Delta\omega = 2D_z/\Delta V$. Experimentally, $D_z \approx 10.4$ V while $\Delta V \approx 1$ V. A ten volt well was used in most measurements as this is typical for well depths in ion spectroscopy experiments.

The identification of the ions as protons was based on comparison of the measured trapping rf voltage with the theoretical value, measurement of the dc voltages at which the ions were lost from the well, and the observation of a large, short-lived ion signal at twice the rf voltage of the signal of interest. The properties of this higher voltage signal were characteristic of H_2^+ .

2. The dependence of the proton number on storage time was determined with the method used in the storage ring trap. Figure XIII shows the decrease of ion number with time both

Figure XII-(a) Oscilloscope trace of the ion number signal. The ions were excited at $\Omega-\omega_z$ and detected at the frequency ω_z . A 5 millisecond sawtooth sweep of the dc voltage was used. About 3×10^3 ions were detected.

Figure XII-(b) Oscilloscope trace of the detected ion noise signal decrease produced by ion cooling. The ion number is constant. The ion oscillation frequency was tuned to the tank circuit resonance frequency at t_o . The integration time constant was about two seconds.

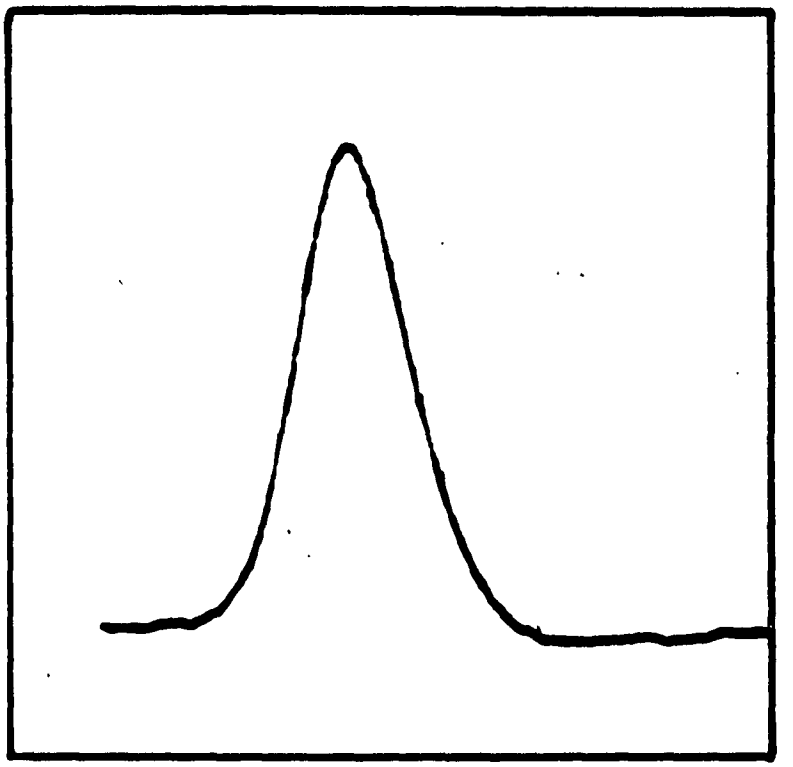

(a)

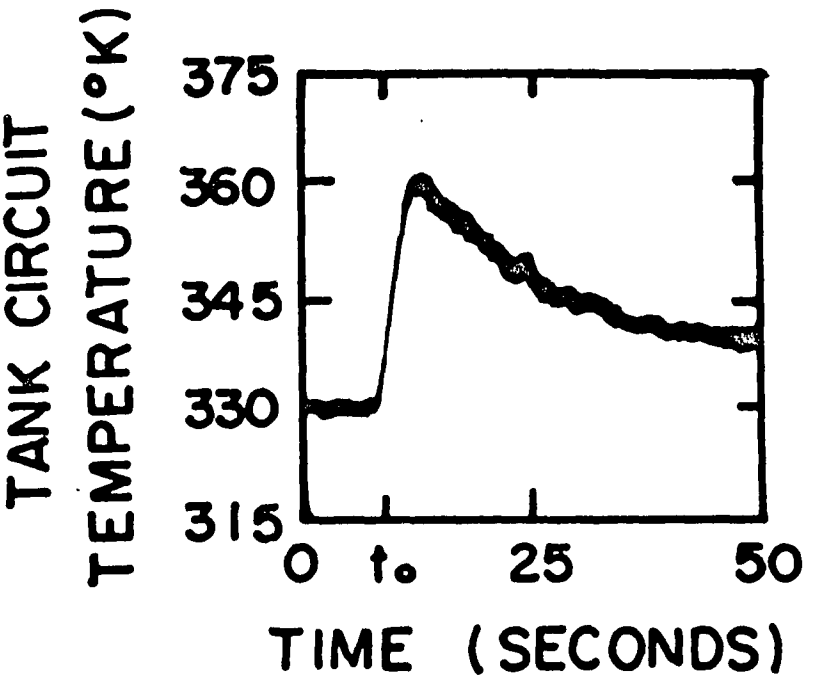
TANK CIRCUIT TEMPERATURE (°K)
375
360
345
330
315
0
t_o
25
50
TIME (SECONDS)

(b)

Figure XIII Decay of the proton population in the axially symmetric ion trap. The rapid decay occurs when the ions are not cooled, while the long time constant decrease was measured with cooled ions.

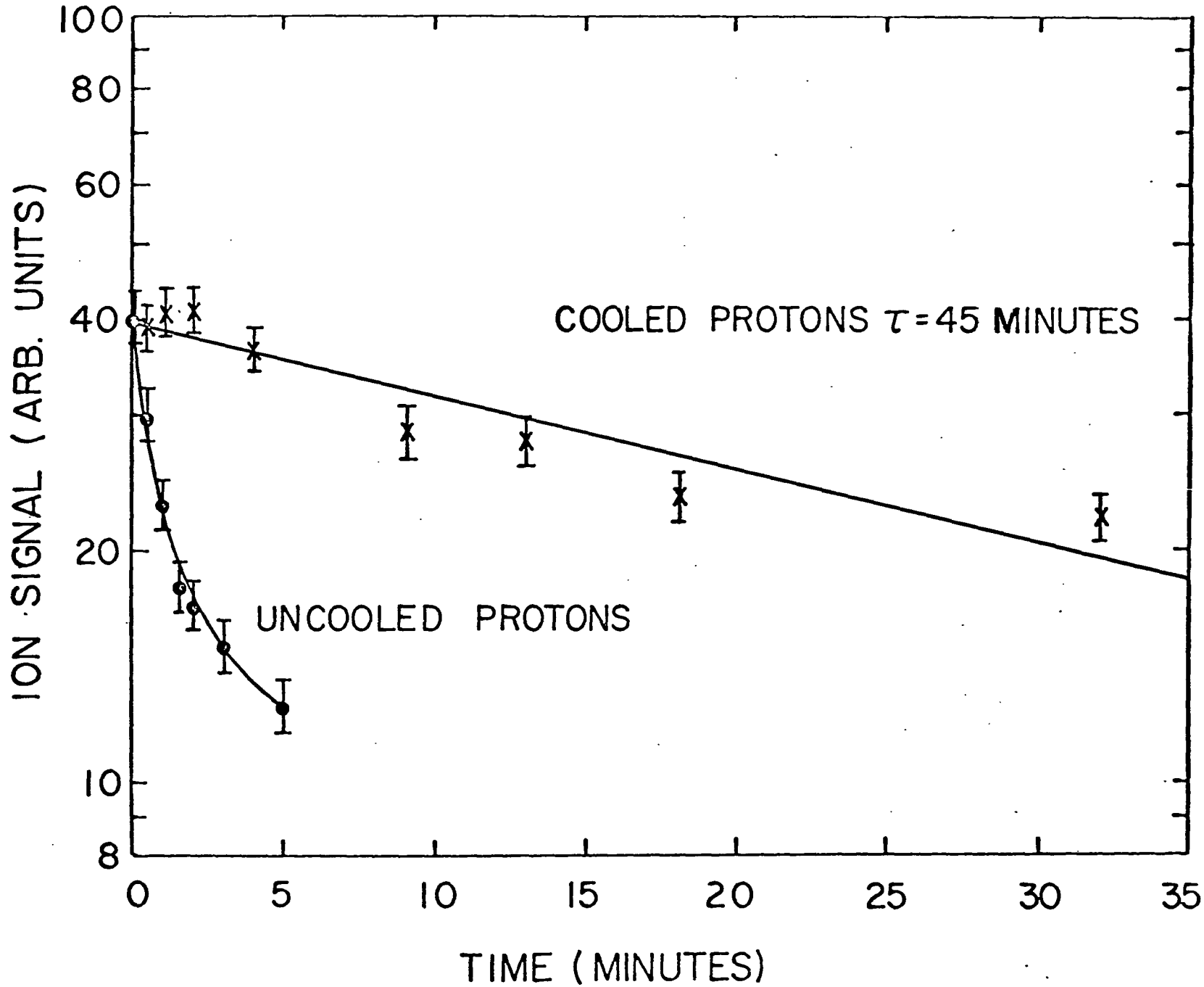
100
80
60
40
20
10
8
ION SIGNAL (ARB. UNITS)
COOLED PROTONS τ = 45 MINUTES
UNCOOLED PROTONS
0
5
10
15
20
25
30
35
TIME (MINUTES)

for cooled and uncooled ions. The rapid initial decrease of uncooled ion number is characteristic, and is used to define the ion lifetime. In the earliest measurements performed with this trap, a trapping rf frequency of 50 MHz was used, giving a non-integral Ω/ω ratio of about 11/1. The initial decrease in ion number had a time constant of about 30 seconds in this situation. Increasing the rf frequency to 146 MHz increased the time constant to about 100 seconds, with a ratio Ω/ω of about 33/1. This indicated that the rf played a part in the rapid initial ion loss, which became essentially independent of pressure for low enough pressures. Moreover, this ion loss rate was affected by the tuning of the rf shunts L_s, C_s shown in Figure X. The shunts were tuned to produce the longest ion lifetime by shorting one and tuning the other to maximize the lifetime, and then repeating the process for the other. This was found to be superior to the alternative of merely tuning each one to resonance. The longest lifetimes were attained with non-zero rf voltages across the shunts, implying the existence of an asymmetry in the trap. The ion lifetime was reduced by $2^{1/2}$ when the relative rf voltage $\Delta V_s/V_o$ was changed by 2.5 per cent from the optimum value.

After the initial sharp decrease in ion number, the rate of loss of ions decreased with sufficiently low pressures. This has been observed elsewhere,[31] and may indicate that the storage time is dependent on ion density. The slow

decrease in system pressure following the initial pressure burst produced by the electron pulse may account for some of the curvature observed in the ion decay plot.

3. The ions were cooled by tuning the ion oscillation frequency to the tank circuit resonance after the creation pulse, since the noise voltage fluctuation on the tank circuit produced by the electron current shot noise was sufficient to throw out some of the ions. After creation, the dc voltage was decreased to a negative value to throw out any remaining H_2^+ ions, and the protons were stored at resonance for a measured time. Detection proceeded in the usual manner. Figure XIII shows that the cooled ion number decreased nearly exponentially with a time constant close to fifty minutes at a pressure estimated at 5×10^{-11} Torr. The lifetime was increased by about a factor of twenty-five as a result of energy being removed by the cooling process.

Evidence that cooled ions had lower energies in the effective potential well could be directly obtained by creating ions in a symmetric well and then decreasing the dc voltage to a fixed value, holding it a few seconds, and raising it again to the original value. For a constant rf voltage this increased the well depth in the z direction while decreasing it in the r direction. In this asymmetric situation, hot ions scattered into the coordinate with small well depth should be lost. The ion number remaining after a measured well depth excursion was compared with the number

trapped while symmetry was maintained to obtain a measure of this loss. For cooled ions, no loss was observed down to D_r = 1.6 V while half the ions were lost with D_r = 1.0 V. For uncooled ions, however, loss began at D_r = 3.7 V, with half the ions gone at D_r = 2.2 V.

4. The noise voltage fluctuation induced on the detection tank circuit by the ions was next observed to definitely establish an ion cooling rate. When the detected voltage was greater than about 0.5 volts the detection was linear, and the rectified dc voltage in the detector bandwidth was proportional to the square root of the mean square noise voltage fluctuation across the tank circuit. The change in the tank circuit temperature due to the presence of the ions was small, so the detected signal was the small voltage difference between two large dc voltages. As a result, the signal voltage was directly proportional to the difference between the heated tank circuit temperature and the equilibrium temperature, ΔT. From equation II-7, this tank circuit temperature difference is proportional to both the temperature of the ions above the tank circuit temperature and the ion number. As the ion temperature decreases, the tank circuit temperature will decrease with the same time constant as long as the ion number remains constant. The cooled ion number decay measurements showed that the ion number can be considered constant for short times. An oscilloscope trace of the decrease of the detected noise signal is shown in

Figure XII-(b). From the theory previously outlined, the tank circuit temperature is expected to decay exponentially to its initial value as the ions come into equilibrium with it. Figure XII-(b) shows that the decay was not exponential and that the temperature signal seemed to indicate that the ions were being held at a temperature above the tank circuit equilibrium temperature by some energy input. However, some ion cooling had definitely occurred.

When the tank circuit temperature difference above this equilibrium signal temperature reached by the ions was plotted on semi-log graph paper, the decay of the ion temperature to equilibrium was found to be exponential within the limits of error. The time constant for temperature decay was taken as an experimental value of the cooling time constant. From equation II-4, the time constant for cooling protons in the absence of temperature limiting perturbations is about 6 seconds, using parameters from Tables II and III. As discussed in section II-2, the uncertainties in this value are fairly substantial. When the relaxation time between the degrees of freedom of the ion motion is shorter than the cooling time constant, the observed time constant will be increased by a factor of three. The experimental demonstration of the existence of this situation is discussed in section VIII-5. The measured exponential decay rate given in Table III was shorter than the estimated time constant value.

The tank circuit Q was kept much larger than the Q of the ion line in order to improve the signal to noise ratio. Experimentally the tank circuit Q could be reduced by putting a physically small carbon resistor in parallel with the tank circuit coil. The observed tank circuit temperature signal amplitude varied directly with the Q for Q values between 50 and 180, while the ion cooling time constant was independent of Q in this range. The signal was too small to make measurements of comparable accuracy for smaller Q values.

The ion linewidth was also observed by monitoring the tank circuit temperature while the ions were swept through resonance linearly. The observed linewidth measured between the half power points agreed with that obtained from the absorption signal measurements. No strong dependence of the ion linewidth on ion number or temperature was observed.

The results of observing the equilibrium ion temperature signal for long times are shown in Figure XIV. After the initial rapid decrease due to cooling, the signal decays slowly with about the same time constant as the ion number decay. Since the tank circuit temperature signal is proportional to both ion number and temperature, this implies that at equilibrium the ion temperature remains constant while the number changes. This effect was investigated further by measuring the created ion number as a function of electron emission for constant pulse length, and then measuring the equilibrium temperature signal level as a function

Figure XIV Decrease of the tank circuit temperature signal with time. The initial sharp drop is due to the decrease in ion temperature while the slow decrease has a time constant close to that measured for cooled ion number loss.

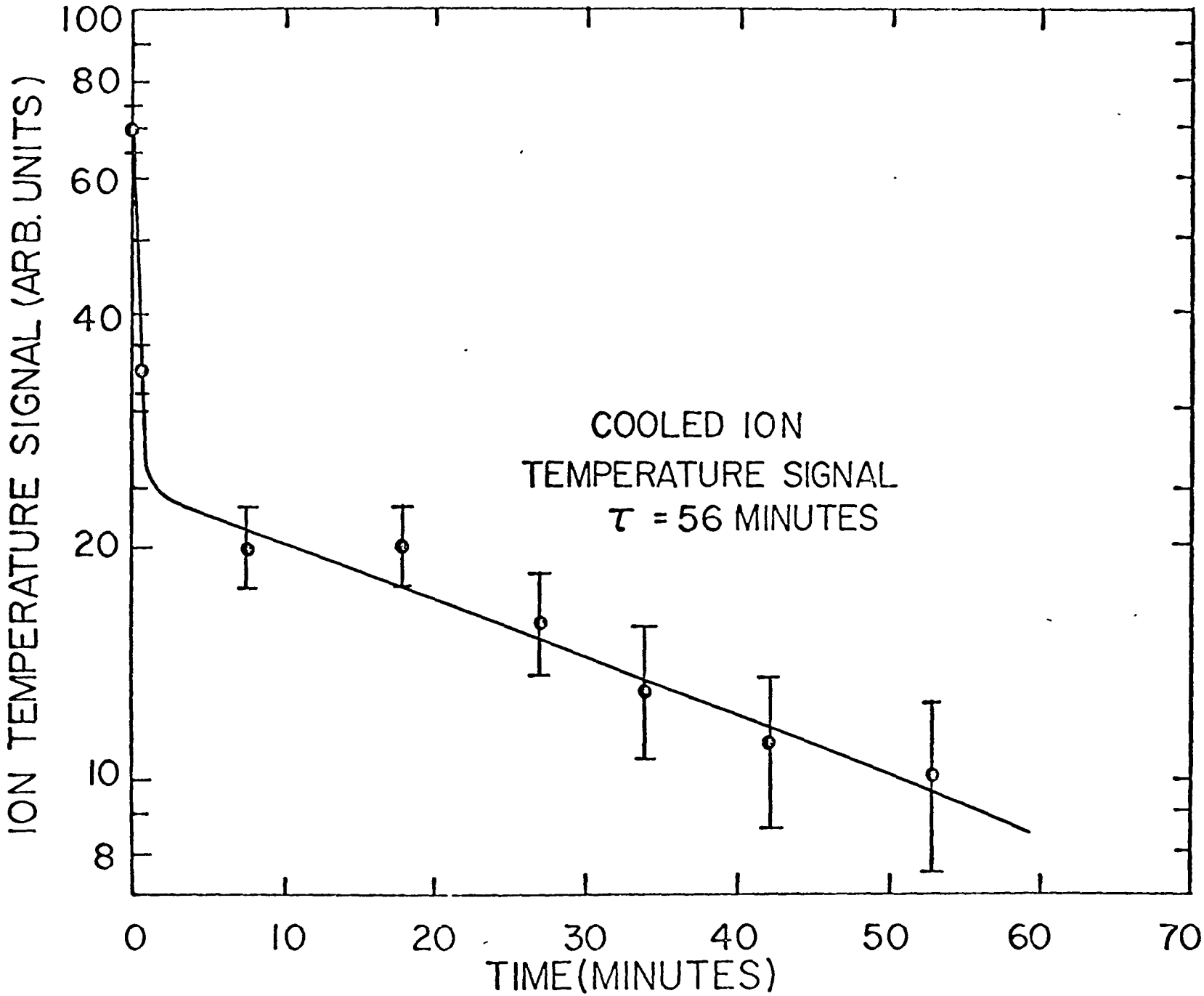
ION TEMPERATURE SIGNAL (ARB. UNITS)
100
80
60
40
20
10
8
0
10
20
30
40
50
60
70
TIME(MINUTES)
COOLED ION
TEMPERATURE SIGNAL
τ = 56 MINUTES

of emission current under the same conditions. The results of these measurements are combined in Figure XV to show how the equilibrium temperature signal varies with ion number. The straight line drawn through the experimental points is for a directly proportional dependence, confirming the original indication that at equilibrium the ion temperature remains constant while the ion number decays.

5. By modulating the force constant of the effective harmonic well that contains the ions at twice the ion oscillation frequency, energy can be transferred to the ions.[33] The degrees of freedom of the ion motion are orthogonal under this type of parametric excitation as long as the frequencies of oscillation differ. After one component of the motion has been heated by a parametric pulse the ions will no longer be in thermal equilibrium and energy will be exchanged to the other degrees of freedom via collisions, assuming the motional coordinates are otherwise uncoupled, until equilibrium is restored. The important collision process will be the one with the largest collision frequency which, at low pressures, should be the Coulomb scattering of the ions.

Experimentally, energy is pulsed into the r motion of the ions at frequency $2\omega_r$ by applying the excitation voltage V_p to the ring electrode of the trap as shown in Figure X. The excitation is symmetric so the center of mass of the ion cloud does not move. After the pulse, the energy enters the z motion slowly and increases the z motion temperature, which

Figure XV Equilibrium ion temperature signal versus ion number. The error bars indicate the standard deviation of a single measurement. The points represent the average of between six and ten measurements.

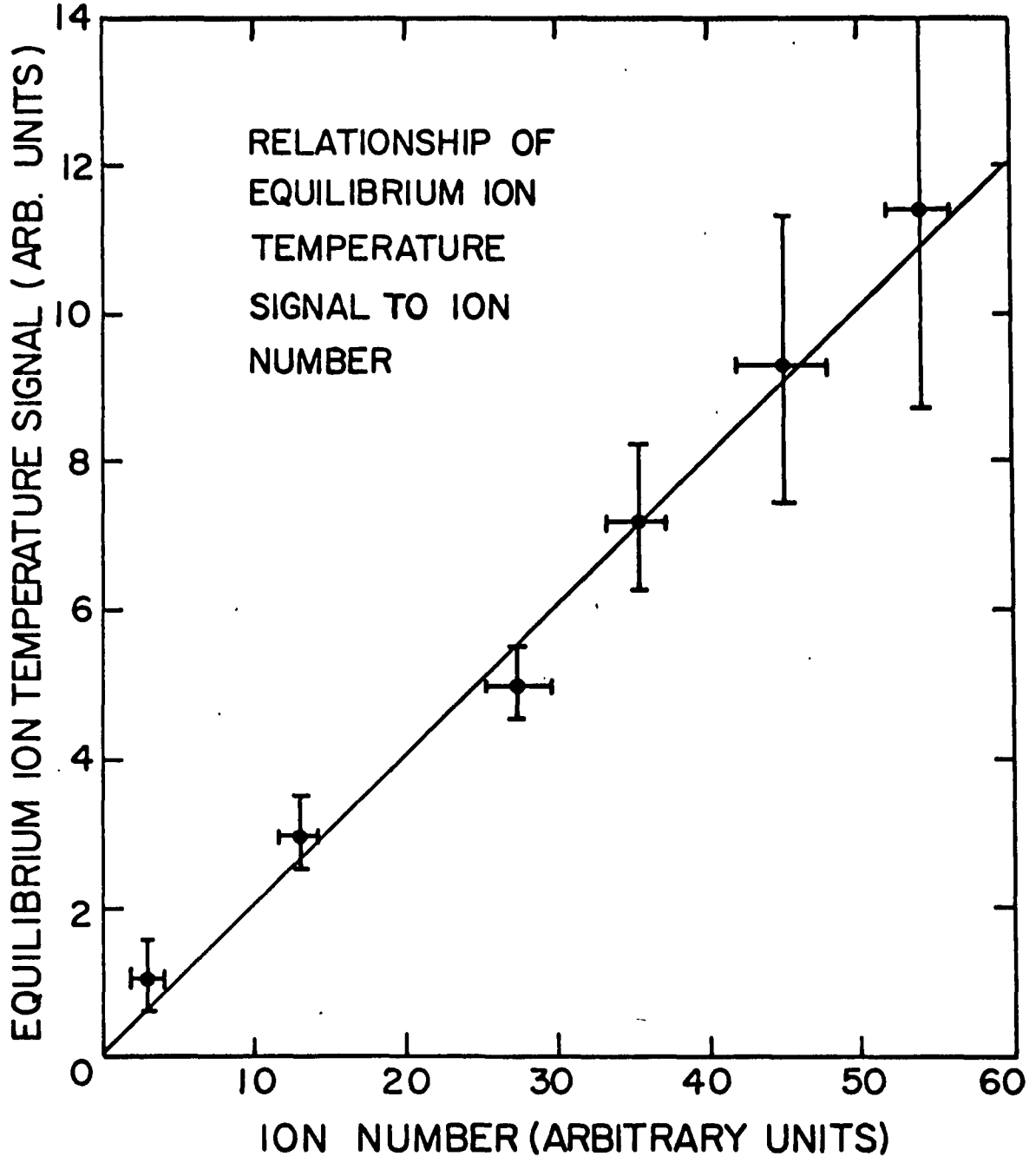
RELATIONSHIP OF
EQUILIBRIUM ION
TEMPERATURE
SIGNAL TO ION
NUMBER
EQUILIBRIUM ION TEMPERATURE SIGNAL (ARB. UNITS)
ION NUMBER (ARBITRARY UNITS)
0
2
4
6
8
10
12
14
10
20
30
40
50
60

is detected in the usual manner. The total system energy is cooled by the tank circuit after equilibrium is established. A number of such pulses were integrated with the multi-channel analyzer system with the results shown in Figure XVI. Both transients in Figure XVI were produced by 10 msec pulses at $2\omega_r$. The shorter response time shown in the lower photograph results from ion excitation by a pulse with one half the amplitude of that used to produce the upper transient. This is consistent with the assumption that the relaxation is produced by ion-ion collisions. When the variation of ion density with temperature is taken into account, the Spitzer time t_{II} (equation VI-4) is proportional to the temperature raised to the third power, so the lower energy ions should exhibit a shorter relaxation time. Assuming that the transient rises at an exponential rate and equating this time constant with the relaxation time, the r-z relaxation time for the higher temperature measurement is about 0.3 seconds, while the lower is about half as much. These times were measured in the 10 volt well. The ratio of the measured relaxation times agrees very well with the ratio predicted by equation VI-4 when the ratio of observed equilibrium ion temperatures is used. The predicted relaxation time calculated using the measured ion equilibrium temperature and number, given in Table III, is about a factor of two less than that observed. Since assumptions about the ion density and effective temperature in a non-equilibrium situation must be made, this difference is probably not significant.

Figure XVI Relaxation transients produced by parametric heating of the r motion of the ions in the trap. The 10 msec pulse was applied at time t_o. The smaller amplitude pulse produced the faster relaxation. Random noise was reduced a factor of eight by integration.

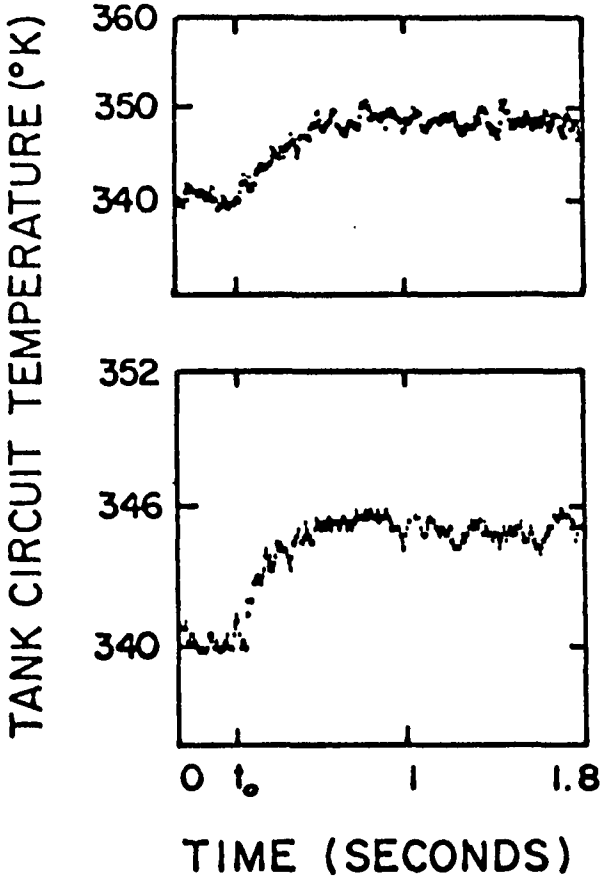
TANK CIRCUIT TEMPERATURE (°K)
360
350
340
352
346
340
0
t_o
1
1.8
TIME (SECONDS)

Furthermore, the measurement was complicated by loss of ions during the integration procedure. Since the ions were heated by the pulse, the loss of ions proceeds at a slightly increased rate during this portion of the measurement cycle. The trap required refilling several times during the measurement, resulting in a further uncertainty in ion number. However, the measurements with hot and cold ions were similar in this respect, so the ratio should not be greatly affected, and the relative magnitudes are still significant. A further relaxation time measurement was made at lower ion temperature in a well of depth 3.9 volts, where much faster relaxation was expected and observed, although no accurate determination of the time constant was made.

The ions could also be excited by applying a weak steady parametric signal at either $2\omega_r$ or $2\omega_z$. This resulted in an increase in the ion temperature signal unless the excitation was strong enough to drive ions from the trap, in which case the signal would increase to a maximum value only about 20 per cent higher than the initial uncooled temperature and then drop to the empty tank circuit temperature. Such a measurement could be used to count the ion number.

6. As previously mentioned, the ion cloud cannot be indefinitely compressed by cooling, so the apparent equilibrium ion temperature may be related to the space charge limited volume of the ion cloud. As the minimum volume is approached,

the rate of energy loss produced by cooling will be modified as $\overline{z}^2$ becomes independent of ion temperature. The harmonic content of the ion current at the fundamental frequency should decrease as the well becomes more flat-bottomed, resulting in a decreased cooling rate. For ions "at rest" at depth D_q the only motion associated with their position is the micromotion, or expansion and contraction of the ion cloud at the frequency Ω . Photographs of stored charged aluminum particles in such a situation have been made.[22] With the much lighter ions, this "lattice" situation will not be reached. However, an estimate of the minimum volume gives a measure of the minimum ion temperature, which we take as $T_o + T_q$ where $kT_q = eD_q$. Using the highest observed ion signal to noise ratio, 400/1, in equation V-1 in a bandwidth of 20 KHz, the maximum ion number trapped was about 7×10^3. From equation VI-3, D_q is about 0.06 V using this ion number in a 10 V well. The next task was to determine the apparent noise temperature of the ions and the tank circuit temperature.

The noise temperature of the tank circuit T_o was determined in the following manner. A measured resistance R_M was put across the half of the tank circuit closest to the electron gun between the end cap and the ring electrode. A quarter watt carbon resistor was used. This resistance appears in parallel with R/4 where R is the resonant tank resistance. The effective resistance R_e is equal to R_M if

R_M is quite small, or alternatively R_e can be calculated from the known tank circuit impedance. A measured dc current produced by the temperature limited emission of the electron gun was next passed through R_e. The shot noise associated with this current heated the tank circuit, and the detected voltage corresponding to this increased temperature was recorded, as was the voltage corresponding to the unheated tank circuit. The thermal voltage fluctuation across one half of the tank circuit at temperature T_o is $\overline{V}_1^2 = 4R_e kT_o \Delta f$, and the increased fluctuation in voltage produced by the shot noise current can be shown to be[34]

$$\overline{V}_2^2/4R_e kT_o df = 1 + IR_e/2(e/kT_o)$$

The ratio, together with the known values of R_e and I gives T_o. The rectified dc voltage from the diode detector is produced by both the tank circuit and noise generated in the first stage of amplification. The contribution from the amplifier alone was determined by removing the tank circuit from the input. As a result, the corrected voltage ratios used were proportional to the relative tank circuit temperatures. From about twenty trials, with different values of R_e and different excitation levels, the tank circuit temperature was found to be $T_o = 328 \pm 8$ degrees K, where the error is the rms deviation of the average temperature. This value is close to 30 degrees over room temperature, indicating a small diode nonlinearity or some heating of the tank circuit

by the monitoring amplifier, or some other systematic error. Since the temperature calibrating system reads high, this value of base temperature T_o is used in absolute temperature determinations. These temperature measurements served to calibrate the detected diode voltage against the excited tank circuit temperature.

To obtain the noise temperature of the ions, the ion-tank circuit system was excited with the shot noise produced by a photon excited photomultiplier tube. The added noise was coupled to the tank circuit with an antenna. The ratio of the effective noise excitation generated tank circuit temperature to the normal temperature was calculated using the temperature calibration just discussed. Ions present oscillating at the tank circuit resonant frequency are assumed to come into thermal equilibrium with the tank circuit as indicated earlier by equation II-5. The validity of this assumption will be discussed later. The external excitation must be applied for times long compared to the cooling time constant τ_o to insure that equilibrium between ions and tank is established. When the excitation is suddenly removed, the tank circuit cools to equilibrium in a time measured by $\tau_{to} = Q_t/\omega_z$, while the ions cool to equilibrium with their much longer cooling time constant. The initial hot ion signal has been produced by a known tank circuit temperature. The equilibrium signal temperature was determined by tuning the ions off resonance and taking a ratio between the hot and cold signals, which is independent of the ion number. The

results of such measurements are shown in Figure XVII for ions in a ten volt well. The increase in ion temperature due to tank circuit heating was found to add to the equilibrium temperature. The equilibrium temperature of the ions in the well was substantially larger than the estimated limit produced by ion space charge.

A determination of ion number can be made from these measurements by measuring the tank circuit temperature produced by the presence of ions at known temperature, and applying equation II-7.

The equilibrium temperature reached by the ions was also measured for several different values of well depth by changing the ion detection frequency and trapping the ions at correspondingly lower voltages. The equilibrium temperature reached by the ions decreased roughly linearly with well depth. The time constant for uncooled ion loss from the trap was independent of well depth and the time constant for cooled ion loss measured at a well depth of 2.6 V was the same as the value for the ten volt well within the limits of error. The number of ions trapped at a given well depth decreased only slightly as the well depth was decreased, so the well was probably not full for many of the higher well depth measurements.

The values for ion number, equilibrium temperature, maximum ion temperature, and various temperature and number dependent time constants are shown as a function of well

Figure XVII Calibration of the equilibrium ion temperature. The error bars indicate the uncertainty in a single measurement, while the points are the average of several measurements.

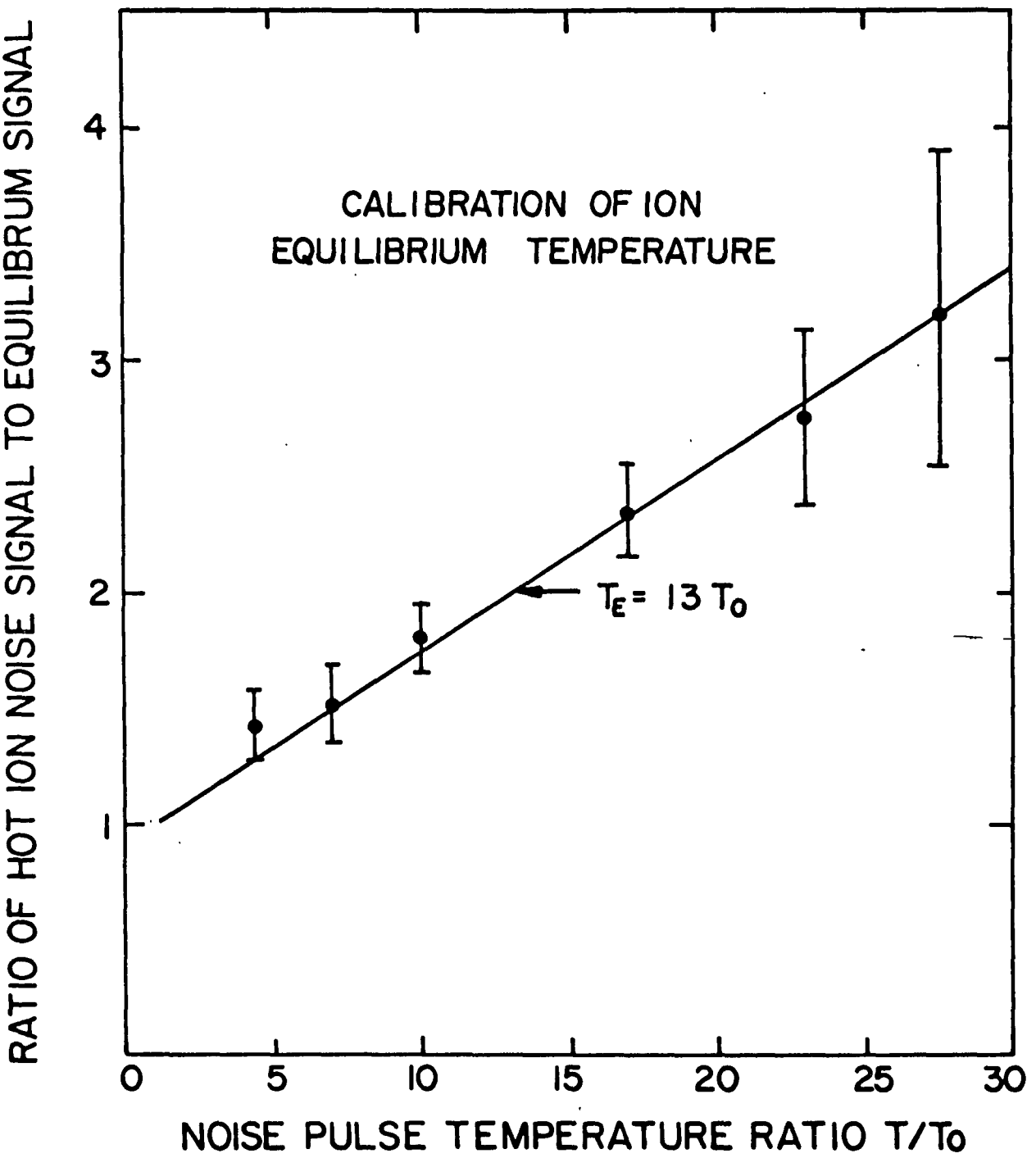
CALIBRATION OF ION
EQUILIBRIUM TEMPERATURE
$T_E = 13\,T_0$
RATIO OF HOT ION NOISE SIGNAL TO EQUILIBRUM SIGNAL
NOISE PULSE TEMPERATURE RATIO T/To
0
5
10
15
20
25
30
1
2
3
4

depth in Table III. The lowest equilibrium temperature attained was about 1000 degrees K for 2 x 10^3 ions in a 2.6 V well. Due to the low ion number and temperature the signal was small enough to make fairly long integration times desirable. Ten second digital averages of the hot ion decay, the equilibrium signal and the empty tank circuit temperature were made by converting the voltage signal to frequency and counting the frequency. The initial hot ion temperature was calculated by dividing the accumulated count by the integrated area under the decaying ion signal, as indicated in Figure XVIII-(c). For larger well depths the signal decay and equilibrium average were obtained directly from chart recordings. An example of such a decay measured with the multi-channel analyzer system using 3.2 second averaging times is shown in Figure XVIII-(b) for the 2.6 V well depth.

The equilibrium temperature reached for the smallest well depth was obtained despite the addition of capacitance to the tank circuit to reduce the frequency to the necessary value. It was found to be experimentally inconvenient to lower the frequency by increasing the inductance due to the unwieldy air coils used. Good coupling was not obtained due to geometrical problems, and the ion signals observed were weak. Ferrite cores could not be used due to nonlinear effects produced by the Ωrf. At the 2.6 V well depth, the total capacitance used was about 23 pF, increasing the

Figure XVIII-(a) Decay of the temperature signal after ions were created and tuned to resonance. The ions were detuned at 55 seconds.

Figure XVIII-(b) Decay of the temperature signal in a 2.6 volt well after heating at resonance by a noise pulse to the temperature T_H. The ions were detuned from resonance at time t_o. About 20 sweeps were integrated. $T_H/T_o = 6.2$

Figure XVIII-(c) Plot of the temperature signal decay indicating the cooling time constant and the integration intervals Δt used to measure the ion temperature.

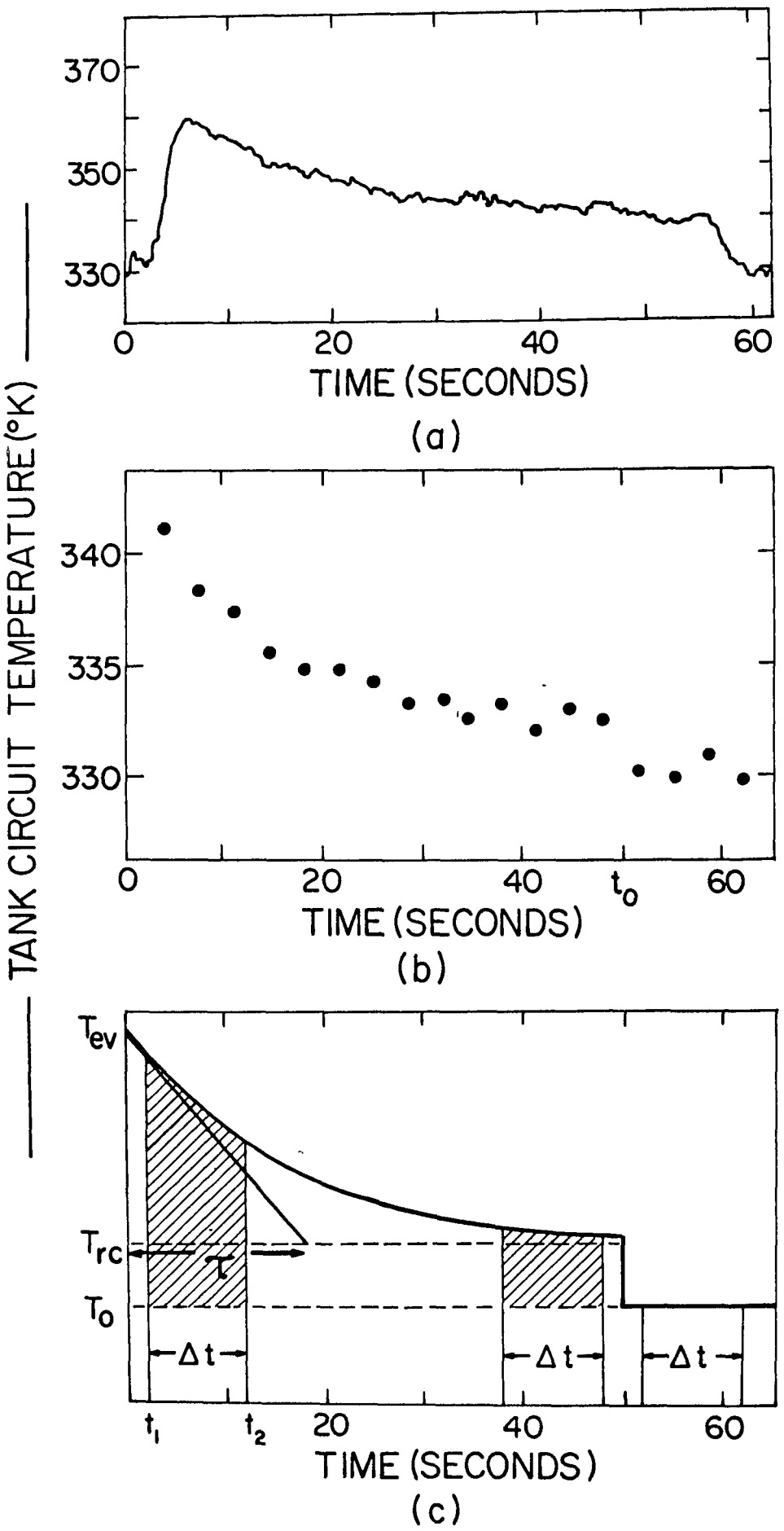
TANK CIRCUIT TEMPERATURE (°K)
370
350
330
0
20
40
60
TIME (SECONDS)
(a)
340
335
330
0
20
40
t_o
60
TIME (SECONDS)
(b)
T_{ev}
T_{rc}
T_o
τ
Δt
Δt
Δt
t_1
t_2
20
40
60
TIME (SECONDS)
(c)

calculated cooling time constant by about 60 per cent over the value in the 10 V well.

The existence of perturbations that effect the ion temperature make a calibration justified by a situation where perturbations are absent somewhat suspect. Conceivable energy gain or loss mechanisms might change the apparent calibration by a factor dependent on ion energy. Rather than discuss each possibility, we enumerate the available experimental checks as a basis for confidence in the measurements.

A rough determination of the rate of energy increase by the ions was made by storing the ions at equilibrium, detuning them for a measured interval, and then recording the maximum signal obtained when they were returned to resonance with the tank circuit. This measurement should be valid as long as ion loss is negligible, which is the case for short times. With the ions off resonance for times up to twenty-five seconds, the rate of temperature rise had a time constant of about 60 seconds, while for longer times the time constant was about 160 seconds. Both time constants were long compared to the cooling time constant. The variation in heating rate as equilibrium is approached seems to indicate a rapidly increasing energy gain rate with temperature decrease.

Returning to the temperature calibration measurements, the relative temperature increase by the ions due to tank

circuit heating shown in Figure XVII is linear even into the temperature region where 70 per cent of the ions initially present are lost during the heating cycle. By using the calibrated temperature and the observed sensitivity η, equation II-7, the ion number $N_t = \eta\tau_{zo}/\tau_{to}$ can be compared to the number N_c obtained from the coherent signal excitation measurements. Incoherent signal to noise ratios using measured values can also be compared to theoretical expressions. Some comparisons are presented in Table III. In general, the measurements appear to be consistent.

7. In an attempt to determine the cause of the ion equilibrium temperature, heating of the ions by stray rf fields was investigated. Possible unexpected emissions from the Ω rf linear amplifier were attenuated with the $\lambda/2$ filter tuned to Ω. This narrowed the bandwidth to less than one MHz. Such a filter might pass transmitter generated harmonics of Ω, so these were attenuated by a low pass filter. Addition or removal of these filters to the rf input circuit had no effect on the ion equilibrium temperature. Moreover, a tuned detector was built to measure coherent sidebands or added noise separated from the rf carrier by the ion oscillation frequency. The measurement was performed with the standard experimental apparatus with the detector in parallel with the low impedance end of the final step-up pi network to the trap. Some noise was detected, but coherent excitation at this frequency with an amplitude

one hundred times the measured noise level failed to heat the ions, indicating that the noise was harmless. The geometry of the trap inhibits ion excitation by such sidebands unless there is a lack of symmetry.

The shielding around the ion trap was not perfect, so the presence of stray rf frequencies inside the shield was investigated in the frequency range from 0.5 to 30 MHz with a radio receiver, and in the higher frequency range using a local oscillator and mixer with the receiver. A few signals were detected, mostly from adjacent apparatus, but eliminating those whose source could be determined had no effect. Since the ion oscillation frequencies were changed over the range of 2.2 to 5 MHz, an accidental resonance seems unlikely. The ions were observed throughout the day and night, but no excitation time dependence was observed, i.e. it was not turned on and off. Turning off the ion pump and TDG showed that the discharges were not exciting the ions. Finally a batch of ions was stored with all leads to the shield except the rf and the detection amplifier removed and shorted. The null results of these measurements coupled with the dependence of the temperature on well depth indicate that the source of heating of the ions was not external to the system.

8. Following the measurements just described, the vacuum system was opened and the rotation of the ring electrode discussed in section VII-2 was discovered. Accurate realignment of the electrodes proved difficult due to the

distortions in the end caps, which limited accuracy to a few thousandths of an inch. The system was then resealed, baked out, and the electrodes were outgassed at a lower temperature than before. After another bakeout and outgas, most of the measurements previously described were repeated at a well depth of 3.9 V. The data, summarized in Table III, shows that the effects of the perturbation were not dramatic. By keeping the capacitance small the cooling time constant was reduced to about 7 seconds. Using the differential tuning arrangement described in section VII the uncooled ion lifetime and equilibrium signal level could be monitored as a function of departure of the potential well from symmetry due to the application of a different rf voltage to each end cap electrode. Taking ΔV_c as the difference in voltage of the end caps and V_c as the end cap voltage at symmetry, the uncooled lifetime of the ions remained constant at 120 seconds for $\Delta V_c/V_c$ as large as 10 per cent, while nearly 20 per cent asymmetry was required to reduce the lifetime by 30 per cent. The equilibrium ion temperature also did not appear to vary substantially over this tuning range. In general, small improvements in uncooled ion lifetime, ion linewidth, and relative ion temperature were observed after the electrode geometry change, implying that further favorable improvements might be expected in a rigorously symmetrized trap.

9. We have already discussed the heating of the ion cloud by elastic collisions and other causes, interpreting the resultant loss of ions as a loss from the high energy tail of the distribution inside the harmonic well. The temperature of the uncooled ions was monitored by tuning the ions to resonance for brief intervals during the otherwise uncooled storage period. When corrected for the cooling effects during the storage intervals, the ion temperature appeared to remain constant while the ion number decreased.

When the ions are cooled, the temperature is decreased while the ion number remains essentially constant. From Figure XVIII-(a) it can be seen that the uncooled ion temperature is about three times the cooled ion temperature. The theoretical time constant for ion loss, equation VI-5, varies exponentially with the well depth to temperature ratio. Using the measured temperature to well depth ratios, the values calculated are more than an order of magnitude above the measured loss time constant of 100 seconds. When the ions are cooled to the equilibrium temperature, T_B increases to over 10^9 seconds while the measured ion lifetime only increases to 3×10^3 seconds. The measured ion loss time constant is nonlinearly temperature dependent but only weakly: a 50 per cent increase in ion temperature above the equilibrium value, generated by a weak parametric heating voltage, produced only a 30 per cent decrease in the cooled ion storage lifetime. This temperature dependence of the

lifetime appears to be inconsistent with both the evaporation theory and with the low energy ion-molecule reaction theory to be discussed, which has a rate independent of energy in the region of validity. The improved agreement of the evaporation theory with experiment at high temperature indicates that at lower temperatures competing processes with less temperature sensitivity may become dominant.

Other possibilities for ion loss are asymmetric charge transfer and ion-molecule reactions, both resulting in different types of ions. Reactions of this type with ions stored in traps have been observed.[35] When asymmetric charge transfer for a given ion is considered as a long range interaction at moderate energies, the theory of Rapp and Francis[36] predicts that the cross section will drop rapidly in the low velocity region. For protons, the cross section is predicted to start dropping at relative kinetic energies about fifty times larger than the energy discrepancy between the ionization energies of the ion and atom.

With the gases normally expected in the vacuum system, discussed in Appendix II, only CO has an energy discrepancy of 0.4 volts or less for collisions with protons. However, CO_2, with an ionization energy of 13.8 volts, is evolved from stainless steel during bakeout[37] and may also be present. Using CO as an example, for one volt ions the charge exchange cross section with protons for an energy discrepancy of 0.4 V is about 10^{-17} cm^2, using the theory. For an anticipated

partial pressure of CO of 10^{-11} Torr, a reaction time $T_r = (n_{CO}\sigma v)^{-1}$ of 2×10^5 seconds is obtained. Changes of a factor of two in the average velocity can result in order of magnitude changes in cross section in this velocity region, but this result is still somewhat above the observed loss time constant of 3×10^3 seconds. The measured cooled ion lifetime varied roughly as P^{-1} in the original vacuum, although the lifetime appeared to be slightly less dependent on pressure at the lowest pressures reached. After the system was opened and resealed the cooled ion lifetime was slightly shorter than before, even at slightly better pressures, and the variation with pressure was much less linear. A factor of ten pressure increase produced by shutting off the ion pump only changed the cooled lifetime by 40 per cent. This anomalous behavior could be due to the nonlinear action of ion pumps while pumping different gases (see Appendix I) or possibly to the selective disappearance of certain gas types due to the multiple bakeouts. It indicates that pressure effects on the ion lifetime cannot be neglected, although their contribution to ion heating appears to be small. The cooled ions could be heated by a large gas burst produced by warming a filament, but a decade pressure increase did not produce a significant increase in cooled ion temperature.

Pursuing the reaction ion loss process further, if the ionization energy of B is greater than that of A in the reaction $A^+ + B \rightarrow A + B^+$, the reaction is endothermic and

will not proceed below some threshold energy. On the other hand, for an exothermic reaction either charge exchange or ion molecule reactions of the type $A^+ + BC \rightarrow (AB)^+ + C$ should occur at or near thermal energies.[38] These two processes can be treated together in this energy range. The ion-molecule reaction theory of Gioumousis and Stevenson[39] is still used in the energy range below 10 eV. This theory predicts a reaction rate independent of energy produced by orbiting collisions in the attractive ion-induced dipole potential. A collision complex is assumed to be formed which subsequently decays. The decay channels include both charge transfer and ion-molecule reactions. This cross section predicts that charge transfer may occur at a rate far larger than predicted by the Rapp and Francis long range interaction theory.

The cross sections and rates for any charge exchange or ion-molecule reaction that is exothermic should be quite comparable, and cold ions could be destroyed at a substantial rate. However, all reactions with the dominant background gases near base pressure are endothermic and should not occur near thermal energies. Of the common gases only H_2O and O_2 could have exothermic charge exchange reactions. Using calculated cross sections, the necessary partial pressure of either of these gases to produce the observed ion lifetime can be obtained. This necessary partial pressure is close to 10^{-11} Torr, so the observed ion loss rate

could come from one or several of these reactions proceeding simultaneously.

It has not been possible to definitely eliminate any of the reaction ion loss possibilities discussed. The weak temperature dependence of the cooled ion lifetime may indicate that an ion distribution modified by nonlinear energy inputs exists. The pressure dependence probably reflects ion loss by reactions. Further measurements with a known background gas composition appear to be necessary.

Table II Small ion trap parameters and data measured with a 10 volt well depth.

SMALL ION TRAP DATA

Field dimension $z_o = 2^{-1/2} r_o$	0.16 cm
Storage volume $V_t = 4\pi r_o^2 z_o/3$	0.034 cm^3
Trapping rf frequency $\Omega/2\pi$	146 MHz
Ion oscillation frequency $\omega/2\pi$	4.4 MHz
Well depth D	10.4 V
Calculated maximum ion density n_{max}	6×10^8 cm^{-3}
Calculated maximum ion number N_{max}	2×10^7
Maximum measured ion density n	2×10^5 cm^{-3}
Maximum measured ion number N	7×10^3
N/N_{max}	3.5×10^{-4}
D_q for maximum measured ion number	0.06 V
Tank circuit capacitance	7 pF
Estimated base pressure	7×10^{-12} Torr

Table III Dependence of small ion trap operating parameters and data on the well depth. The symbols used are defined as follows:

V_o	Peak trapping rf voltage
C	Tank circuit capacitance
$3\tau_{zo}$	Ion cooling time constant
$T_B(T_m)$	Ion loss time constant at the temperature T_m.
$T_B(T_e)$	Ion loss time constant at the temperature T_e
T_m	Hot ion temperature
T_e	Equilibrium ion temperature
N_c	Ion number measured by exciting a coherent ion signal
N_t	Ion number from tank circuit temperature measurements.

DEPENDENCE OF PARAMETERS AND DATA ON WELL DEPTH

Well Depth D (V)	10.4	4.6	2.6	3.9
$\omega/2\pi$ (MHz)	4.4	2.95	2.2	2.7
V_o (volts)	485	215	123	183
C (pF)	7	10	23	7
$3\tau_{zo}$ (sec)	13	13	17	7.3
Q_i (Ions)	20	--	--	30
Q_t (tank circuit)	180	--	--	--
$T_B(T_m)$ (sec)	100	100	100	120
$T_B(T_e)$ (sec)	2.6×10^3	--	2.4×10^3	2.4×10^3
$(T_e - T_o)/T_o$	12	5.3	1.7	2.1
$(T_m - T_o)/(T_e - T_o)$	3	2.1	3.1	3.5
$(T_m - T_o)/T_o$	36	11.1	5.3	7.4
kT_e/e (V)	0.33	0.16	0.07	0.08
kT_m/e (V)	0.93	0.30	0.16	0.21
eD/kT_m	11	15	16	18.5
eD/kT_e	32	29	37	49
N_c (typical)	3×10^3	1.6×10^3	2×10^3	1.6×10^3
N_t (typical)	3×10^3	2.3×10^3	2×10^3	2×10^3

IX SUMMARY AND DISCUSSION

The research reported here has demonstrated the feasibility of long term ion storage in both radio-frequency storage ring traps and in extremely small axially symmetric quadrupole traps. Both types of trap may be used to advantage in certain types of ion spectroscopic measurements. A radiative cooling technique especially applicable to light ions has been demonstrated with some success in the axially symmetric trap. "Bolometric" detection,[8] made possible by the cooling technique, has made available information about stored ion relaxation times, and admits the possibility of measuring the energy splitting of internal ion coordinates by coupling these coordinates to the translational motion of the ions in the trap.

Once a cooling rate fast compared to ion heating rates was achieved, the ion cooling and detection proceeded as anticipated with one major exception: the apparent lower limit on the ion temperature in the well is the main limitation on the cooling technique, which makes a further study of this limitation desirable. A definite experimental cause of ion heating has not been established, although it appears to be associated with the trapping rf field, possibly through electrode geometry generated nonlinearities. Using the lowest measured temperature and other demonstrated techniques,[7] the relativistic Doppler limit on the $_3$He ion hfs

could be reduced to about 0.5 Hz, with a fractional linewidth $\Delta\nu/\nu$ of 5×10^{-11}. On the other hand, heavy ions at the same temperature would have a substantially smaller Doppler width, allowing much smaller fractional linewidths. The cooling time constant increases as $Z^{-1}(A/Z)^{1/2}$ for ions with mass Am, charge Ze, assuming a constant well depth is maintained. As an example, a cooling time constant for doubly ionized Thallium of $\tau_o = 37$ seconds in the quadrupole trap can be extrapolated. This is not long compared to feasible ion storage times. The relative hfs linewidth would be $\Delta\nu/\nu \approx 8 \times 10^{-13}$. The availability of the ion-atom collisional cooling technique, which produces much faster cooling rates for heavy ions, limits the appeal of radiative cooling for heavy ions despite the larger perturbations of the ionic systems by the collisions.

The sensitivity for the "bolometric" detection technique for arbitrary ion number[8] is $\eta = N/N_c(1 + N/N_c)$, and is largest when $N \geq N_c$, the critical ion number. Neglecting motional relaxation corrections, $N_c = \tau_{zo}/\tau_{to} = 8D_zC/eQ_IQ_t$ is independent of the ion mass and oscillation frequency. For the quadrupole trap, N_c was about 10^6 ions, while the measured sensitivity was less than one per cent. Decreased ion excitation rates should allow larger ion numbers to be trapped, increasing the sensitivity. The lack of agreement of the measurements with the ion evaporation theory predictions may also be due to Ω - rf heating effects.

Due to the larger capacitance associated with the storage ring trap structures, the cooling time constants for ions stored in these traps are substantially longer than in small axially symmetric traps. However, the use of electronic feedback damping methods to increase the damping rate may be possible.[40,41] The cooling rate with the methods suggested is increased at the expense of an increased base temperature, which does not become a disadvantage until it exceeds any other lower limit on the ion temperature. Enhanced ion cooling rates have yet to be definitely established.

Despite these disadvantages, the storage ring type trap may be quite useful for ion spectroscopy experiments not involving this type of cooling. The long beam interaction region of the racetrack configuration would be desirable for ion interactions with low intensity neutral beams such as are available from state selectors. The separation of the ion creation, polarization and detection functions is then possible.

Finally, analogous to the method for electrons,[8] ions could be stored and cooled in Penning type traps. The cooling and trapping should be simplified by the static trapping fields used in these traps.

APPENDIX I

Vacuum Technique and Vapor Loaded Pump Measurements:

After assembly, welded and brazed parts of the vacuum shell were checked for leaks using a CEC 24-101A helium leak detector with a sensitivity of 10^{-6} std cc/sec. The helium was either blown on the suspected joint with a hypodermic needle or the part was placed in a helium balloon. Fortunately almost all faulty welds showed up on this detector.

After machining, both the vacuum shell and metal apparatus parts were degreased with Trichlorethylene using an ultrasonic cleaner when possible. Following several rinses in ethyl alcohol, the parts were thoroughly scrubbed with Scotch-brite using Labtone as a detergent. Several rinses in hot and cold distilled water followed, and the parts were dried in a warm air oven and stored in aluminum foil until use.

Glazed ceramic insulators and parts made from Alsimag machinable ceramic were cleaned by baking to 900 degrees C in air, while parts machined from Boron Nitride were cleaned with #320 Aloxite cloth and then baked to 800 degrees C in hydrogen or to 500 degrees C in vacuum.[42] This served to drive out water vapor as well as clean the parts without changing the dimensions of the part. Ceramic parts were stored in glass tubes or wrapped in aluminum foil following this procedure.

A high temperature lubricant Fel-Pro C-100 was used on the bolts of the Varian Conflat flanges when the system was assembled. The system was evacuated by a mercury diffusion pump through either a copper tube that was subsequently sealed off with a Varian pinch-off tool, or through a glass connection which was later sealed off by the glass blower. The bakeout oven was of the aluminum foil type using General Electric infrared lamps for heat. The glass in the region of glass to metal seals was coated with Aquadag to equalize the temperature of the glass and metal parts during the heating or cooling portions of the baking cycle. This was done following a crack in an uncoated seal during a non-equilibrium situation. To inhibit oxidation the pressure in the system was held below 5×10^{-5} Torr while the oven temperature was raised to 400 degrees C. The diffusion pump evacuated the system to between 10^{-6} and 10^{-7} Torr after bakeout at which time the ion pump was turned on and the system was sealed off from the diffusion pump. Base pressures varied slightly from system to system, but an indication of 10^{-11} A on the TDG could always be attained in a leak free system after several days of bakeout and system stabilization.

The presence of leaks in the system was detected in a number of standard ways, depending on the pressure region in which their effects became apparent. Tesla coil excited discharge color served as an indicator in the roughing

pressure range for systems with glass parts. From roughing pressure to about 10^{-8} Torr the change in ion pump current resulting from plugging the leak with Acetone was substantial. Below 10^{-8} Torr the change in ion pump current when helium was substituted for air outside the system was used.[44] For the smallest leaks, the pump current was bucked out as much as possible with dc current from a battery and plastic balloons were built around suspected parts of the system. When the balloons were alternately filled with helium and air, the modulation of the pump current could be observed. This technique, although laborious, was the only successful one found for leaks in the 10^{-11} Torr range.

After a low system base pressure was reached, a general method for determining if leaks were the limiting factor was to shut off the ion pump and monitor the pressure rise in the system with a TDG or other suitable gauge. With a small leak free system, the pressure would rise about a decade and would then be held constant by the pumping speed of the gauge. If a leak were present, the pressure would continue to rise slowly following the rapid initial increase until pressures in the 10^{-8} region or higher were reached.

A well known property of ion pumps is the rapid decrease in pumping speed observed in the 10^{-8} to 10^{-10} Torr pressure region.[45] A factor of five decrease, apparently independent of gas type, is typical. Changes in the distribution of electrons in the Penning gauge pumping structure

have been observed as a function of pressure,[46] which may be related to the pumping action. One possible method of increasing the pumping speed on a chamber at low pressure is to maintain the pump in the high speed region by an appropriate pressure of adsorbable vapor in the pump. Suitable traps can keep this vapor out of the chamber to be evacuated, while not substantially inhibiting the flow of other gas types to the pump. Cesium, with a vapor pressure of about 10^{-6} Torr at room temperature, is a suitable adsorbable vapor; while both gold and carbon surfaces have been used to adsorb cesium.

Measurements with an ion pumped glass vacuum system carried out by Mr. S. Hoverson demonstrated that gold was superior to carbon as a Cs adsorber and that base pressures of 10^{-13} A (TDG) could be obtained when the system, but not the gauge, was held at minus seven degrees C in a dry ice loaded refrigerator. At room temperature the pressure was generally above the base value obtained without Cs in the system, except after a bakeout which drove the Cs back into the reservoir. The decrease in pressure with temperature could be attributed to improved adsorption on the trap surfaces and to decreased Cs vapor pressure in the pump.

A predominantly metal vacuum system was next assembled to further study these effects. The system, shown schematically in Figure XIX, was essentially the system used for the storage ring ion trap apparatus, but with a minimum four

Figure XIX Diagram of vacuum system used for the adsorbable vapor loaded ion pump low pressure pumping speed measurements.

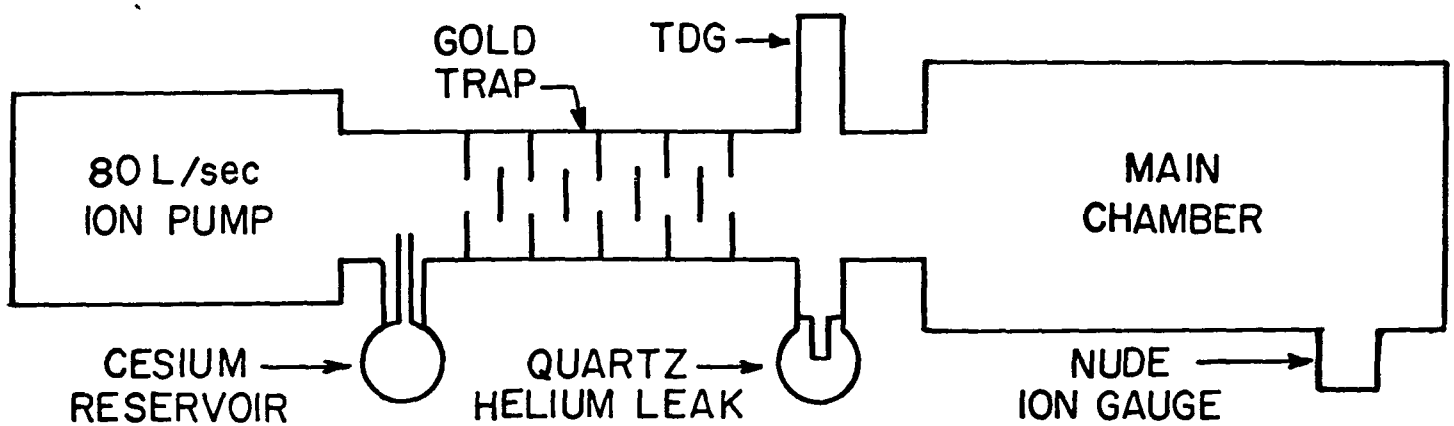
GOLD
TRAP
TDG
80 L/sec
ION PUMP
MAIN
CHAMBER
CESIUM
RESERVOIR
QUARTZ
HELIUM LEAK
NUDE
ION GAUGE

bounce Cs trap inserted between the 80 liter/second ion pump and the main chamber, and a Cs reservoir and conventional Helium leak installed. A filament failure in the Varian nude ion gauge left only the General Electric TDG as a pressure monitor. The trap consisted of a four inch outside diameter stainless steel tube divided into sections defined by stainless steel plates mounted on two supporting rods. A plate with a hole in the center was followed by a solid plate with diameter slightly larger than the preceding hole, and then another plate with a hole. This sequence comprised one section of the trap, through which a molecule could pass with a minimum of one bounce. Four sections were used, and the inside surfaces were covered with Engelhard UR #01-FM unfluxed paste gold paint during assembly. The conductance of the structure was about 35 liters per second for air, but substantially higher for the light gases expected at low pressures. The Cs reservoir was separated from the pump volume by a one l/second conductance glass tube which decreased the flow of Cs to the pump. The flow rate could be increased by driving Cs up the tube using an infrared lamp. The Cs was multiply distilled, both before and after it was let into the system through a break-off tip. No effect of the Cs on the base pressure of the system, about 10^{-11} Torr obtained after a 400 degree C bakeout, was immediately observed. Even after driving Cs up the glass tube the pressure did not immediately increase or decrease. However, after

several months the pressure had risen to about 5.5×10^{-11} A (TDG) in the main chamber, while the pump current indicated that the pump was around 10^{-8} Torr.

To determine the cause of the pressure increase, the different parts of the system were selectively cooled with dry ice. Cooling the main chamber decreased the TDG current to 4.5×10^{-11} A, indicating that some Cs had leaked through the gold trap. Next the trap was cooled, which decreased the pressure slightly more, while cooling the pump decreased the pressure to 1×10^{-11} A, the original base pressure of the system. Apparently the pump emits noncondensable gases at an increased rate while pumping Cs at substantially higher pressures.

The main chamber of the system was next baked out at 300 degrees C with the pump 70 degrees cooler to drive Cs back into the reservoir from both the pump and main chamber. After the bake, the pump current was 0.02 mA, one fifth of the original value, while the TDG indicated 3×10^{-12} A. Dry ice placed on the main chamber had no effect on the pressure, indicating that no Cs was present there. Over a period of several days both gauge and pump pressures rose, so the system was rebaked. The lowest chamber pressure attained was 1.2×10^{-12} A with dry ice on the pump and trap and 2×10^{-12} A without dry ice. In both cases the pump current was greater than 20 μA, indicating an effective pump pressure of around 10^{-8} Torr.

Next the helium leak was operated at a constant rate to determine the effect of the Cs on the pumping speed of helium. With the initial pressure at 1.6×10^{-11} A at room temperature, the leak rate was increased until at equilibrium the total current indication was 6.2×10^{-11} A, with the current component due to helium taken as the difference between these two values. With the leak rate held constant, dry ice was applied to the system, decreasing the pressure indication to 4.8×10^{-11} A. When the leak was turned off, the pressure dropped to 2.3×10^{-12} A. The relative helium pressure remained constant, implying no change in the pumping speed. This was also found to be true when the pressures for comparable leak rates before and after Cs was let into the system were compared.

Although it seems clear that the presence of Cs in the pump can inhibit the pumping rate for other gases, no unassailable evidence for enhanced pumping speeds has been obtained. For instance, the improvement in base pressures may merely be due to the effect of the multiple bakeouts on the system. However, it is also clear that the presence of some Cs in the pump does not raise the base pressure, and the lower base pressures could be due to a favorable compromise between conflicting processes. When the pump voltage was increased from 3000 to 6000 V the pressure of noncondensable gas increased, apparently because of increased sputtering by the heavy Cs ions. Perhaps a lighter adsorb-

able gas would reduce the gas generation problem while a gas pumped in a more conventional manner than He should be used as a test gas.

APPENDIX II

Vacuum Gauge Calibration:

A current related to the rate of ionization of the residual gas in the vacuum system was measured with a General Electric Triggered Discharge Gauge (TDG). This gauge does not suffer the x-ray limitations of a Bayard-Alpert gauge in the pressure range of interest, and its inventors claim it is effective into the 10^{-14} Torr range.[47] The advertized sensitivity of the TDG is one A/Torr for N_2, but it is well known that the sensitivity decreases with pressure.[48,49] A calibration in a typical system was made between the TDG and a Varian Associates nude Bayard-Alpert gauge (BAG). Using helium as a calibration gas, the results duplicated those of Kietzmann[50] above 2×10^{-11} A (TDG). The BAG consistently gave a higher pressure indication, ranging from a factor of six at 2×10^{-11} A (TDG) to a factor of three at 10^{-9} A (TDG). However, the BAG may give high indications due to the desorption of ions from the grid, which contribute to the measured ion current for pressures less than 4×10^{-8} Torr.[47] The true pressure in the system will apparently lie between the values given above.

Since the sensitivity of the TDG depends on the type of gas being ionized, it is important to know the types of residual gas present in the system. No mass spectrometer was available,[51] so the experience of others must be consulted. The gases generally observed at pressures below

10^{-10} Torr are[52] H_2, CO, and N_2, with He a major component in an ion pumped glass system, due to the low pumping speed for helium. In addition H_2O has been observed.[53] We chose a model of the background gas with equal parts of H_2 and He, with the partial pressures of CO and N_2 down by a factor of three. Using TDG sensitivities measured[48] below 10^{-9} Torr, the base pressure of the small vacuum system used in ion cooling appears to be about 7×10^{-12} Torr. This corresponds to a TDG current of 7×10^{-13} A with an estimated average sensitivity of $\bar{S} = 0.1$ A/Torr. Ion lifetime measurements were made at an average system working pressure of about 5×10^{-11} Torr, which should be primarily produced by H_2 and CO. The pressure average is taken over the longest storage interval for the ions.

APPENDIX III

Pulsed Helium Leak:

The helium leak was a standard quartz tube type with a reservoir holding about 25 cm^3 of $_3He$ at about 10 Torr. A heating coil surrounding the quartz tube in the reservoir produced a constant flux of helium through the quartz into a small volume consisting mostly of a one liter per second Varian ion pump. This volume was connected by a conductance of 10^{-4} liters/second to the main vacuum system. The small conductance was produced by shrinking one inch of 0.01 inch diameter stainless steel capillary into a block of stainless steel. When the ion pump was turned on by pulsing the high voltage, the leak was effectively off, since the influx of helium was removed by the pump. When the pump was turned off, the equilibrium flow of helium into the system matched the flow through the leak. The "equivalent circuit diagram"[54] for the system is shown in Figure XX where the circuit elements are labelled by their vacuum system analogues. Defining the helium flux through the leak as Q Torr l/sec., the steady state pressure of the vacuum system with the leak on is $P_{on} = Q/S_s$ where S_s was the pumping speed of the system pump for helium. With the leak off, $P_{off} \approx QC/S_sS_p = P_{on}C/S_p = 10^{-3}P_{on}$ for $C = 10^{-4}$ liter/sec., $S_p = 10^{-1}$ liter/sec. The time constant for pressure rise in the system is set by the ratio of the volume of the system to the pumping speed, and

was several seconds for the experimental situation. P_{on} was $\approx 5 \times 10^{-9}$ Torr.

Figure XX Equivalent circuit for the pulsed helium leak.

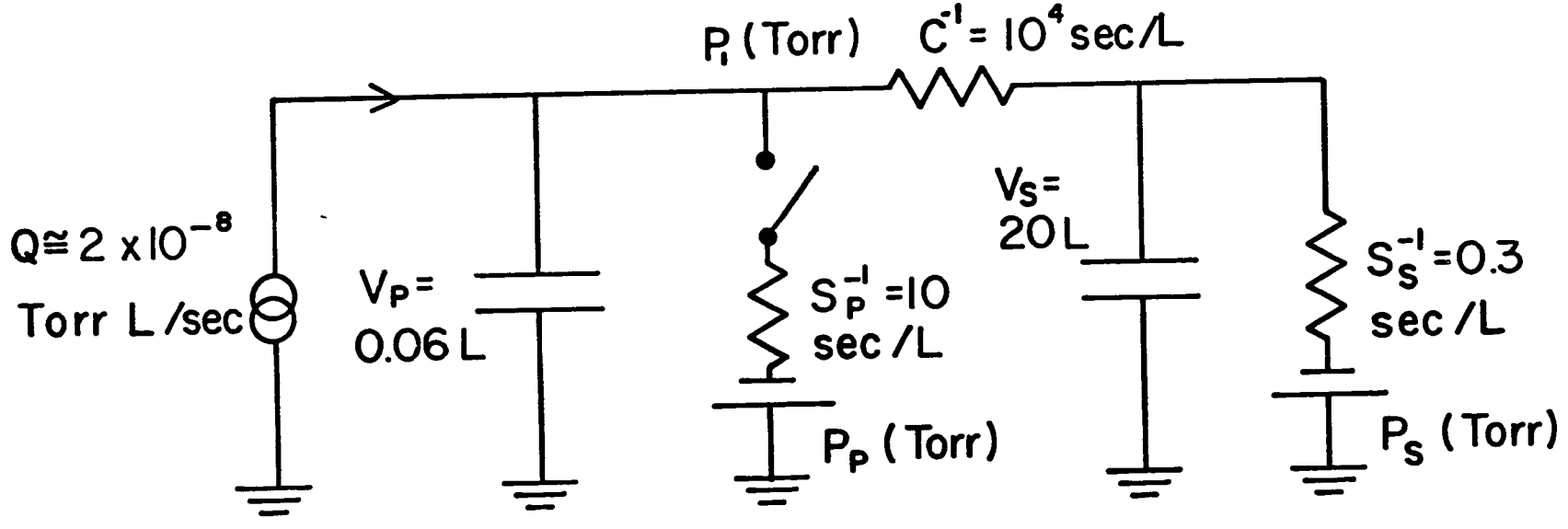
P_t (Torr)
$C^{-1} = 10^4$ sec/L
$Q \cong 2 \times 10^{-8}$
Torr L/sec
$V_P =$
0.06 L
$S_P^{-1} = 10$
sec/L
P_P (Torr)
$V_S =$
20 L
$S_S^{-1} = 0.3$
sec/L
P_S (Torr)

FOOTNOTES

1. E. N. Fortson, F. G. Major, and H. G. Dehmelt, Phys. Rev. Letters 16, 221, (1966).
2. F. G. Major and H. G. Dehmelt, Phys. Rev. 170, 91, (1968).
3. H. G. Dehmelt and K. B. Jefferts, Phys. Rev. 125, 1318, (1962).
4. C. B. Richardson, K. B. Jefferts, and H. G. Dehmelt, Phys. Rev. 165, 80, (1968).
5. K. B. Jefferts, Phys. Rev. Letters 20, 38, (1968).
6. H. A. Schuessler, S. C. Menasian, and E. N. Fortson, Bull. Am. Phys. Soc. 13, 67, (1968).
7. H. A. Schuessler, E. N. Fortson, and H. G. Dehmelt (to be published).
8. H. G. Dehmelt and F. L. Walls, Phys. Rev. Letters 21, 127, (1968).
9. E. Fischer, Z. Physik 156, 1, (1959).
10. F. G. Major, Thesis, University of Washington, University Microfilm, Ann Arbor, Michigan. (1962).
11. W. Paul and M. Raether, Z. Physik 140, 262, (1955).
12. N. W. McLachlan, Theory and Application of Mathieu Functions, (Oxford University Press, London, 1947).
13. H. Motz and C. J. H. Watson, Advances in Electronics and Electron Physics 23, (Academic Press, Inc., New York, 1967), p. 153.

14. H. G. Dehmelt, Advances in Atomic and Molecular Physics 3, (Academic Press, New York, 1967), p. 53.

15. T. Drees and W. Paul, Z. Physik 180, 340, (1964).

16. D. A. Church and H. G. Dehmelt, (to be published).

17. H. G. Dehmelt, Advances in Atomic and Molecular Physics, (to be published).

18. W. Shockley, J. Appl. Phys. 9, 635, (1938).

19. S. Ramo, Proc. I. R. E. 27, 584, (1939).

20. J. D. Jackson, Classical Electrodynamics, (Wiley, New York, 1963).

21. F. E. Terman, Radio Engineers' Handbook, (McGraw-Hill, New York, 1943).

22. R. F. Wuerker, H. Shelton, and R. V. Langmuir, J. Appl. Phys. 30, 342, (1959).

23. G. R. Huggett and S. Menasian, private communication.

24. F. v. Busch and W. Paul, Z. Physik 164, 581, (1961).

25. Obtained from the Refractories and Electronics Division, Carborundum Company, Latrobe, Pa.

26. Obtained from the American Lava Corporation, Chattanooga, Tennessee.

27. I. E. Dayton, F. C. Shoemaker, and R. F. Mozley, Rev. Sci. Instrum. 25, 485, (1954).

28. H. S. W. Massey and E. H. S. Burhop, Electronic and Ionic Impact Phenomena, (Oxford University Press, London, 1956).

29. R. H. Neynaber and S. M. Trujillo, Phys. Rev. 167, 63, (1968).

30. L. Spitzer, Physics of Fully Ionized Gases, (Wiley [Interscience], New York, 1956).

31. P. H. Dawson and N. R. Whetton, J. Vac. Sci. Tech. 5, 1 and 11, (1968).

32. W. H. Kohl, Materials and Techniques for Electron Tubes, (Reinhold Publishing Co., New York, 1956).

33. L. D. Landau and E. M. Lifshitz, Mechanics, (Addison-Wesley Publishing Co., New York, 1956).

34. H. C. Torrey and C. A. Whitmer, M. I. T. Radiation Laboratory Series 15, McGraw-Hill Book Co., Inc., New York and London, 1948).

35. G. Rettinghaus, Z. angew. Phys. 22, 321, (1967).

36. D. Rapp and W. E. Francis, J. Chem. Phys. 37, 2631. (1962).

37. Y. E. Strausser, 1967 Transactions of the 14th National Vacuum Symposium of the A.V.S., (1967), p. 131.

38. J. Futrell and F. Abramson, Advances in Chemistry Series (American Chemical Society, 1966), p. 107.

39. G. Gioumousis and D. P. Stevenson, J. Chem. Phys. 29, 294, (1958).

40. F. Walls and H. G. Dehmelt, private communication.

41. S. C. Menasian, private communication.

42. F. Rosebury, Handbook of Electron Tube and Vacuum Technique, (Addison-Wesley Publishing Co., Reading, Mass., 1965).

43. L. E. Prescott, Rev. Sci. Instrum. 33, 485, (1962).

44. J. W. Ackley, A. E. Barrington, A. B. Francis, R. L. Jepson, C. F. Lothrop and H. Mandoli, 1962 Transactions of the Ninth National Vacuum Symposium of the American Vacuum Society, (MacMillan Co., New York, 1962), p. 380.

45. S. L. Rutherford, 1963 Transactions of the Tenth National Vacuum Symposium of the American Vacuum Society, (MacMillan Co., New York, 1963), p. 183.

46. J. R. Young, J. Vac. Sci. Tech. 5, 102, (1968).

47. J. R. Young and F. P. Hession, 1963 Transactions of the Tenth National Vacuum Symposium of the American Vacuum Society, (MacMillan Co., New York, 1963), p. 234.

48. W. J. Lange, J. H. Singleton, and D. P. Eriksen, J. Vac. Sci. Tech. 3, 338, (1966).

49. J. R. Young, J. Vac. Sci. Tech. 3, 345, (1966).

50. B. E. Kietzmann, Varian Report VR-32, Varian Associates, Palo Alto, California (1965).

51. Due to voltage limitations, all the ion traps studied could scan at most a few mass numbers.

52. W. D. Davis, 1962 Transactions of the Ninth National Vacuum Symposium of the American Vacuum Society, (MacMillan Co., New York, 1962), p. 363.

53. K. B. Jefferts, private communication.

54. A. E. Barrington, High Vacuum Engineering, (Prentice-Hall, Inc., New Jersey, 1963).

VITA

David Arthur Church was born on April 3, 1939 in Berlin, New Hampshire, son of Andrew I. and Barbara B. Church. He attended the Gorham, New Hampshire public schools and entered Dartmouth College in 1957, graduating with a Bachelor of Arts in Physics in 1961. He next attended the University of Washington, receiving the Master of Science degree in Physics in 1963. During the same year he married Diane Claire Burnham in Seattle.